

https://dspace.org/

Aspects of the theory of inversion as applied to geophysical problems.

Cooper, Gordon Robert John.

1997
http://hdl.handle.net/10539/22950

Downloaded from a DSpace repository. https://dspace.org/

Figure 3.4 : Misfit vs Iteration for some sample boreholes for L_1 and L_2 inversion 47

Figure 3.5 : Kurtosis 49

Figure 3.6 : Misfit and kurtosis for L_1 and L_2 inversion for a sample borehole . . 49

Figure 3.7 : L_2 inversion for a sample borehole for different damping schemes . 51

Figure 3.8 : L_1 inversion for a sample borehole for different damping schemes . 53

Figure 4.1 : Magnetic model used to illustrate convergence properties 56

Figure 4.2 : Misfit as a function of body horizontal position for the model shown in Figure 4.1 56

Figure 4.3 : Convergence as a function of body initial horizontal position for the model shown in Figure 4.1 58

Figure 4.4 : Misfit as a function of body position for the model in Figure 4.1 . . 60

Figure 4.5 : Result of inverting the model in Figure 4.1 from a grid of different starting positions 60

Figure 4.6a : A portion of Figure 4.5 shown in more detail 61

Figure 4.6b : A portion of Figure 4.6a shown in more detail 61

Figure 4.7a : The Cantor set 63

Figure 4.7b : The Mandelbrot set 63

Figure 4.8 : Estimation of the fractal dimension of the basin of convergence of the model in Figure 4.1 65

Figure 4.9 : Behaviour of inversion trajectories 66

Figure 4.10a : The Newton-Raphson method of root finding 68

Figure 4.10b : Using the Newton-Raphson method to find the roots of $z^3 - 1 = 0$ 68

LIST OF FIGURES

page

Figure 1.1 : Example 2.5D gravity model 2

Figure 1.2 : Inversion of one model parameter - local gradients 6

Figure 1.3 : Misfit surface for the inversion of one model parameter 6

Figure 1.4 : Example of the genetic coding of a magnetic model 12

Figure 2.1 : Example magnetic model 17

Figure 2.2 : Model geometry 17

Figure 2.3 : Body properties dialog 24

Figure 2.4 : Selection of a body 24

Figure 2.5 : Numerical body entry dialog 27

Figure 2.6 : Numerical corner modification dialog 27

Figure 2.7 : Dialog for editing the remanent properties of a body 29

Figure 2.8 : Body movement dialog 29

Figure 2.9 : Body inversion dialog 31

Figure 2.10 : Hardcopy output dialog 31

Figure 2.11 : Regional and anomaly fields 33

Figure 2.12 : Regional field removal using Mag2dc 33

Figure 2.13 : Data filtering options 35

Figure 3.1 : Robust fitting of a straight line 38

Figure 3.2 : Location of boreholes whose data is shown in Figure 3.3 38

Figure 3.3 : Sample borehole temperature perturbation curves 44

5.6 Inversion of the density contrast of the body 105

5.7 Placing constraints on the position of the body 105

5.8 Inversion of multiple parameters simultaneously 108

5.9 Using chaotic inversion as an alternative to the Monte Carlo inversion technique 113

5.9 Using chaotic inversion to escape local minima 113

5.10 Conclusions 116

CHAPTER SIX - PROPERTIES OF THE MISFIT SURFACE

6.1 Introduction 119

6.2 Misfit surfaces 119

6.3 Improving convergence by fitting quadratic Functions to the misfit surface 121

6.3.1 Choosing a step size 125

6.3.2 Effect of noise 128

6.4 Extension to higher dimensions 130

6.5 Avoidance of local minima 136

6.5.1 Effect of noise 142

6.6 Conclusions 142

CHAPTER 7 : CONCLUSIONS AND SUGGESTIONS FOR FURTHER RESEARCH . 147

REFERENCES 150

CHAPTER FOUR - CONVERGENCE PROPERTIES OF INVERSION

4.1 Introduction 55

4.2 Convergence 55

4.2.1 Inversion of one parameter 55

4.2.2 Inversion of two parameters 57

4.2.3 Fractals 59

4.2.4 Fractals and Inversion 62

4.3 Effect of damping the inversion 69

4.4 Conclusions 72

CHAPTER FIVE - ASPECTS OF CHAOTIC DYNAMICS IN THE INVERSION OF GEOPHYSICAL DATA

5.1 Introduction 74

5.2 Chaotic dynamics and inversion 75

5.3 Generation of chaotic inversion 75

5.4 Inversion of the horizontal position of the body 77

5.4.1 Bifurcations 80

5.4.2 Transient behaviour 87

5.4.3 Fourier analysis of the motion 89

5.4.4 Lyapunov exponents 91

5.4.5 Phase space reconstruction 93

5.4.6 Correlation dimension 99

5.4.7 Damping 102

5.5 Inversion of the angle of rotation of the body 102

2.5 Description of Mag2dc and Grav2dc 22
2.5.1 Model editing options 23
2.5.1.1 Changing the body properties 23
2.5.1.2 Adding a new body to the model 26
2.5.1.3 Changing the shape of a body 28
2.5.1.4 Changing the remanent magnetisation of a b , 28
2.5.1.5 Options that affect the entire body 28
2.5.2 Inversion options 30
2.5.3 Miscellaneous options 30
2.5.3.1 Model output 30
2.5.3.2 Modifying the regional field 32
2.5.3.3 Filtering the field data 32
2.5.3.4 Changing the way that the model is displayed . . 34
2.6 Conclusions 36

CHAPTER THREE - NON-LEAST SQUARES INVERSION

3.1 Introduction 37
3.2 Borehole temperature data 39
3.3 The forward model 41
3.4 Inversion 42
3.5 Damping 48
3.6 Conclusions 54

CONTENTS

Page

Declaration ii

Abstract iii

Dedication v

Acknowledgements vi

List of figures xi

List of tables xvi

Philosophy xvii

CHAPTER ONE - INTRODUCTION

1.1 Forward and inverse modelling 1

1.2 Linear and non-linear inversion 5

1.3 Matrix inversion techniques 7

1.4 Ridge-regression 9

1.5 Local minima problems 10

1.6 Other techniques 11

1.7 Description of the work undertaken in this project 12

CHAPTER TWO - OBJECT ORIENTED GEOPHYSICAL SOFTWARE DEVELOPMENT

2.1 Introduction 14

2.2 Object oriented programming philosophy 14

2.3 Application to gravity and magnetic modelling 16

2.4 Calculation of the forward model 20

ACKNOWLEDGEMENTS

I would like to thank my supervisors, Dr. A. Cichowicz and Professor C. Wright, for their help, assistance, and suggestions throughout this project. I would like to thank Dr. M.Q.W. Jones for suggesting that I study the inversion of borehole temperature data and for his guidance with this portion of the project. I am also grateful to Lyn Whitfield for doing some of the draughting work involved.

TO MY PARENTS

ensure that a broad range of possible solutions was examined by the inversion, and to escape from local minima when these were encountered. Chaotic inversion can be used as an alternative to the Monte Carlo technique, over which it has some advantages.

Finally, the project involved the writing of a large quantity of geophysical software using object-oriented techniques, the structure of which is described in detail.

ABSTRACT

Inverse theory provides an important tool that the geophysicist can use to explore the structure of the Earth. This thesis examines several new approaches to the inverse problem, and suggests ways of improving the conventional least-squares technique. Non least-squares inversion was applied to borehole temperature data from South Africa, and when the norm of the inversion was controlled by the statistics of the misfit, it reduced by over 50% the number of iterations required for the inversion to converge upon a solution. Various damping schemes were also examined, and the use of the misfit in controlling the damping is shown to provide the best solution of those studied (Cooper and Jones, In press).

Improvements to the efficiency of the inverse process were also achieved by the fitting of parabolic forms to portions of the misfit surface, using both the misfit value and the gradient of the surface, for gravity data. The presence of nearby minima other than the one that the inversion has just converged to can also be detected in this manner.

The set of initial models that converged to a particular solution using least-squares inversion was studied for magnetic data, and it was noted to have a fractal nature. The fractal dimension of the set was found to be inversely proportional to the damping of the inverse problem.

The inverse process was pushed into a chaotic state by the modification of the least-squares inversion equation. The chaotic state was studied, and exploited to

I declare that this thesis is my own unaided work. It is being submitted for the Degree of Doctor of Philosophy in the University of the Witwatersrand, Johannesburg. It has not been submitted before for any degree or examination in any other university.

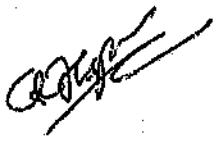

3rd day of December 1997

ASPECTS OF THE THEORY OF INVERSION AS APPLIED TO GEOPHYSICAL PROBLEMS

Gordon Robert John Cooper

A dissertation submitted to the Faculty of Science, University of the Witwatersrand, Johannesburg, in fulfillment of the requirements for the degree of Doctor of Philosophy

Johannesburg 1997

Since the inverse of an orthogonal matrix is its transpose, the inverses of U and V are calculated trivially. The inverse of a diagonal matrix is another diagonal matrix whose non-zero elements are simply the reciprocal of the original matrix. So ;

$$Z^{-1} = V\,[\,\mathrm{diag}(1/w_j)\,]\,U^T \qquad (1.8)$$

Hence the inverse of A^TA may be easily found once the matrices U,V, and W have been calculated. If A^TA is singular, then some of the smaller values of W_i will be incorrect and will produce an invalid solution. To counter this problem, the smallest values of W_i are set to zero, which has the effect of damping the inversion. When using single precision (4 byte word in Microsoft Fortran) variables, the singular value cutoff is normally set to 10^{-6} ; that is, any values of W_i that are less than 10^{-6} of the biggest value of W_i are set to zero. Although this is throwing information away, the values of W_i that are discarded are assumed to be invalid. The basic idea is that the parameter change vector that corresponds to a very small value of W_i will be very large, and probably erroneous.

SVD can additionally be used to counter the numerical inaccuracies that arise in the calculation of A^TA when A is a large matrix. Instead of solving equation 1.3, equation 1.9 is used (Lines and Treitel, 1984);

$$P = A^{-1}e \qquad (1.9)$$

Using SVD to calculate the inverse of A gives ;

converge on the required solution. The solution is reached in an iterative manner because the local gradient of the misfit surface is used, which is generally not the same as the gradient that would optimise the model the most effectively. Figure 1.2 shows the situation. In the gravity model shown in Figure 1.1, the density contrast is a linear parameter while the position of the body is a non-linear parameter. The greater the degree of non-linearity that is present in the model, the greater the difficulty that inversion schemes such as equation 1.3 will have, since they assume linearity.

1.3 Matrix Inversion Techniques

The inversion of the matrix A^TA can cause problems. Simple techniques such as Gauss-Jordan elimination (Jeffrey 1979, p.389) can produce unstable solutions if A^TA is singular, that is one of the rows or columns is a multiple of another. When matrices are inverted numerically (using computers, for example), additional problems can occur. One row or column may not be exactly a multiple of another, but they may be so similar that numerical roundoff error makes the matrix singular. Another problem is that roundoff errors can acculmulate during the computation, and this can cause the matrix inversion to produce the wrong solutions. This is particularly likely if the matrix A^TA is large (Lines and Treitel, 1984). One solution to these problems is to use the procedure of Singular Value Decomposition (SVD). This can be used to invert a square matrix Z by splitting it into three other matrices U,V, and W, where U and V are orthogonal and W is diagonal (Press et al 1992, p.51) .

$$Z = U W_i V^T \qquad (1.7)$$

Figure 1.2 : Inversion of One Parameter - Local Gradients

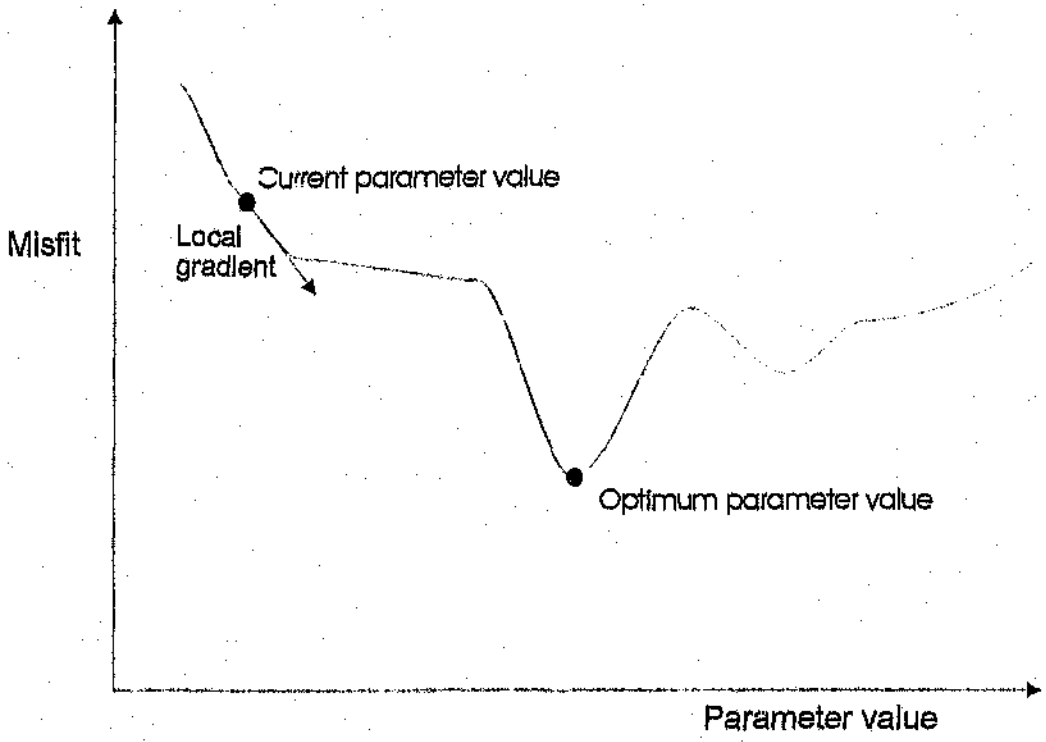

The incorrect assumption that the gradient measured at any point is the same for all parameter values results in equation 1.3 not producing the optimum parameter value in a single application.

Figure 1.3 : Schematic Misfit Surface for the Inversion of One Parameter

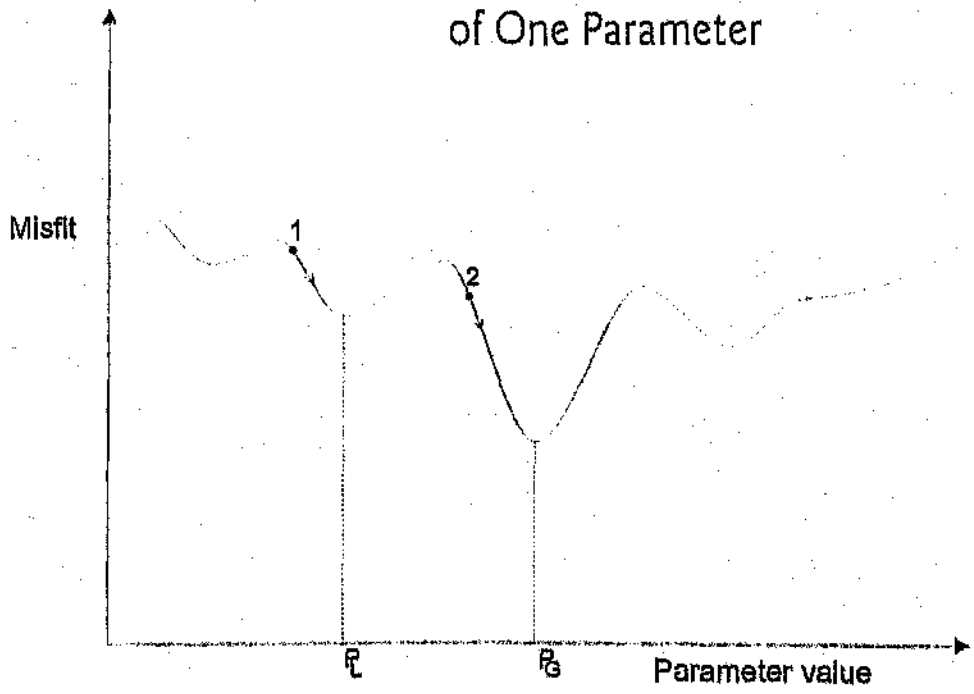

In certain situations, such as tomography for example, some model parameters are overdetermined while others are underdetermined. The inversion process also produces an estimate of the uncertainty with which each parameter is known. For the overdetermined situation the covariance of the solution given by ;

$$[\text{cov } P] = \sigma^2 (A^T A)^{-1} \qquad (1.6)$$

Where σ^2 is the variance of the field data (Menke 1989, p.58). Unfortunately, the geophysical problem is not so simply solved in practice, and there are many difficulties (see section 1.5 for example). Nevertheless, inversion is a valuable tool that is used routinely by the applied geophysicist in his daily work. It has been applied to almost all aspects of geophysics, including reflection seismology (Cohen and Bleistein, 1979, Cooke and Schneider, 1983), seismic refraction (Hampson and Russel, 1984), gravity data (Oldenburg, 1974), resistivity (Inman, 1975), and electromagnetic methods (Oristaglio and Worthington, 1978 ; Constable, Parker, and Constable, 1987).

1.2 Linear and Non-Linear Inversion

In a linear system the output scales with the input, that is , for a system f, if $f_{in} \rightarrow f_{out}$, then $\alpha f_{in} \rightarrow \alpha f_{out}$ (Pippard 1985, p.40). If the geophysical response of the model to a parameter is linear, then equations 1.3 and 1.5 will produce the model parameter values P that minimse the misfit directly. If however the response is non-linear, then equations 1.3 and 1.5 will at best produce a set of parameter changes dP to the original model that result in a reduced misfit, and must be used iteratively to

that can fit the data is estimated intuitively by the geophysicist as the modelling is performed.

In inverse modelling, the field data are analysed mathematically to produce a model that will fit the data. The parameters that are to be inverted are selected, and an initial value ('starting guess') for each is provided. The solution that best fits the data in a least-squares sense, when the model response is a linear function of the model parameters (see section 1.2), is then given by (Lines and Treitel, 1984) :

$$P = (A^TA)^{-1}A^Te \qquad (1.3)$$

where e is the n point misfit (or error) matrix between the model and the data given by :

$$e_i = O_i - C_i \qquad (1.4)$$

and O_i and C_i are the observed and calculated data values at point i. The superscript T represents the transpose of a matrix, and the superscript -1 represents the inverse of a matrix. The total misfit (as plotted in Figures 1.2 and 1.3 for example) is $1/n\sum_{i=1}^{n}|e_i|^2$ .Equation 1.3 defines the Gauss-Newton or Moore-Penrose method, and is the solution for the overdetermined case, where there are more field data points than there are model parameters (i.e. n>m) . If there are more parameters than data points then the model parameters are underdetermined, and the solution is given by (Dimri 1992, p.53) :

$$P = A^T(AA^T)^{-1}e \qquad (1.5)$$

situation is made worse by the fact that the field data are sampled at a finite set of discrete positions, and at these positions the data measurements are contaminated by noise from many sources. Some form of prior knowledge about the range of values that the model parameters (such as the shape and position of the bodies, for example) are allowed to take on can constrain the number of possible solutions (Menke 1989, p.49).

In forward modelling, some of the parameters are varied to determine the eff. on the model. Eventually the calculated response from the model will match the field data, and the model will be deemed to be a possible representation of the physical structure of the Earth. So :

$$f(P) = O \qquad (1.1)$$

where O is the m point matrix of observed field data, P is the n point parameter matrix, and $f(P)$ is the response of the model which is described by the parameters P. When the response of the model to the parameters is linear (see section 1.2) then :

$$A.P = O \qquad (1.2)$$

where A is termed the data kernel (Menke, 1989 p.9).

Because of the problem with non-uniqueness, if possible, several different geophysical methods would be used together with data from boreholes and constraints from surface geology to minimise errors in the the model parameters. The range of models

Figure 1.1 : Example 2.5D Gravity Model

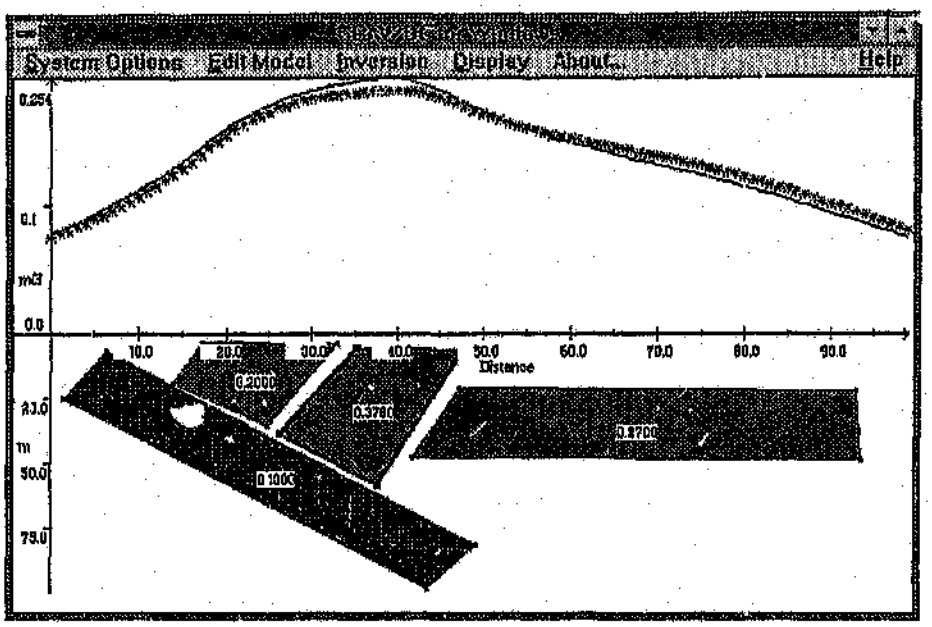

The solid line in the upper portion of the plot shows the calculated gravitational response of the polygonal bodies in the lower portion. The observed field data is shown as a series of asterisks *, and the body density contrasts (in $g.cm^{-3}$) are shown in the centre of each body.

CHAPTER 1 : INTRODUCTION

The determination of the structure of the Earth has been a problem central to geophysics for some time. There are many different geophysical methods available, such as seismological (earthquake and controlled source), magnetic, gravity, electromagnetic, and others (see Telford et al, 1990). All the methods exploit the contrasting physical properties of different types of rocks in such a way as to yield information about the geology of the subsurface. Measurements are made of some quantity, such as the strength of the geomagnetic field, and these measurements are then analysed, a process which generally involves the use of a computer to reduce the data (for example, to correct for known factors such as instrument drift), to filter the data (to remove or suppress unwanted noise), and then to derive a model of earth structure.

1.1 Forward and Inverse Modelling

Figure 1.1 shows an example of a gravity model. The upper portion of the figure shows a line of asterisks * which show the value of the gravitational field as measured in the field (after data reduction and regional field removal), and a solid line. The latter is the theoretical gravitational anomaly produced by the polygonal bodies in the lower half of the figure. The density contrasts of the bodies (in $g.cm^{-3}$) are superimposed upon them. Details of the model geometry and the calculation of the anomaly are given in section 2.4. The object of modelling is to find a body which will cause an anomaly that fits the observed field data. Unfortunately, gravity modelling (and geophysical modelling in general) is non-unique i.e. there will be a range of different models that will fit the data equally well (Lines and Treitel, 1984). The

Figure 6.8 : The gravity model of Figure 6.5 with 50% noise added 129
Figure 6.9 : Comparison of parabolic inversion and the ridge-regression technique in the inversion of gravity data - noise added 131
Figure 6.10 : Misfit surface for the model in Figure 6.2 for the parameters of depth and horizontal position 132
Figure 6.11 : Comparison of parabolic inversion and ridge-regression inversion for the inversion of body position and depth in a gravity model 134
Figure 6.12 : Comparison of parabolic inversion and ridge-regression inversion for the inversion of body position and angle of rotation in a gravity model 135
Figure 6.13 : Local minimum problem 137
Figure 6.14 : Misfit as a function of horizontal position for the model in Figure 6.13 139
Figure 6.15 : Quartic fit to misfit surface 139
Figure 6.16 : Quartic fit to misfit surface using data points and surface gradient 141
Figure 6.17 : Inversion of angle of rotation of body 141
Figure 6.18 : Misfit surface for the rotation of the body in Figure 6.17 143
Figure 6.19 : The model in Figure 6.13 with noise added 143
Figure 6.20 : Quartic fit to misfit surface using data points and surface gradient for the model in Figure 6.19 145
Figure 6.21 : The gravity model in Figure 6.17 with noise added 145
Figure 6.22 : Quartic fit to misfit surface for the model in Figure 6.21 146

LIST OF TABLES

Table 3.1 : Rock properties 40
Table 3.2 : Efficiency of L_2 inversion compared to L_1 inversion 45

position and angle of rotation 111

Figure 5.23a : Bifurcation diagram for the inversion of body position and rotation (plot of misfit) 111

Figure 5.23b : Bifurcation diagram for the inversion of body position and rotation (plot of horizontal position) 112

Figure 5.23c : Bifurcation diagram for the inversion of body position and rotation (plot of rotation angle) 112

Figure 5.24 : Sample trajectory from the chaotic inversion of body position and body angle of rotation for the model inFigure 5.22 114

Figure 5.25 : Misfit surface as reconstructed from a chaotic trajectory for the inversion of body position and angle of rotation 115

Figure 5.26 : A local minima problem 117

Figure 5.27 : Using chaos to escape a local mimima problem 117

Figure 6.1 : Schematic misfit surface for the case when two model parameters are inverted 120

Figure 6.2 : Example gravity model 120

Figure 6.3 : Example misfit surfaces for three parameters in the inversion of a gravity model 122

Figure 6.4 : Quadratic fit to a schematic misfit surface 123

Figure 6.5 : Gravity model used for body horizontal position inversion 123

Figure 6.6 : Comparison of parabolic inversion and the ridge-regression technique in the inversion of gravity data 126

Figure 6.7 : Gravity model used for body vertical position inversion 129

Figure 5.9a : Transient behaviour near a bifurcation point 88

Figure 5.9b : Number of iterations required for convergence against distance from a bifurcation event 88

Figure 5.10 : Power spectrum of data from a chaotic trajectory (Γ = 5.0) Horizontal body position inversion 90

Figure 5.11a : Divergence of nearby trajectories during chaotic motion 92

Figure 5.11b : Example calculation of Lyapunov exponent 92

Figure 5.12 : Analysis of a chaotic body horizontal position trajectory (Γ=5.0) 96

Figure 5.13 : Embedding of data in phase space 98

Figure 5.14a : Correlation sum vs distance R for different embedding dimensions, body horizontal position inversion (Γ = 5.0) 100

Figure 5.14b : Correlation dimension against embedding dimension, body horizontal position inversion (Γ = 5.0) 100

Figure 5.15 : Effect of damping upon inversion behaviour 103

Figure 5.16 : Bifurcation diagram for horizontal body position inversion (k=2.5)104

Figure 5.17 : Bifurcation diagram for horizontal body position inversion (k=5.0)104

Figure 5.18 : Model used for body rotation inversion 106

Figure 5.19 : Misfit bifurcation diagram for the model in Figure 5.18, body angle of rotation being inverted 107

Figure 5.20 : Angle of rotation bifurcation diagram for the model in Figure 5.19107

Figure 5.21a : Constrained inversion of body horizontal position 109

Figure 5.21b : Bifurcation diagram for the inversion of body horizontal position in the model shown in Figure 5.21a 109

Figure 5.22 : Model used to demonstrate simultaneous chaotic inversion of body

Figure 4.11 : Convergence to minima as a function of position for magnetics (damping factor k=10.0) 70

Figure 4.12a : Fractal dimension as a function of damping coefficient 71

Figure 4.12b : Percentage of starting positions for inversion that converge to the minimum on the same side of the profile that they started upon 71

Figure 4.13 : Convergence to minima as a function of position for magnetics (maximum X change allowed per iteration=100km, Y change allowed 50km) . . 73

Figure 5.1 : Gravity model used to demonstrate chaotic inversion 76

Figure 5.2 : Misfit surface for inversion of the model in Figure 5.1 with respect to body horizontal inversion 78

Figure 5.3a : Misfit against inversion iteration for the model in Figure 5.1 (Γ=1.0) 79

Figure 5.3b : Iteration scheme for the case when Γ=1.0 79

Figure 5.4a : Misfit against iteration for the model in Figure 5.1a (Γ = 4.0) . . . 81

Figure 5.4b : Iteration scheme for the case when Γ= 4.0 81

Figure 5.5a : Misfit against iteration for the model in Figure 5.1a (Γ = 5.0) . . . 82

Figure 5.5b : Iteration scheme for the case when Γ= 5.0 82

Figure 5.6a : Bifurcation diagram for the inversion of the horizontal position of the model in Figure 5.1a 83

Figure 5.6b : Bifurcation diagram for the inversion of the horizontal position of the model in Figure 5.1a 83

Figure 5.7 : A period-doubling bifurcation event in phase space 85

Figure 5.8 : The Feigenbaum constants 85

```
    End;
    If Body[BodyT].Hidden=False then For Point:=1 to
     NoObsPts do MagC^[Point]:=MagC^[Point]
      -Body[BodyT].Magnetics[Point];
    Calculate(BodyT);
   End;
End;
```

The method checks to see if any corners of the body are tied to any corners of other bodies. If a corner of a body is tied to that of another body, then movement of either will cause the movement of both. This allows the easier modification of regions where anomalous bodies abut onto one another. This code performs the movement of the tied corner and the recalculation of its anomaly. The BreakLinks method in the body object breaks all such links associated with the body when required. The total magnetic anomaly for all of the bodies that make up the model is stored in the array MagC. It is considered bad programming practice to access the data fields of an object directly, without using the methods associated with that object.

Each dialog that is used in Mag2dc and Grav2dc to request information of any kind from the user is also an object. They will be discussed in detail below.

2.4 Calculation of the Forward Model

Both Mag2dc and Grav2dc use a 2.5D algorithm to calculate the magnetic field anomaly produced by the causative bodies. The profile direction is assumed to cut the bodies being modelled at 90 degrees, the bodies themselves being represented by polygonal shapes of up to 50 sides. The profile bisects the bodies, which extend along strike an equal distance. Figure 2.2 shows the model geometry.

```
Body[1].Move(10,20);
```

The code for the Move method is shown below :

```
Procedure TBody.Move(Dx,Dy:Real);
Var
 I                    : Integer;
Begin
 For I:=1 to NoCorners do
  Begin
   If Corners[I].Ypos + Dy <0.0001 then Dy:=
    -Corners[I].Ypos + 0.0001;
  End;
 For I:=1 to NoCorners do Corners[I].Move(Dx,Dy);
End;
```

The method checks that the movement will not bring the body above the surface of the ground, and if this is the case then it reduces the vertical movement accordingly. Then it calls the Move method of the Corners object to perform the actual movement. The Move method code for the corner object is :

```
Procedure TCorner.Move(Dx,Dy:Real);
Var
 TempC,Point          : Integer;

Begin
 Xpos:=Xpos+Dx;
 Ypos:=Ypos+Dy;
 If Tied=True then
  Begin
   Body[BodyT].Corners[CornerT].Move(Dx,Dy);
   If Body[BodyT].Corners[CornerT].Ypos < 0.0 then
     Body[BodyT].Corners[CornerT].Ypos:=0.0001;
   If CornerT=1 then
    Begin
     TempC:=Body[BodyT].NoCorners;
     Body[BodyT].Corners[TempC].Xpos:=
       Body[BodyT].Corners[1].Xpos;
     Body[BodyT].Corners[TempC].Ypos:=
      Body[BodyT].Corners[1].Ypos;
```

```
End;
```

The body is an object of type Tobject (i.e. Tobject is its ancestor type), which is the most primitive type of object available in Turbo Pascal. The variables that describe the body are listed first. As well as details describing the susceptibility, remanence, strike length and the anomaly produced by the body, information pertinent to inversion is also stored (such as which parameters of the body are to be inverted, and the limits that are to be set upon their values). The procedures (known as *methods*) are listed last, and are used to move and rotate the body. The purpose of the *Constructor* Init is to allocate any memory required by the body and to initialise all of the variables that are used by the body. If necessary, a *Destructor* could also be used, to release the memory used by the body when the body was deleted from the model. The definition of the body makes use of another object type called TCorner, which describes the behaviour of the vertices of the body. The code for this object is listed below :

```
PCorner=^TCorner;
Tcorner=Object(TObject)
  Xpos,Ypos                    :  Real;
  Tied                         : Bcolean;
  BodyT,CornerT                : Integer;
  InvHC,InvVC                  : Boolean;
  Constructor Init;
  Procedure Move(Dx,Dy:Real);
End;
```

As an example of how this object is used, suppose it is required to move body 1 10m horizontally and 20m deeper. Then the program statement would look like ;

Figure 2.1 : Example Magnetic Model

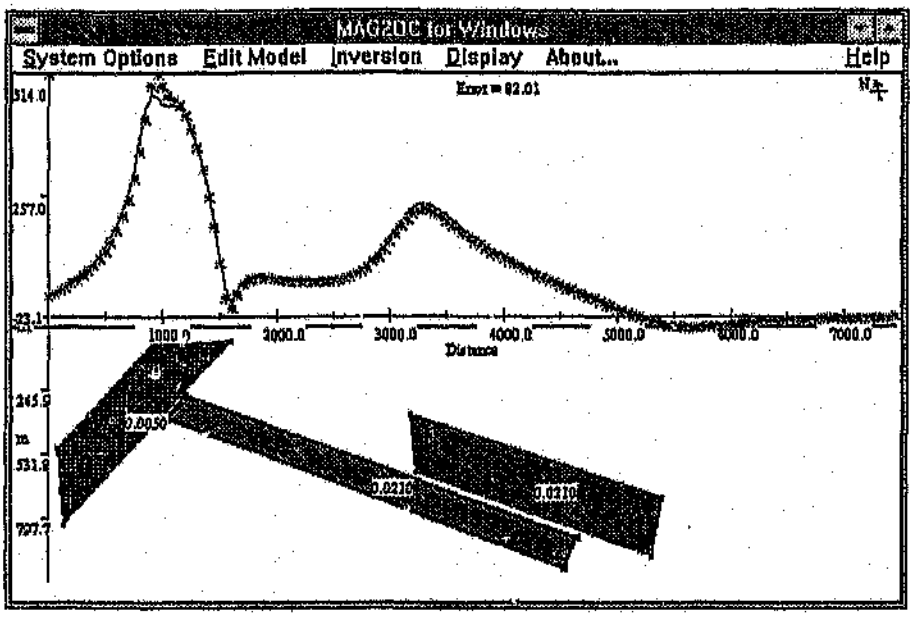

Figure 2.2 : Model Geometry

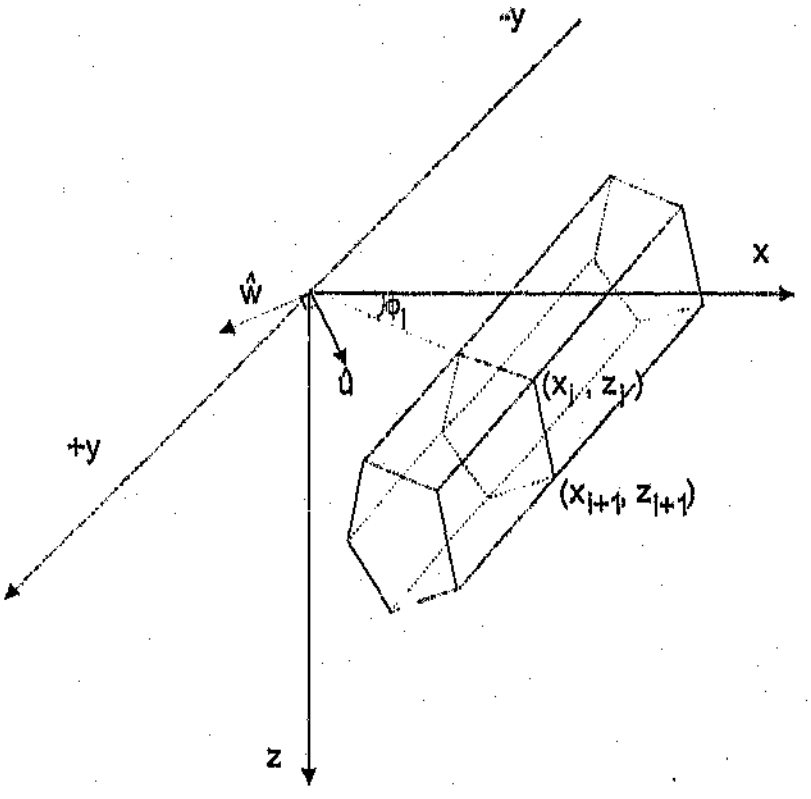

A sample body is shown superimposed on the model geometry. It is of polygonal cross-section and has corners (x_i, z_i). It lies at 90 degrees to the x axis, and extends to a limited extent on each side of it. The other terms are described in the text

OOP has proved useful when applied to a wide variety of different problems, such as control systems (Bricker 1990 ; Gowan 1991), voltage network design (Nicolson, 1993), real-time software (Baas, 1993), and many others. Studies have been performed that show the superiority of the OOP approach over more traditional structured programming techniques in many situations (Meyer 1988 ; Nitch 1992).

2.3 Application to Gravity and Magnetic Modelling

An example model is shown in Figure 2.1 . Mag2dc uses a Talwani algorithm (which is described in section 2.4) to calculate the 2.5 dimensional anomaly over a number of bodies of polygonal cross-section which lie at 90 degrees to the profile direction. These bodies are shown in the lower portion of Figure 2.1. The upper portion shows the calculated magnetic anomaly from the model (the solid line) and the field data (the line of asterisks *).

The bodies that make up the model are shown in the lower portion of Figure 2.1. Each body in the model is described by an object, which contains data about the body (such as its susceptibility or strike length) and procedures that act upon it (to move or turn it, for example). Sample code describing a body is shown below ;

```
PBody=^TBody;
 Tbody=Object(TObject)
  Suscept,Inten,Inc,RemAng,Strike   : Real;
  Smin,Smax,Hmin,Hmax,Vmin,Vmax     : Real;
  RotMin,RotMax                     : Real;
  NoCorners                         : Integer;
  Remanent,Hidden,InvS,InvH         : Boolean;
  InvV,InvRot                       : Boolean;
  Corners              : Array[1..MaxCorners] of TCorner;
  Magnetics            : Array[1..MaxPts] of Real;
  Constructor Init;
  Procedure Turn(Angle:Real);
  Procedure Move(dx,dy:Real);
  Procedure BreakLinks;
```

These aims are achieved by tightly integrating the data and the procedures that act upon it in the form of an *object*. This is known as *encapsulation*. Objects can be used to build other objects (known as the *descendants* of the original ancestor object) which have access to the data and procedures of the original object.

Pascal is a strongly typed language, meaning that the nature (integer, real, etc) of all variables must be defined in each procedure. This helps prevent problems with variables of different types being mistakenly assigned to each other, or variables of incorrect (in the sense that the type is different to that expected) type being passed to a procedure or function. Languages such as Fortran and Basic do not require that the type of a variable is explicitly specified before it is used. Turbo Pascal for Windows adds OOP functionality to the Pascal language. As well as encapsulation and inheritance, it also supports *polymorhpism*, whereby several different copies of a procedure can exist, and the decision as to which is called depends on the type of the data that is passed to it. Because the data type may not be known until the program is run, the decision as to which procedure to call cannot be made until this time.

Other OOP compilers that are commercially available include C++ (which is C with OOP enhancements, available from Microsoft, Borland, and Zortech, amongst others), Delphi (from Borland - which became available in late 1995 after most of the software used in this project had been written), as well as older languages such as Smalltalk, LISP, Prolog, Modula-2, and Ada. Not all of these languages provide full OOP functionality however, and the use of OOP facilities is not always made compulsory by the compiler.

CHAPTER 2 : GEOPHYSICAL MODELLING SOFTWARE DEVELOPMENT USING THE OBJECT ORIENTED PROGRAMMING PARADIGM

2.1 Introduction

Software to model and invert gravity and magnetic data was developed as an integral part of this project. The software made extensive use of object oriented techniques, which proved well suited to geophysical problems. Turbo Pascal 1.5 (Borland, 1992) for Microsoft Windows 3.1 was used as the development language because of its implementation of the object oriented programming philosophy, and the speed of execution of the resulting code. Commercial geophysical software could not have been used in this project because the source code is not made available to users.

2.2 Object Oriented Programming Philosophy

Software development is an extremely labour intensive process. Software costs can easily exceed hardware costs in a project, particularly since hardware (such as processors, memory, and disk space) becomes cheaper and more powerful as technology improves. Object oriented programming (OOP) is a way of writing and debugging structured programs that are easier to test and maintain (and are therefore cheaper to produce) than non-OOP programs. OOP also attempts to make code more reusable, thus reducing development costs further. Since maintenance of software can make up as much as two-thirds of the total software development costs (Steward, 1979), strategies that aim to make the maintenance of code as simple as possible are particularly useful.

considerably. Chapter 6 describes the use of knowledge of the shape of the misfit surface for the same purpose.

c. To look at local minima problems in detail and to see what strategies could be used to get around them. Chapter 4 examines the nature of the set of models that converge to a given minimum for magnetic data. Chapter 5 uses chaotic dynamics to ensure that a large range of possible models is sampled during the inversion, so that the probability of convergence to a local minimum rather than the global minimum is reduced. Chapter 6 discusses using knowledge of the shape of the misfit surface to determine whether another minimum exists adjacent to the one that the inversion has just converged to.

Throughout this project the aim has been to analyse mathematical aspects of inverse theory. It was *not* the aim of the project to perform any kind of geological interpretation of geophysical data using inverse methods. The concept was to develop tools that would be of use to others, such as geophysicists or geologists, in their work. The demonstration of the techniques presented here has mainly been performed on synthetic data, since it is easy to construct problems (such as local minima) that are both difficult or insoluble for standard inverse methods, and which simultaneously allow the principles of the new methods to be clearly seen.

In this thesis the standard procedure of referencing work by other authors where it has been used has been followed. All non-referenced material is the work of the author, or is considered common knowledge (e.g. the equation for the roots of a quadratic equation).

random mutations have produced a benefit to the model (i.e. improved the fit) are retained, while the models that have been harmed (i.e. that have made the fit worse) are discarded.

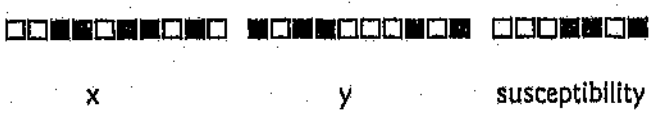

Figure 1.4 : The horizontal and vertical position of a body, and its susceptibility, are encoded as three portions of a binary string. A solid square ■ represents a binary 1, and an empty square □ a binary zero. The more bits that are assigned to store a particular parameter, the greater the resolution with which that parameter can be known.

1.7 Description of the Work Undertaken in this Project

The aim of this project was to attack the problem of the inversion of geophysical data from several different angles, and it is therefore split into several distinct portions ;

a. The magnetic and gravity modelling programs required for chapters 4, 5, and 6 necessitated the writing of large quantities of software (since the source code of commercial software was not available), and a description of the software and the object-oriented methodologies used is given in chapter 2.

b. To find ways to improve the efficiency i.e. improve the speed of convergence, of inversion. Chapter 3 describes the application of non least-squares inversion to a set of borehole temperature data collected in South Africa, which improved the efficiency

simultaneously, then the gravity (with anomalies of the order of tens of mgals) will be dominated by the magnetics (with anomalies of up to several thousand nT) unless some form of scaling is performed (see section 5.8).

1.6 Other Techniques

An inversion method that is often used when the model response is too non-linear for the Gauss-Newton method to work effectively is the Monte Carlo technique. This involves running hundreds or thousands of forward models with parameters chosen randomly and then selecting the ones that give the best fit (Press, 1969). This method is not liable to local minima problems, since each model that is run is independent of the previous models. It has the disadvantage that it requires large amounts of computer processing time to run the forward models. Anderssen et al (1972) applied the technique to modelling the density of the Earth, and modified it statistically to ensure that only physically realistic models were generated.

A variation on the Monte Carlo method, called genetic algorithms, has been used successfully with geophysical data (Horne and MacBeth, 1994, Sambridge and Drijkoningen, 1992). In this method the models are encoded into binary strings in an analogous manner to human DNA (see Figure 1.4). The models are then bred together, and the ones whose response fits the data best are retained and bred further ('survival of the fittest'). In addition a random element is added to the process by the switching of a single bit in a certain proportion of the models. This simulates random mutations caused in DNA by radiation. The 'radiation level' can be varied by controlling the rate at which random bits are swapped. The models in which the

1.5 Local Minima Problems

The ridge-regression and Gauss-Newton methods are both prone to local minima problems. The objective of the inversion is to find the model whose response has the best fit to the data, but it frequently happens that instead of reaching the set of parameters that produce the smallest misfit possible (the global minimum), the inversion becomes stuck in a local minima on the misfit surface. Figure 1.3 shows the problem for the case when there is only one model parameter being inverted. From the starting point 1 the inversion reduces the misfit at first, until the parameter reaches the point P_L. The global minimum at P_G cannot be reached from P_L, since small perturbations to the value of P about P_L result in a worse misfit. If however the inversion had been started from point 2 then it would have converged successfully to the global minimum P_G. In general, if a poor initial model is used then there is a greater likelihood that the inversion will become trapped in a local minimum.

One use of inverse theory that can partially help to solve the local minima problem is the joint inversion of two geophysical datasets that be. the same geology. For example, magnetic and gravity profiles over an ore body can be inverted simultaneously (Menichetti and Guillen, 1983). Such joint inversion can be useful, since the inversion may take one parameter out of a local minimum of one data type in the course of modifying another. In addition, since the noise present in the two datasets will be uncorrelated (depending on the types of data used), its effect will be reduced. Care must be taken when applying joint inversion to scale the datasets correctly, or the data with the greatest numerical values will tend to dominate (Vozoff and Jupp, 1975). For example, if gravity and magnetic data are to be inverted

$$P = V [\text{diag}(1/w_j)] U^T e \qquad (1.10)$$

1.4 Ridge-Regression

Despite the use of SVD, the inversion of the matrix A^TA may still cause problems i.e. generate invalid models. One solution is to use the technique of Marquadt-Levenburg (Marquadt, 1963, Levenburg, 1944), sometimes referred to as ridge-regression (Inman, 1975). Equation 1.3 is modified to become :

$$P = (A^TA + kI)^{-1}A^Te \qquad (1.11)$$

where k is a constant and I is the identity matrix. The factor k acts to damp the inversion, preventing P from assuming arbitrarily large values when A^TA is singular. It works by placing an upper limit on the parameter change vector. However if the model response is a non-linear function of the parameter's values and hence the inversion process is iterative, then the greater the value of k, the slower the inversion will converge to the minima. Even if the inversion is linear with respect to all of the model parameters (see section 1.2) more than one iteration will be required for convergence to the minima if the value of k is non-zero.

The value of the constant k affects the size of the model (where the size is given by P^TP) as well as the damping (Menke, 1989 p.52). The larger k is, the smaller will be the resulting model in general, but setting k too large can result in too slow convergence of the inversion. This is investigated in detail in chapter 3.

Figure 2.5 : Numerical Body Entry Dialog

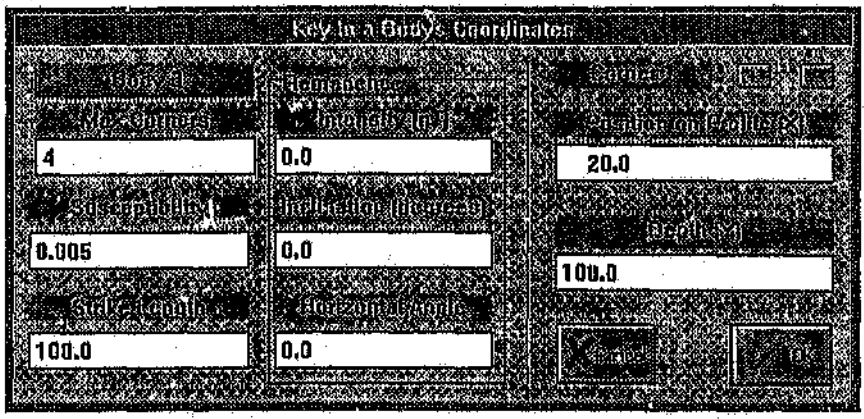

Figure 2.6 : Numerical Corner Modification Dialog

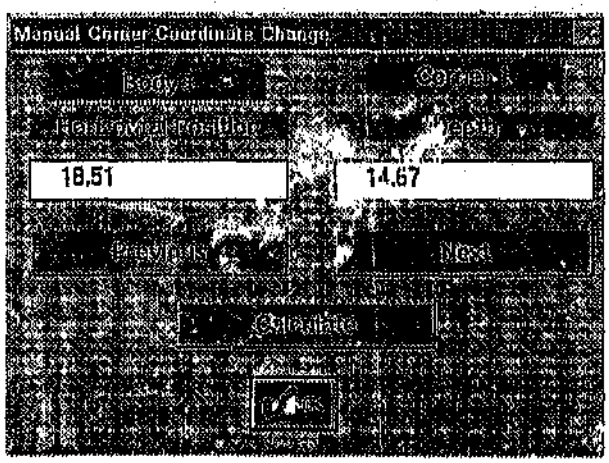

checked.

2.5.1.3 Changing the Shape of a Body

This can be performed by clicking with the mouse on the corner that is to be moved, then clicking on the new position, which will cause the model to be recalculated and updated. Alternatively, the new coordinates can be entered numerically. Body corners can be added or deleted by clicking upon them with the mou Figure 2.6 shows the numerical corner modification dialog. This method is necessary if body corners are to be moved off the ends of the profile (to prevent edge effects), since the mouse cursor obviously cannot be moved offscreen.

2.5.1.4 Changing the Remanent Magnetisation of a Body

Remanent magnetisation is the magnetisation that the body would possess in the absence of any external magnetic fields (Blakely, 1995 p.89). It is a vector quantity, but rarely has sufficient magnitude to alter the resultant field direction from that of the geomagnetic field by a significant amount. In Mag2dc it is described by three parameters : an intensity (in nT), an inclination from the horizontal plane (positive downwards), and a horizontal plane angle (degrees clockwise from magnetic North). The dialog is shown in Figure 2.7. Inversion of the remanent parameters can also be performed from this dialog.

2.5.1.5 Options that Affect the Entire Body

Available editing options that affect the whole body (as opposed to just the position of a corner) include moving, rotating, and copying it. The move dialog is

projected from the cursor position to a point outside of the model. Each side of the polygon making up each body in the model is then checked to see if it intersects this line. If there are an odd number of intersections then the point lies within the body currently being tested and this becomes the current body. If there are an even number of intersections then the point lies outside the body, and the next body is checked. This process works no matter whether the body is concave or convex. Figure 2.4 illustrates the process.

The calculations involved are computationally trivial and the user is aware of no delay between double-clicking on a body and the properties dialog appearing.

All dialogs used in Mag2dc and Grav2dc are *modal*, i.e. the user is unable to perform any other action with the program (except putting it into the background) until the dialog is closed.

2.5.1.2 Adding a New Body to the Model

This can be done either by clicking onscreen at the desired locations of the body corners in a clockwise manner (the cursor position is shown onscreen, and in addition the corners can be made to snap to a user-defined grid if desired), or by entering the body corners numerically onscreen in a dialog, or by reading in the body coordinates from an ASCII file on disk. The latter is useful if the initial model has been digitised from a seismic section, for example. The numerical entry dialog is shown in Figure 2.5. After each corner's coordinates are entered, pressing the + and - buttons will enable the next corner to be entered or the previous corner's coordinates to be

$$\Delta g_z(x_0) = -2\gamma G\rho\Sigma_i z\cdot n_i \log\frac{u_{i+1}+R_{i+1}}{u_i + R_i}$$
$$+ 2G\rho\Sigma_i \frac{x_i z_{i+1} - z_i x_{i+1}}{\Delta x_i^2 + \Delta z_i^2}\left[\Delta z_i \log\frac{r_{i+1}(Y + R_i)}{r_i(Y + R_{i+1})}\right. \quad (2.4)$$
$$\left. + \Delta x_i\left(\tan^{-1}\frac{u_{i+1}Y}{w_i R_{i+1}} - \tan^{-1}\frac{u_i Y}{w_i R_i}\right)\right]$$

where G is the gravitational constant and ρ is the density contrast (in $g.cm^{-3}$) of the body. n_i is the normal to the ith side of the body, and • denotes the scalar product. The gravitational or magnetic response of the body to a change of density or magnetisation is linear, as can be seen from equations 2.1 - 2.4. The body position is described by the coordinates (x_i,z_i), and hence the geophysical response of the body to operations such as rotation or translation is non-linear. This fact becomes relevant in chapters 4,5, and 6.

2.5 Description of Mag2dc and Grav2dc

The programs are similar in many respects and will therefore be discussed together. Turbo Pascal 1.5 for Windows does not allow any data structure (including objects) to be greater than 64Kb in size, and this has restricted the maximum number of data points that can be modelled to 650. There can be up to 16 bodies in a model, each with up to 50 corners. Any computer capable of running Microsoft Windows 3.1 has sufficient memory and processing power to run these programs, but an 80586 based or better machine is preferred. The source code for the software consists of over 10000 lines per program, and it is therefore not listed in this work. There are almost 50 menu options available within both Mag2dc and Grav2dc ; only the most important ones will be discussed here. A full 'Windows Help' facility has been written for each program. The help file was written using Microsoft Word, then compiled into

output to ASCII, HP-GL, or DXF file formats. It may also be copied to the Windows clipboard for ease of importation into other packages. The hardcopy output dialog is shown in Figure 2.10 .

2.5.3.2 *Modifying the Regional Field*

Selection of the correct regional field is critical to the whole modelling process. Separation of the regional field from the observed data will leave the residual anomaly caused by the target structure (Blakely, 1995 p.128), and if an incorrect regional field is chosen then an incorrect anomaly will remain. Figure 2.11 shows the concept. Both Mag2dc and Grav2dc allow a linear regional field to be subtracted from the observed data. Clicking with the right mouse button sets the regional field value at the right side of the profile, while clicking the left button sets it on the left side. Figure 2.12 shows a regional field being selected for some magnetic data. The equation of the regional field removed is displayed after it has been removed.

2.5.3.3 *Filtering the Field Data*

Noisy data can be smoothed using a simple weighted moving average filter, as shown in Figure 2.13 . The amount of smoothing can be increased by increasing the filter size - that is a five point filter with weights (1, 1, 1, 1, 1), will produce more smoothing than a three point filter (1, 1, 1). The result of the filtering can be previewed by pressing the Test Filter button. The weights can be set to produce highpass (E.g. -1, 2, -1) and edge detection filters (1, 0, -1) (See Richards, 1993 p. 118-130 for more details on space domain filtering techniques). While the output from these latter filters cannot be modelled directly by Mag2dc or Grav2dc, it can be

Figure 2.9 : Body Inversion Dialog

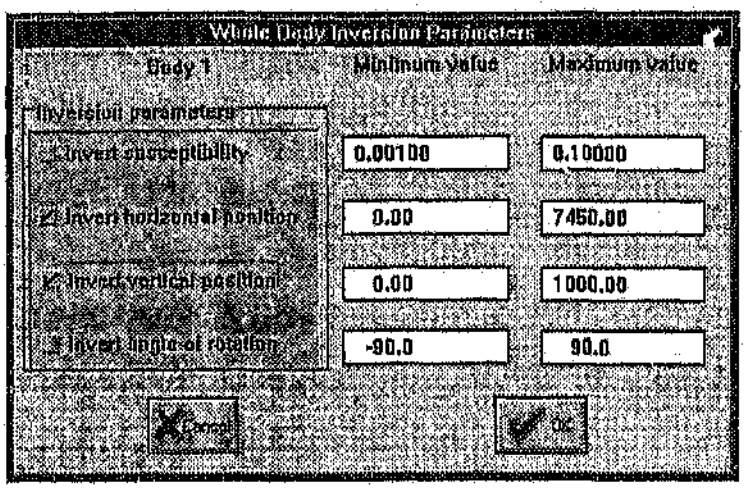

Figure 2.10 : Hardcopy Output Dialog

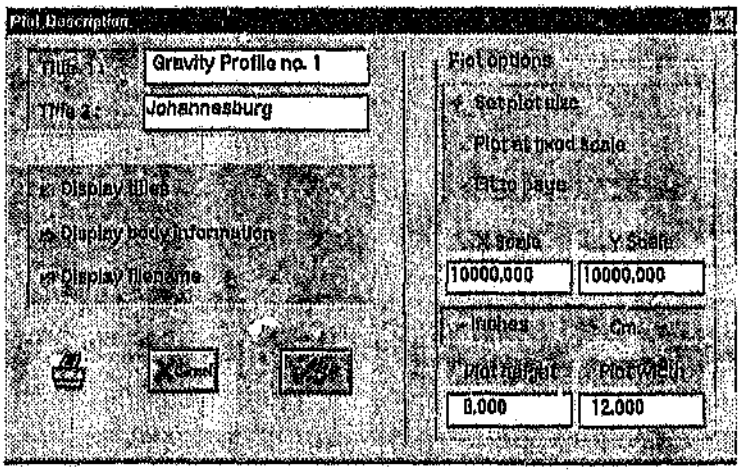

shown in Figure 2.8. In addition to moving a body by pressing the + and - buttons (which operate in a similar manner to those described above) a body may also be moved by holding the mouse down upon it, then dragging it to the new location. When the mouse button is released the body position is fixed and the anomaly is updated.

2.5.2 Inversion Options

The body position, shape, angle of rotation, density and susceptibility may be inverted using the options in the 'Invert' menu. Body corner positions may be inverted in either a horizontal or a vertical plane, or in both. A maximum of 10 body parameters may be inverted simultaneously due to the memory restrictions of Turbo Pascal mentioned previously. The body parameter selection dialog is shown in Figure 2.9. Selection of body corners for inversion is done by clicking on them ; once for inversion in a horizontal plane, twice for vertically, three times for both horizontally and vertically, and four times to deselect the corner for inversion. The current status of the corner with respect to inversion is shown by a double-headed arrow that points in the directions of inversion that are currently selected.

The mathematical details of the inversion process itself is discussed in detail in chapters 4 and 5.

2.5.3 Miscellaneous Options

2.5.3.1 Model Output

The model can be printed on any Windows supported printer (to scale), or

Figure 2.7 : Dialog for Editing the Remanent Properties of a Body

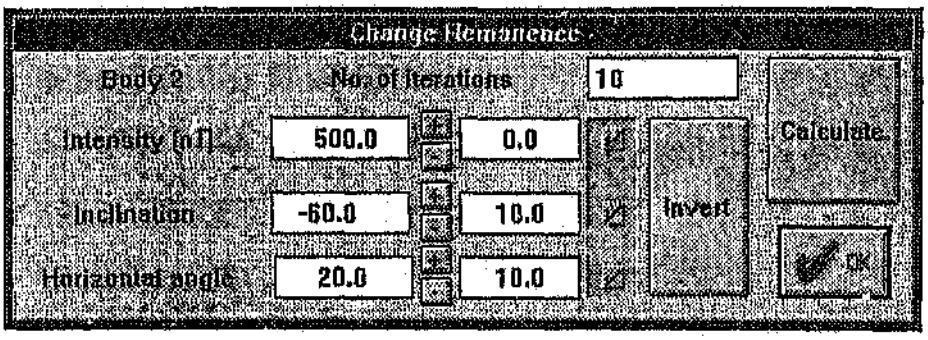

Figure 2.8 : Body Movement Dialog

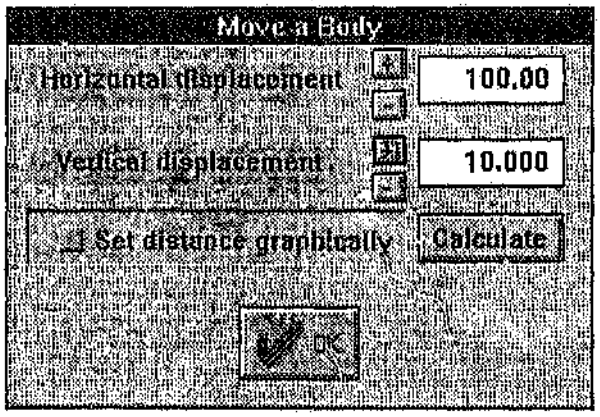

```
PProperties =^Properties;
Properties = Object(TDialog)
 Procedure SetUpWindow; virtual;
 Function CanClose: Boolean; virtual;
 Procedure Plus(Var Msg:TMessage); virtual id_first +
id_Plus;
 Procedure Minus(Var Msg:TMessage); virtual
id_first+id_Minus;
 Procedure Calc(Var Msg:TMessage); virtual id_first +
id_Calc;
 Procedure SusPlus(Var Msg:TMessage); virtual id_first +
id_SusPlus;
 Procedure SusMinus(Var Msg:TMessage); virtual id_first
+ id_SusMinus;
 Procedure DepthPlus(Var Msg:TMessage); virtual id_first
+ id_DepPlus;
 Procedure DepthMinus(Var Msg:TMessage); virtual
id_first + id_DepMinus;
 Procedure WidthPlus(Var Msg:TMessage); virtual id_first
+ id_Wplus;
 Procedure WidthMinus(Var Msg:TMessage); virtual
id_first + id_Wminus;
 Procedure InvSuscept(Var Msg:TMessage); virtual
id_first + id_InvSus;
 Procedure InvDepth(Var Msg:TMessage);  virtual id_first
+ id_InvDepth;
End;
```

There are two methods present in addition to the ones that respond to the pressing of buttons on the dialog. These are 'Procedure SetUpWindow', which initialises the dialog with the current data that describes the body, and 'Function CanClose', which reads back the final settings of the variables when the OK button is pressed, and updates the model accordingly. The keyword *virtual* after each procedure name indicates that the program will determine at runtime which object has called the procedure. This is known as *late binding* (Swan,1991 p.119), and is necessary since it is not known until runtime which object has called the procedure.

The body properties dialog can be called up either from the main menu or by double-clicking on a body. To determine which body has been selected, a line is

Figure 2.3 : Body Properties Dialog

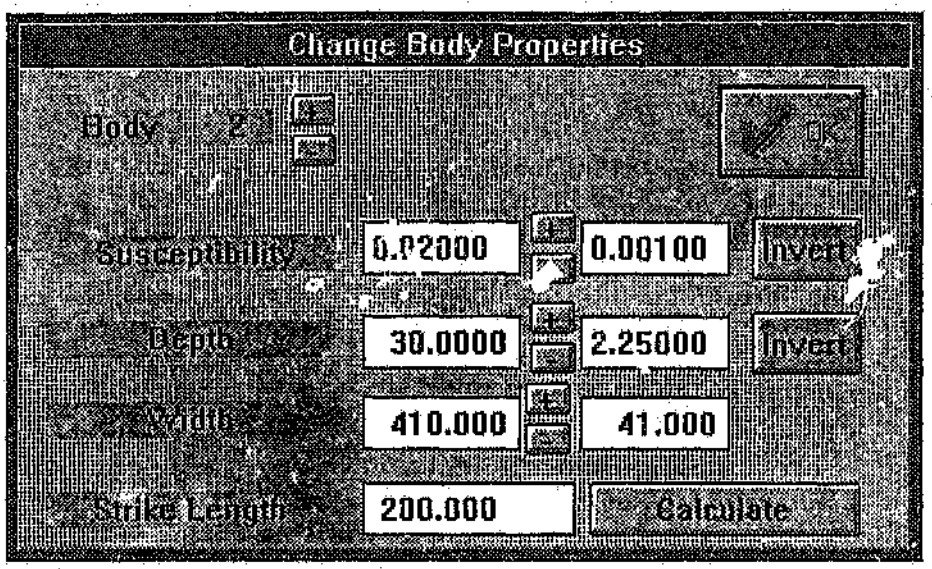

Figure 2.4 : Selection of a Body

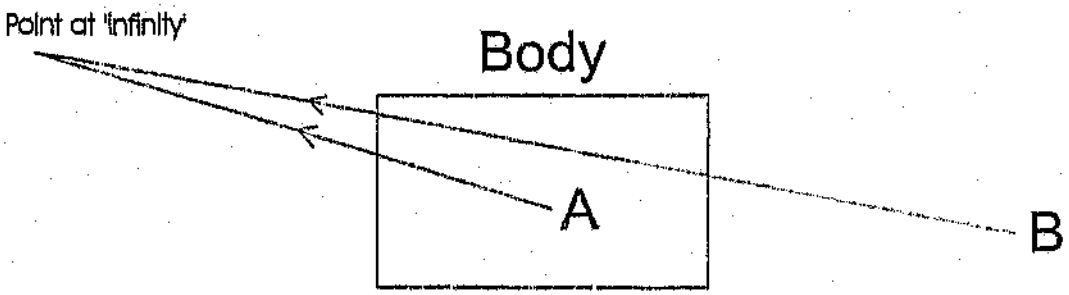

Points A and B are positions where the mouse has been clicked. Point A lies inside the body, and the line from it to 'infinity' intersects the body only once.

Point B lies outside the body, and the line from it to 'infinity' intersects the body twice.

.hlp format using the RoboHelp compiler (Blue Sky Software, 1991).

2.5.1 Model Editing Options

2.5.1.1 Changing the Body Properties

The susceptibility, width, strike length, and depth can be changed in Mag2dc using the dialog shown in Figure 2.3 The number of the current body is shown in the upper left of the dialog. All actions are carried out on the current body, which is displayed in a bolder outline than the other bodies. A body can be made current by clicking on it with the mouse. Clicking on the small +/- buttons next to the body number will cause the next/previous body to become current. To change the susceptibility of the body, enter the new value then press the 'Calculate' button. The anomaly will then be recalculated and updated Alternatively, pressing the small +/- buttons next to the susceptibility will cause the increment shown in the adjacent box to be added or subtracted respectively, and the model will be recalculated and redrawn. The user may set the increment at will. A similar process applies to the body depth and width. The depth is the distance from the surface to the shallowest body corner. The width is the maximum horizontal separation between two body corners. When the width is changed the body is expanded or contracted about a vertical line through its centre.

The code for the body properties dialog is given below as an example of the style used in the rest of the dialogs.

The components of the anomaly at a point outside the causative body in the magnetic case are given by (Rasmussen and Pedersen, 1979) :

$$\Delta B_z(x_0) = -2J \sum_i \frac{\Delta x_i}{(\Delta x_i^2 + \Delta z_i^2)} [(j_x \Delta x_i + j_z \Delta z_i) \log \frac{r_i (R_{i+1} + Y)}{r_{i+1} (R_i + Y)} + (j_x \Delta z_i - j_z \Delta x_i) (\tan^{-1} \frac{u_{i+1} Y}{w_i R_{i+1}} - \tan^{-1} \frac{u_i Y}{w_i R_i})] \quad (2.1)$$

$$\Delta B_x(x_0) = 2J \sum_i \frac{\Delta z_i}{(\Delta x_i^2 + \Delta z_i^2)} [(j_x \Delta x_i + j_z \Delta z_i) \log \frac{r_i (R_{i+1} + Y)}{r_{i+1} (R_i + Y)} + (j_x \Delta z_i - j_z \Delta x_i) (\tan^{-1} \frac{u_{i+1} Y}{w_i R_{i+1}} - \tan^{-1} \frac{u_i Y}{w_i R_i})] \quad (2.2)$$

$$\Delta B_y(x_0) = -2J j_y \sum_i (\tan^{-1} \frac{u_{i+1} Y}{w_i R_{i+1}} - \tan^{-1} \frac{u_i Y}{w_i R_i}) \quad (2.3)$$

where the profile is in the x plane, z is down, and y is orthogonal to both (see Figure 2.2). The corners of the body are located at (x_i, z_i) and are ordered in a clockwise manner. J is the magnetisation of the body. $R_i = \sqrt{(u_i^2 + w_i^2 + Y^2)}$, $r_{i+1} = \sqrt{(u_{i+1}^2 + w_{i+1}^2)}$, $w_i = -x_i \sin\phi_i + x_{i+1}\cos\phi_i$, $u_i = x_{i+1}\cos\phi_i + z_i \sin\phi_i$. The body has a strike length of Y on each side of the profile.The angle ϕ is shown in Figure 2.2. If the strike length of the body is made infinite then equation (2.3) will become zero.

For the gravity case the anomaly is given by (Rasmussen and Pedersen, 1979) :

Figure 2.13 : Data Filtering Options

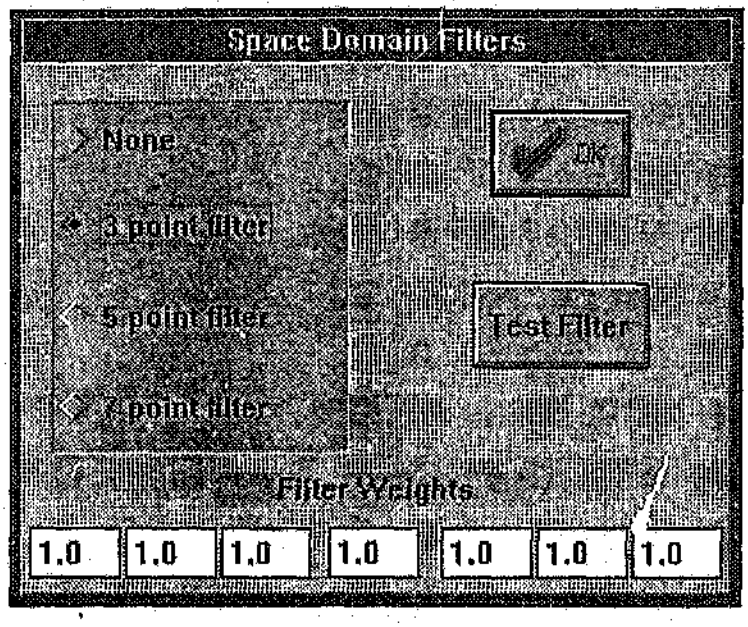

Figure 3.3 : Sample Borehole Temperature Perturbation Curves

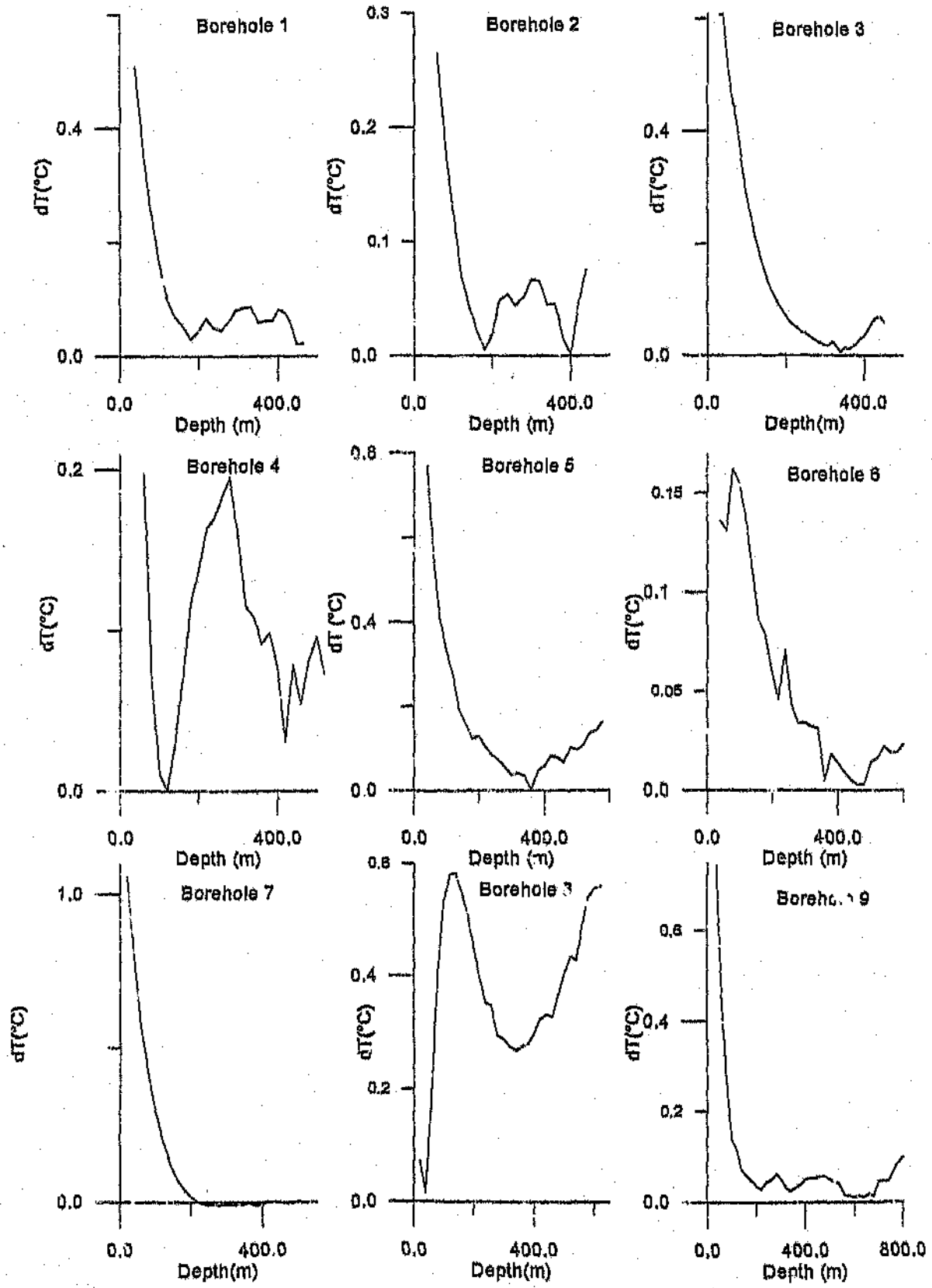

The temperature perturbation was estimated by removing the deep linear trend from the observational data.

(see equations 1.3 and 1.11 for an explanation of the terms in equation 3.6). The starting model used for all the boreholes considered consisted of zero surface temperature perturbations at all past times. Because the resolution attainable by the modelling decreases with increasing time of the temperature step from the present, larger time width steps were used further back in time (Beltrami and Mareschal, 1995). Ridge-regression was used rather than equation 1.3 because the solution of the heat equation backwards in time is unstable (Beltrami and Mareschal, 1995), and solutions with large, unphysical, ground surface temperature changes were not wanted.

Figure 3.3 shows the observed temperature perturbation from several boreholes, which was estimated by subtracting the deep linear increase in temperature from the actual observations. Most of the boreholes show a decrease in temperature with depth over the first few hundred metres, followed by an increase in temperature at greater depths. Boreholes 4 and 8 have been disturbed, and have noisy profiles. Such disturbances can be caused by changing groundwater flows which will alter the rock temperature, or by the removal or planting of trees in the area around the borehole, since this will affect the heat flux on the ground surface that is received from the Sun.

The data were initially inverted using the L_2 norm technique, and Figure 3.4 shows the misfit as a function of the inversion iteration for several typical boreholes. The inversion process was terminated when it produced no further decrease in the misfit.

surface temperature $T_0(t)$ is then given by (Carlslaw and Jaeger, 1959);

$$\Delta T(z) = \frac{z}{2\sqrt{(\pi\kappa)}} \int_0^{\infty} T_0(t)\ t^{-3/2} e^{\frac{-z^2}{4\kappa t}}\ dt \qquad (3.4)$$

The surface temperature history can be approximated by a series of N instantaneous changes of surface temperature T_j at past times t_j, in which case the temperature disturbance is given by ;

$$\Delta T(z) = \sum_{j=1}^{N} T_j\ erfc\left(\frac{z}{2\sqrt{(4\kappa t_j)}}\right) \qquad (3.5)$$

Forward calculation is therefore relatively simple if the surface temperature history is known.

3.4 Inversion

The surface temperature history is not generally known, and part of the value of inversion is the constraints that it can place on this parameter. A starting model is chosen which consists of a series of instantaneous surface temperature changes at different times in the past. An initial subsurface temperature distribution is calculated, then the inversion generates a new series of surface temperatures which progressively better match those that were actually measured down the borehole. For L_2 inversion the parameter change vector dP was calculated from :

$$dP = (A^TA + kI)^{-1}A^Te \qquad (3.6)$$

Measured temperature perturbations can be interpreted using forward modelling and inversion. The forward modelling involves a solution of the diffusion equation in one dimension for given surface temperature models, and the results can then be compared with observed borehole temperature data.

Inversion permits an independent estimation of the surface temperature history. It has been performed using both the L_2 and L_1 norm approaches. Modifications to both the L_2 and the L_1 methods can be made that significantly increase their effectiveness.

The borehole temperature data were collected using a thermistor probe three core cable Wheatstone bridge apparatus (see Richardson and Oxburgh, 1978), which was capable of measuring absolute temperatures to within 0.05°C, and temperature differences to within 0.005°C. The locations of the boreholes used are shown in Figure 3.2 .

3.3 The Forward Model

Assuming that the earth is homogenous and isotropic, and that heat generation is negligible, then the subsurface temperature distribution is a solution to the diffusion equation (since the curvature of the Earth can be neglected, the cartesian coordinate system is used):

$$\kappa \frac{\partial^2 \Delta T}{\partial z^2} = \frac{\partial \Delta T}{\partial t} \qquad (3.3)$$

where z is depth, t is time, T is temperature, and κ is the thermal diffusivity of the rock. The present temperature perturbation $\Delta T(z)$ for a semi-infinite solid with past

The temperature distribution in the Earth's crust is controlled by the heat flux from the interior, the thermal properties of crustal rocks, and a number of environmental factors including past surface temperature changes. Variations in the surface temperature propagate as temperature waves into the Earth, such that the amplitude of the perturbations decreases with depth, and that the higher frequency oscillations are attenuated more rapidly. The depth at which a temperature wave's amplitude decreases to 1/e of that at the surface (the 'skin depth') varies with the rock's thermal properties, but is typically about 0.2m for diurnal variations, 3m for annual variations, and 70m for oscillations with a period of 500 years. Values of the relevant physical properties of some South African rocks and skin depths for a 500 year surface temperature oscillation are shown in Table 3.1 to illustrate the range of parameters encountered. Climatically induced perturbations are superimposed on the normal increase of temperature with depth. Observations made down boreholes can therefore be used to model past surface temperature changes (e.g. Pollack 1993, Lewis and Wang 1992).

Table 3.1 : Rock Properties (M.Q.W. Jones, unpublished data, 1996)

Rock Type	Density $Kg.m^{-3}$	Specific heat capacity $J.kg^{-1}K^{-1}$	Thermal Conductivity $W.m^{-1}K^{-1}$	Thermal Diffusivity $10^{-6}m^2s^{-1}$	Skin depth m
Karoo Basalt	2740	930	1.85	0.73	61
Bushveld Complex Norite	2830	900	2.24	0.88	66
Bushveld Complex Pyroxenite	3220	910	3.59	1.23	79
Witwatersrand Quartzite	2710	850	6.09	2.64	113

temperature data upon the number of iterations required by the inversion. It also considers various ways to ensure that the data are fitted by the model with the minimum size while increasing the number of iterations required by the inversion as little as possible (See Cooper and Jones, 1997).

The data interpretation performed using the software based on the methodology described here indicated an increase of 1-2°C over the last two hundred years of the ground surface temperature in Southern Africa. The details are presented in Jones, Tyson, and Cooper, (1997) along with corroborating climatological evidence.

3.2 Borehole Temperature Data

Measurement of the temperature distribution in the top few kilometres of the Earth's interior has largely been aimed at determining the heat flux from within the Earth for studies of geodynamic processes which measurements have a number of practical applications including estimation of virgin rock temperatures and heat loads on deep mining and tunnelling operations (for example Sheer et al., 1984), heat transfer studies associated with radioactive waste disposal (Craig, 1989), modelling of thermal maturation processes in hydrocarbon deposits (Royden et al., 1980 ; Pollack and Cercone, 1994), and understanding the regional distribution of diamondiferous kimberlites and their genesis (Jones, 1988 ; Thompson et al., 1995). A relatively new application of geothermal research is the study of global climatic change.

Figure 3.1 : Robust Fitting of a Straight Line

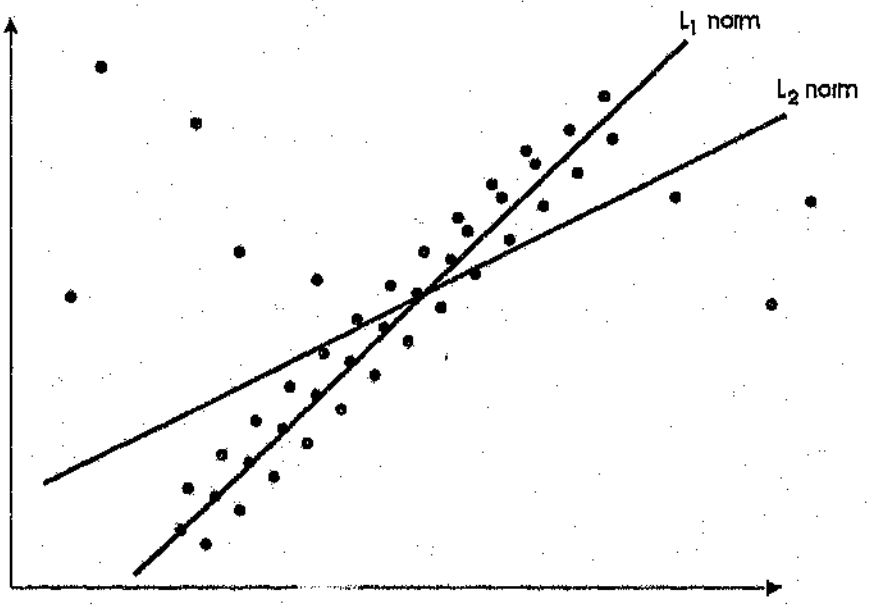

Figure 3.2 : Location of Boreholes Whose Data are Shown in Figure 3.3

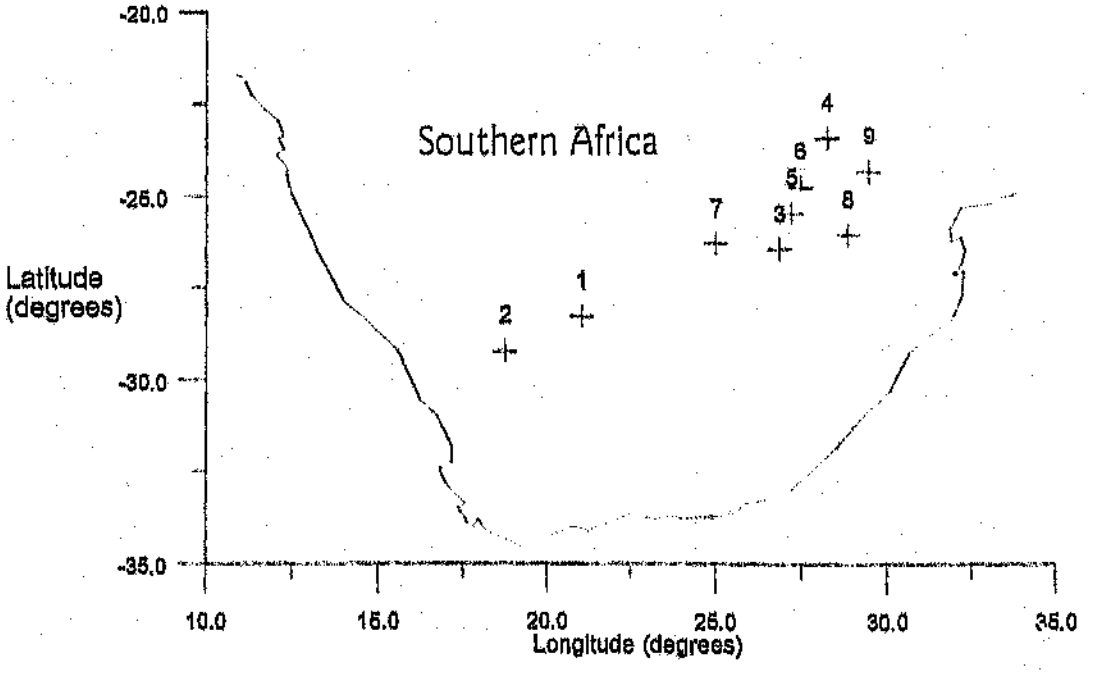

CHAPTER 3 : NON LEAST-SQUARES INVERSION

3.1 Introduction

The Gauss-Newton inversion discussed in chapter 1 was designed to minimise the sum of the squares of the residuals between the observed data and the model response. This is the L_2 norm case. The general case is given by (Menke 1989, p.37) ;

$$L_n \text{ norm} \qquad ||\, e_n \,|| \qquad = \qquad \left[\sum |e_i|^n\right]^{1/n} \tag{3.1}$$

where e_i is the misfit between the model response and the data at the ith datapoint. Use of the L_2 norm is appropriate if the data obey Gaussian statistics, while the L_1 norm should be used if the misfit follows the exponential distribution (Menke 1989, p.133). This is given by :

$$P(d) = \frac{1}{\sqrt{2}\sigma} e^{\frac{-|d - \langle d \rangle|}{\sigma}} \tag{3.2}$$

Where the data d has mean $\langle d \rangle$ and variance σ^2. Since the L_1 norm weights the data according to the absolute value of the distance from the mean, it is less sensitive (more robust) to outliers than the L_2 norm, which would weight them according to the square of that distance. Figure 3.1 shows the difference between an L_2 fit of a straight line to data and a robust fit (Press et al 1992, p.695). The robust fit is less affected by the outlying data points and gives a more reasonable looking fit (in this case).

This chapter studies the effect of varying the norm of the inversion of borehole

2.6 Conclusions

The modelling and inversion of magnetic and gravity data can be performed in the Microsoft Windows environment with relative ease using the programs Mag2dc and Grav2dc. The use of object-oriented technology greatly facilitated the writing of the programs, on which the work in chapters 4, 5, and 6 was based.

useful in the detection of subtle features in smooth data.

2.5.3.4 Changing the Way that the Model is Displayed

The bodies in the model can be labelled with their numbers or susceptibilities/densities. The bodies can be colour coded using their susceptibilities or densities using either a grey or a colour scale. Dark shades of grey are assigned to low values and light shades to (relatively) high values. The colour scale uses cold colours (blue tones) for low values, warm colours (red tones) for high values, and green tones for intermediate values. The bodies can also be displayed in plan view, which shows the different strike lengths of the bodies.

The calculated anomaly curves may be shown as individual anomalies for each body, or as the total anomaly for all of the bodies. Alternatively, the difference between the total anomaly and the observed data can be plotted. The misfit between the observed and calculated data is calculated and displayed onscreen during the modelling.

A portion of the model can be zoomed in upon either by entering numerically the coordinates of the new horizontal and vertical display limits, or by drawing a 'rubber band' box with the cursor around the region of interest.

If borehole information exists, then this can be read in from an ASCII file and the borehole plotted on the model. Up to three boreholes may be read in to a model.

Figure 2.11 : Regional and Anomaly Fields

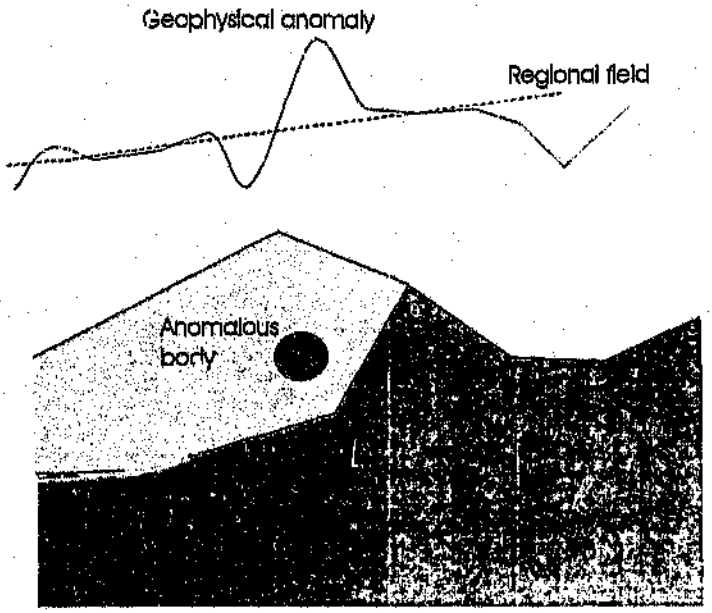

The solid line shows the geophysical response measured along the profile. The dotted line shows the (geophysicist-selected) regional field (after Blakely 1995, p.128).

Figure 2.12 : Regional Field Removal Using Mag2dc

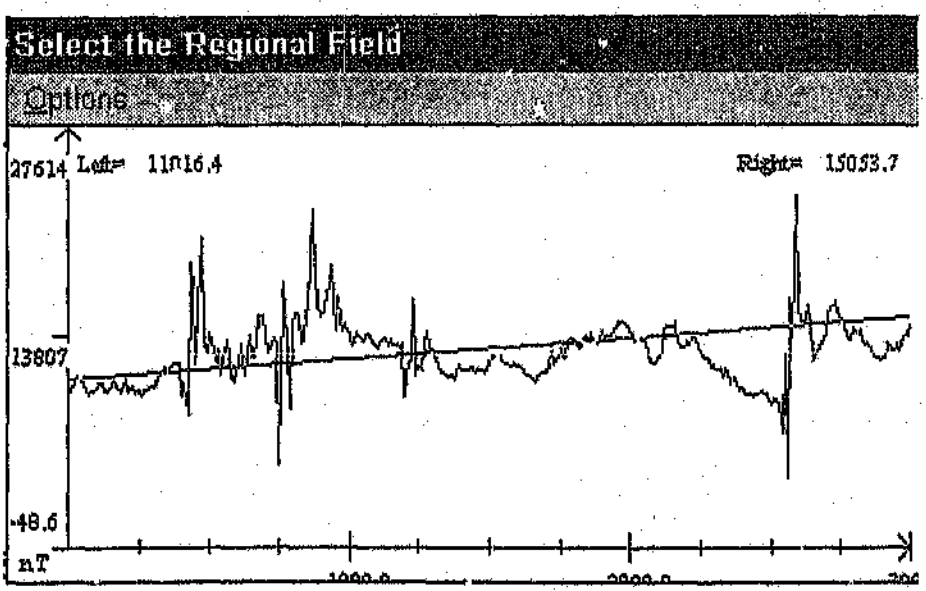

Figure 4.1 : Magnetic Model Used to Illustrate Convergence Properties

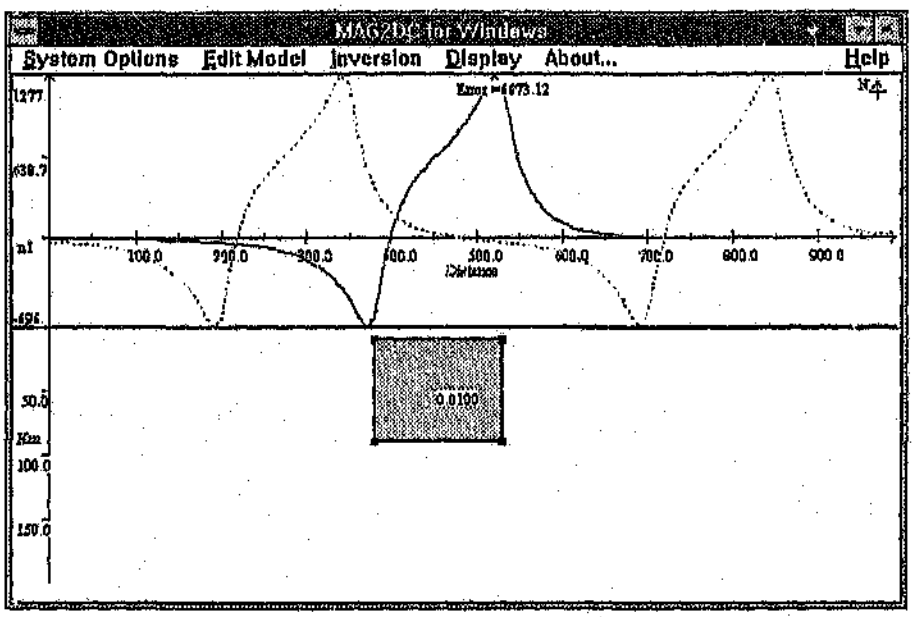

The model is 2.5 dimensional, and extends to 100km distance at 90 degrees to the profile, on each side. The model response is drawn with a solid line and the observed data are drawn with a dotted line. The susceptibility of the body is superimposed upon it.

Figure 4.2 : Misfit as a Function of Body Horizontal Position for the Model Shown in Figure 4.1

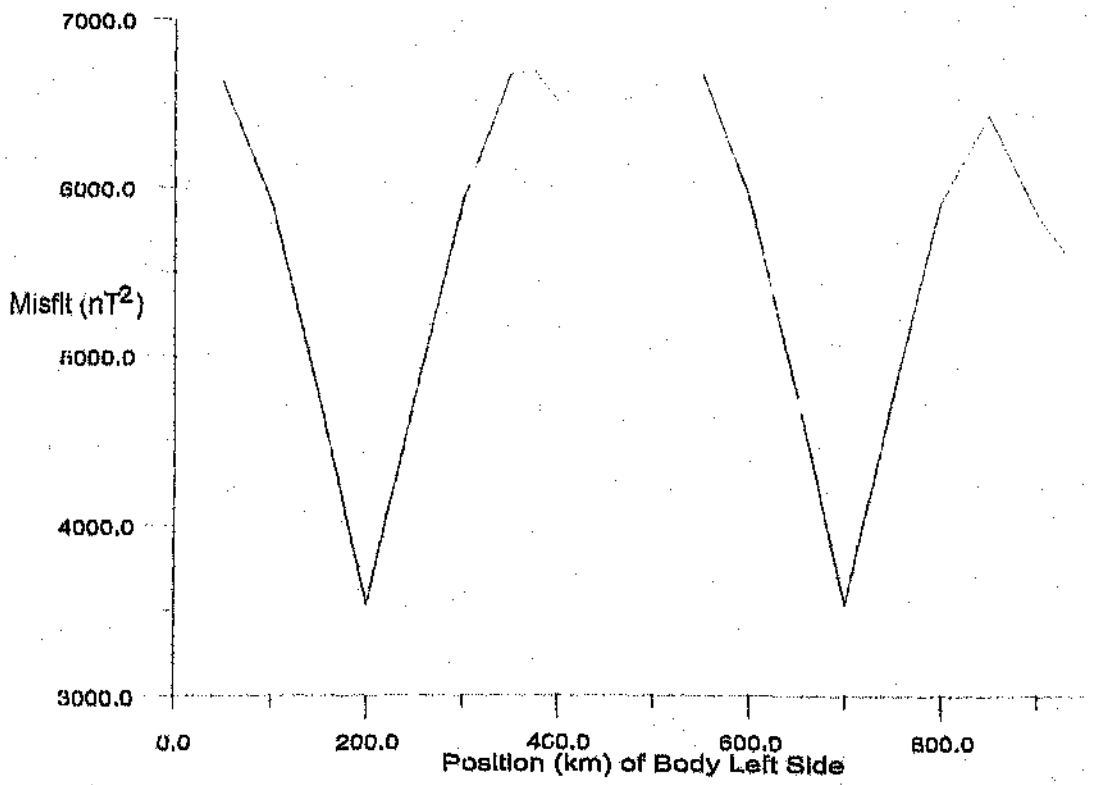

CHAPTER 4 : CONVERGENCE PROPERTIES OF INVERSION

4.1 Introduction

When the misfit surface for a model parameter has more than one minimum it is generally assumed that the Gauss-Newton inversion process will converge to the one that is nearest to the starting model. This hypothesis is studied for some one and two parameter magnetic models.

4.2 Convergence

4.2.1 Inversion of One Model Parameter

Consider the magnetic model shown in Figure 4.1. The body has the correct shape, susceptibility, and depth to fit either of the two anomalies on the profile (equation 2.3 gives the magnetic anomaly caused by the model). The misfit between the observed and calculated anomalies is plotted out as a function of the position of the body on the profile in Figure 4.2. As can be seen, there are two main minima corresponding to the positions of the two anomalies, a much shallower intermediate minimum between them, and a reduction in the misfit at the edges of the profile. Given a particular starting point on the profile, the model will converge to either one of the two main minima, or to neither. The latter possibility corresponds to moving the body to either end of the profile, which also reduces the misfit. The minimum in the middle of the profile proved too shallow to capture the body. Figure 4.3 shows a plot of the position that the inversion converges to as a function of the starting position on the profile. As expected, the inversion converges to the position of the nearest minimum (located at either 200km or 700km) as the misfit surface indicated.

model or the smallest misfit or both. However, in some cases when the starting guess for the model was too far from the solution the inversion was found to converge extremely slowly. This was because e was very large and Δe was very small. The final misfit and model size were satisfactory, but 10-20 times as many iterations were required to reach it.

Figure 3.8 shows a similar plot for the same borehole data, this time using L_1 inversion. In this case the results of L_2 inversion were mirrored in that method 1) gave the smallest misfit (though again, not by much) and the largest model. Method 3) again produced the smallest model, and no problems were encountered with slow improvement of the inversion misfit. For all methods except method 1 the model size produced by L_1 inversion was slightly larger than for L_2.

3.6 Conclusions

The inversion of borehole temperature data can be greatly improved by the use of techniques other than the standard least-squares approach. The choice of which norm to use depends on the statistics of the data. If the damping of the inversion is adjusted using the misfit between the observed data and the calculated curves, then improvements can be made in the resulting model size with minimal effect on the final fit reached. If this is not done then the model sizes became large and conflicted with data from other sources, such as average air temperature data (Tyson et al, 1997). The best results were obtained by combining the L_1 inversion with the improved damping method.

Figure 3.8 : L_1 Inversion for a Sample Borehole using Different Damping Schemes

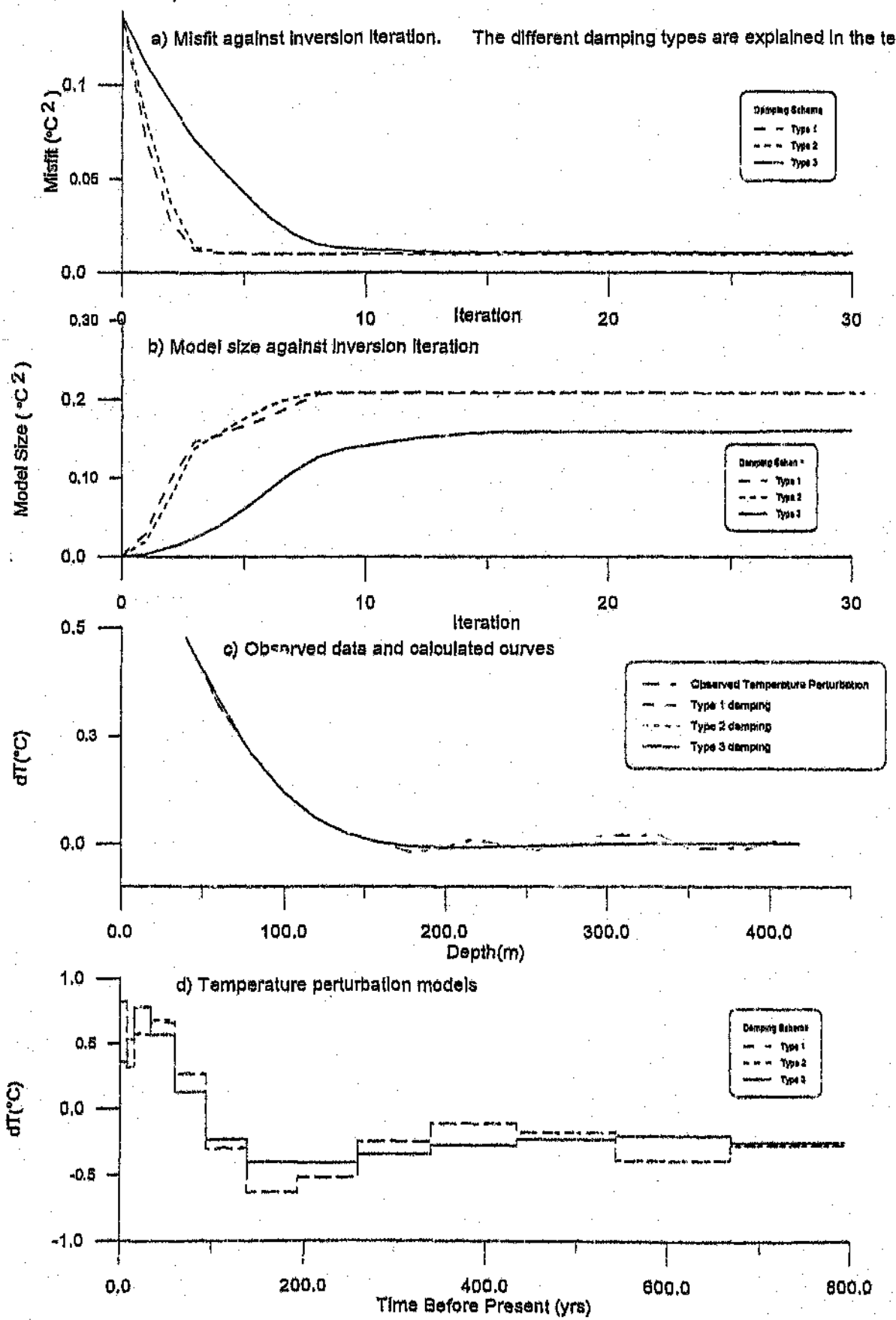

If k is relatively large (compared to the values in the matrix A^TA) then the misfit will decrease slowly with each iteration, whereas if k is relatively small then the misfit can be reduced more rapidly. Unfortunately, if A^TA is singular or near singular then a small value of k cannot prevent the inversion process from diverging and causing the misfit to get worse. A common procedure is to reduce k at each iteration that the misfit decreases, and to increase k if the misfit increases (Lines and Treitel, 1984).

The parameter k performs a second function. The larger the value of k, the more the inversion will try and minimise the size of the model (where the model size is given by P^TP, and P is the n point parameter matrix), at the expense of fitting the data (Menke, 1984, p.52). If k is zero then the inversion will produce the model with the smallest misfit, regardless of the model size (providing it converges).

There are of course an infinite number of possible methods for controlling the damping of the inverse process. For example, the damping can be based on the model size, or on the rate of change of the model with iteration (Constable, Parker, and Constable, 1987 ; Leslie, 1995). Here we focused on using the misfit as the basis for determining the damping. Three different methods of selecting k were examined : 1) k was increased by 50% if the misfit became worse from one iteration to the next, and decreased by a similar amount if the misfit decreased, 2) k was calculated from $e^Te/e_0^Te_0$ (where e_0 is the matrix of the initial misfit values e_i), which results in the misfit being reduced gradually at first, then faster later as e decreases, and 3) k was calculaced from $\Delta e^T\Delta e$, where Δe is the change in the misfit from one iteration to the next. Since this will have a large value if the misfit either increases or decreases, equation 3.12 was used

Figure 3.7 : L_2 Inversion for a Sample Borehole for Different Damping Schemes

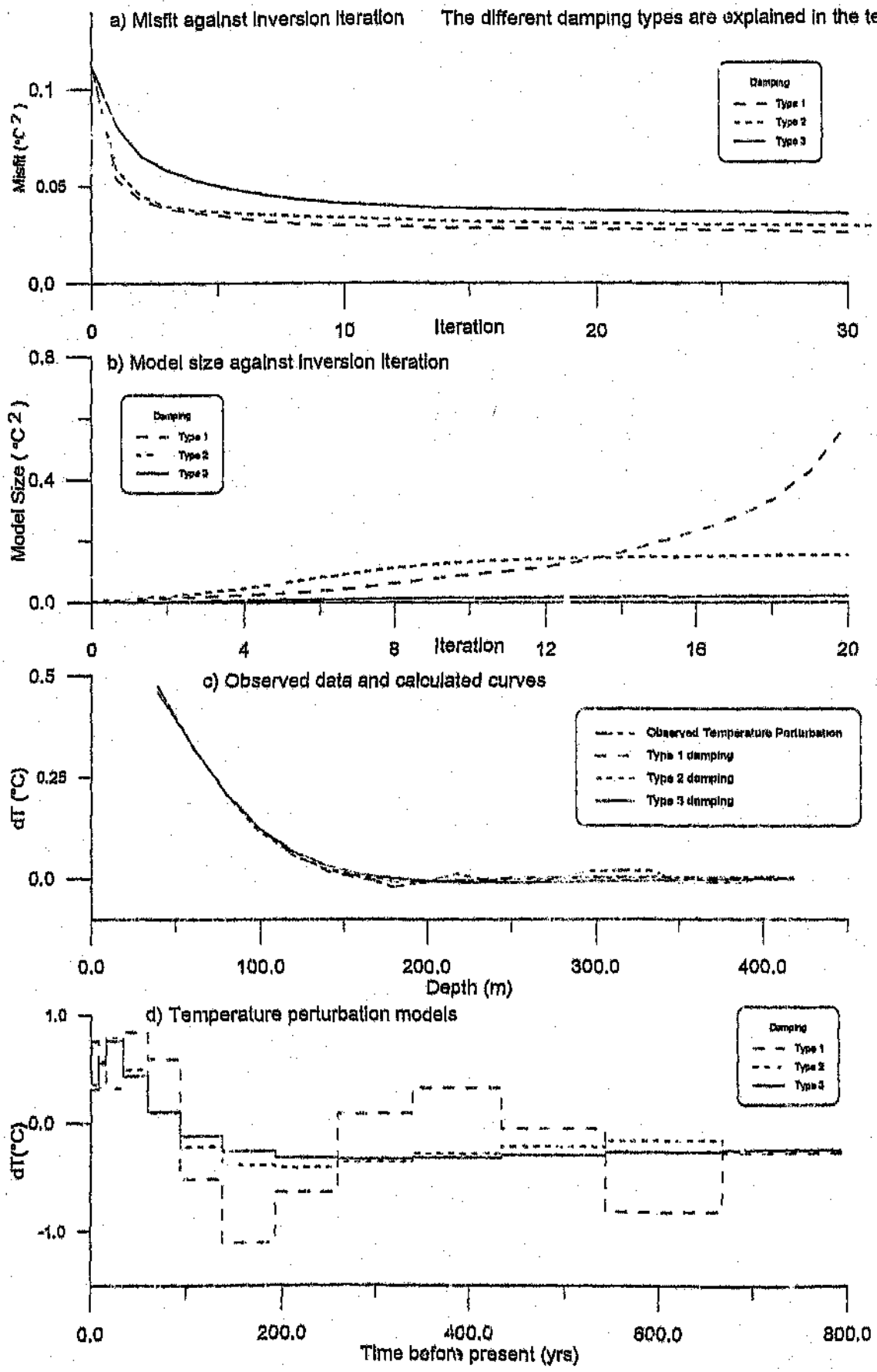

if k is relatively large (compared to the values in the matrix A^TA) then the misfit will decrease slowly with each iteration, whereas if k is relatively small then the misfit can be reduced more rapidly. Unfortunately, if A^TA is singular or near singular then a small value of k cannot prevent the inversion process from diverging and causing the misfit to get worse. A common procedure is to reduce k at each iteration that the misfit decreases, and to increase k if the misfit increases (Lines and Treitel, 1984).

The parameter k performs a second function. The larger the value of k, the more the inversion will try and minimise the size of the model (where the model size is given by P^TP, and P is the n point parameter matrix), at the expense of fitting the data (Menke, 1984, p.52). If k is zero then the inversion will produce the model with the smallest misfit, regardless of the model size (providing it converges).

There are of course an infinite number of possible methods for controlling the damping of the inverse process. For example, the damping can be based on the model size, or on the rate of change of the model with iteration (Constable, Parker, and Constable, 1987 ; Leslie, 1995). Here we focused on using the misfit as the basis for determining the damping. Three different methods of selecting k were examined : 1) k was increased by 50% if the misfit became worse from one iteration to the next, and decreased by a similar amount if the misfit decreased, 2) k was calculated from $e^Te/e_0^Te_0$ (where e_0 is the initial misfit), which results in the misfit being reduced gradually at first, then faster later as e decreases, and 3) k was calculated from $\Delta e^T\Delta e$, where Δe is the change in the misfit from one iteration to the next. Since this will have a large value if the misfit either increases or decreases, equation 3.12 was used

Figure 3.5 : Kurtosis

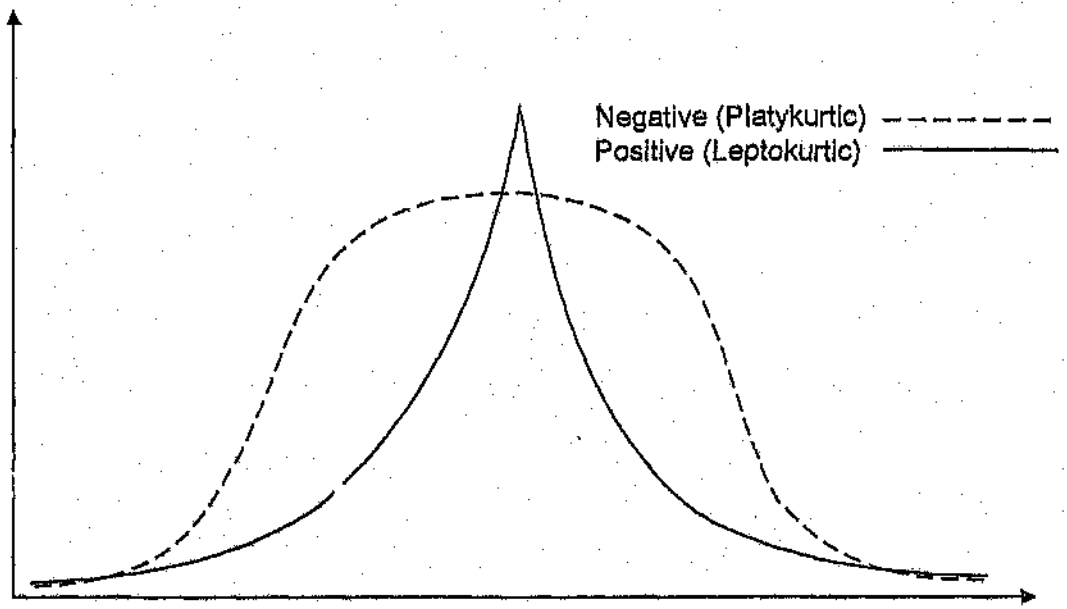

Distributions showing positive and negative Kurtosis (compared to a Normal distribution) are shown.

Figure 3.6 : Misfit and Kurtosis for L_1 and L_2 Inversion for a Sample Borehole

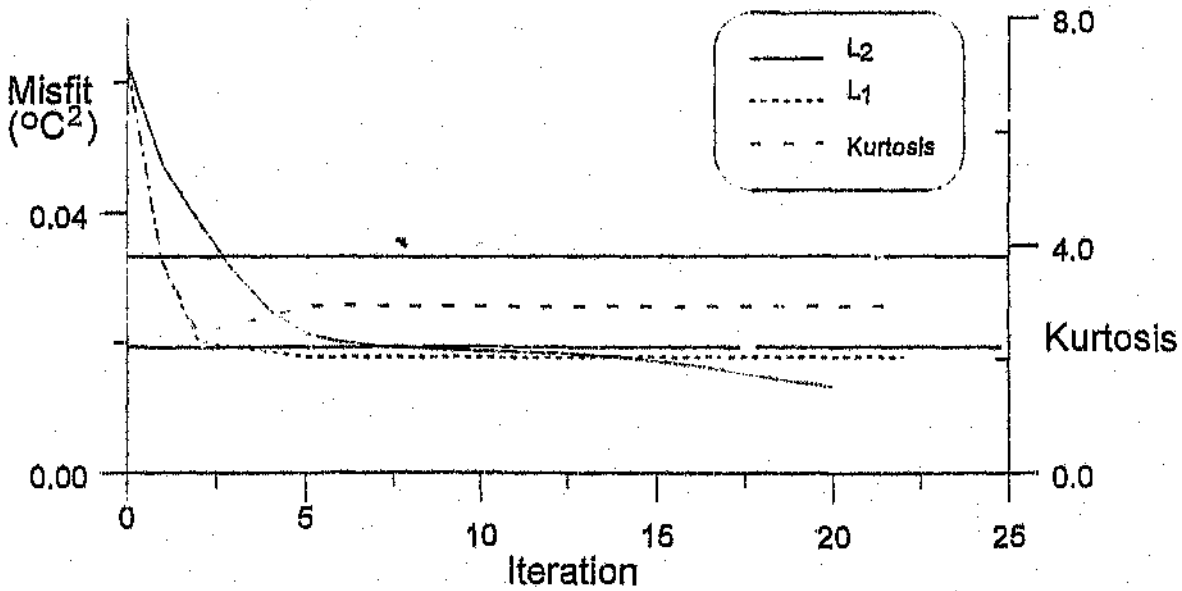

The two horizontal lines at values of the kurtosis of 2.2 and 3.8 show the suggested range of values within which L_2 inversion should be used.

where μ_2 is the second moment of the distribution, and is given by :

$$\mu_2 = \frac{1}{n-1} \sum_{i=1}^{n} (x_i - \langle x \rangle)^2 \qquad (3.10)$$

and μ_4 is the fourth order moment, given by :

$$\mu_4 = \frac{(n^2 - 2n - 3)}{(n-1)(n-2)(n-3)} \cdot \sum_{i=1}^{n} (x_i - \langle x \rangle)^4 - \frac{3(n-1)(2n-3)}{n(n-2)(n-3)} \mu_2^2 \qquad (3.11)$$

where $\langle r \rangle$ is the mean of the residuals $\langle r_i \rangle$ (Kijko, 1994). Harter (1972) proposed the following empirical relation : If *kur* > 3.8, use L_1 norm. If 2.2 < *kur* < 3.8 then use the L_2 norm, and if kur<2.2 then use the L_∞ (Chebyschev) norm. For the borehole temperature profiles analysed, these criteria proved accurate, with *kur* varying as the inversion proceeded, but generally exceeding 3.8 initially. When *kur* falls below 3.8 then the inversion can switch to L_2 norm to achieve the final minimisation of the misfit. Figure 3.6 shows the variation of the kurtosis with iteration for borehole 2 from Figure 3.4 . It can be seen that the kurtosis is above 3.8 until the third iteration and the L_1 inversion reduces the misfit more rapidly than the L_2 inversion up to this point. After the third iteration however the kurtosis remains in the range 2.2 - 3.8 and the L_2 inversion then produces the most improvement. The kurtosis should therefore be monitored during the inversion, and the norm of the inversion changed according to its value.

3.5 Damping

The parameter *k* in equation 3.7 controls the damping of the inversion process.

Figure 3.4 : Misfit vs Iteration for Some Sample Boreholes for L_1 and L_2 Inversion

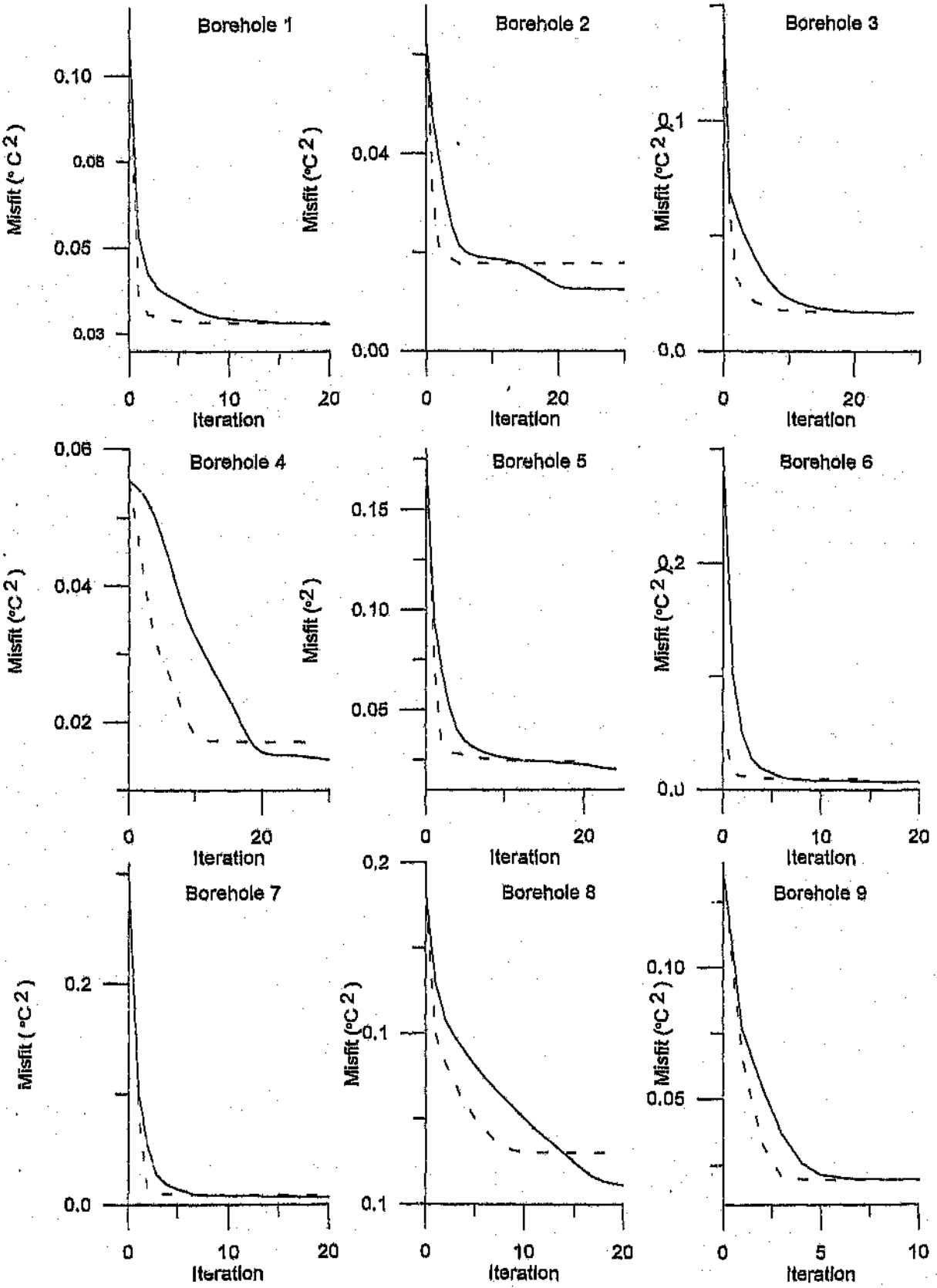

The misfit from L_2 inversion is plotted with a solid line, and the misfit from L_1 inversion is plotted with a dashed line.

Table 3.2 : Efficiency of L_2 Inversion compared to L_1 Inversion

Borehole	No. of iterations required with L_2	No. of iterations required with L_1	$N(L_1) / N(L_2)$
1	10	3	0.30
2*	16	8	0.50
3	20	12	0.60
4*	19	11	0.58
5*	11	6	0.55
6	10	4	0.40
7	7	3	0.43
8*	13	7	054
9	9	4	0.44

Boreholes marked by an asterisk * reached final misfits with L_2 inversion that were smaller than reached by L_1.

Why does the L_1 inversion perform more effectively than the L_2 ? It can be shown that the choice of the order n of the inversion L_n depends on the statistics of the residuals. When there are many outliers in the distribution L_1 is superior to the L_2 (Kijko, 1994). The choice of norm n to be used can be estimated from the kurtosis of the residuals. This in turn depends on the fourth order moment of the data distribution, and is a measure of the peakedness or flatness of the distribution compared to a Gaussian distribution, as shown in Figure 3.5 (Press et al., 1992 p.606). The kurtosis is given by ;

$$kur = \mu_4 / \mu^2_2 \qquad (3.9)$$

Equation 3.6 can be adapted to allow the data points to have different weightings, in which case (Menke, 1989 p.54) :

$$dP = (A^TWA + kI)^{-1} A^TW e \qquad (3.7)$$

where W is the n point diagonal weighting matrix. The weighting matrix can be used to place constraints upon the solutions produced by the inversion. If W_i is proportional to the absolute value of the differences between the observed and calculated curves at point i, then L_1 inversion is being used (Gersztenkorn et al, 1986) i.e.

$$W_i = | e_i |^{-1} \qquad (3.8)$$

This performed much better, with the misfit being minimised in about half the number of iterations compared with the L_2 method. This is illustrated in Figure 3.4 for several boreholes. The final misfit reached for the L_2 inversion was sometimes lower than that for L_1, in which case the inversion should start with L_1 then use L_2 later. Table 3.2 compares the number of iterations required for the L_1 inversion to reach its minimum misfit value, and the number of iterations taken by the L_2 inversion to reach the same value.

Figure 4.10a : The Newton-Raphson Method of Root Finding

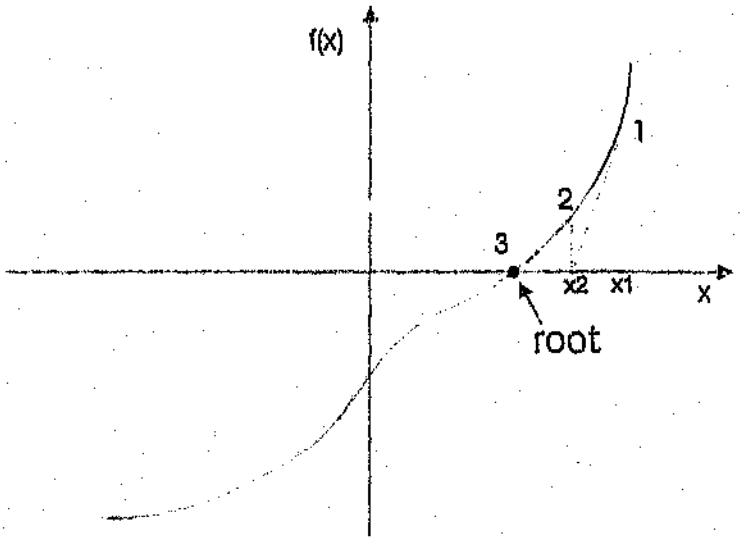

The initial guess for the value of the root is x1, which is improved by the Newton-Raphson method to a value x2. This in turn is improved further until the root is reached with the required accuracy.

Figure 4.10b : Using the Newton-Raphson Method to Find the Roots of $Z^3 - 1 = 0$

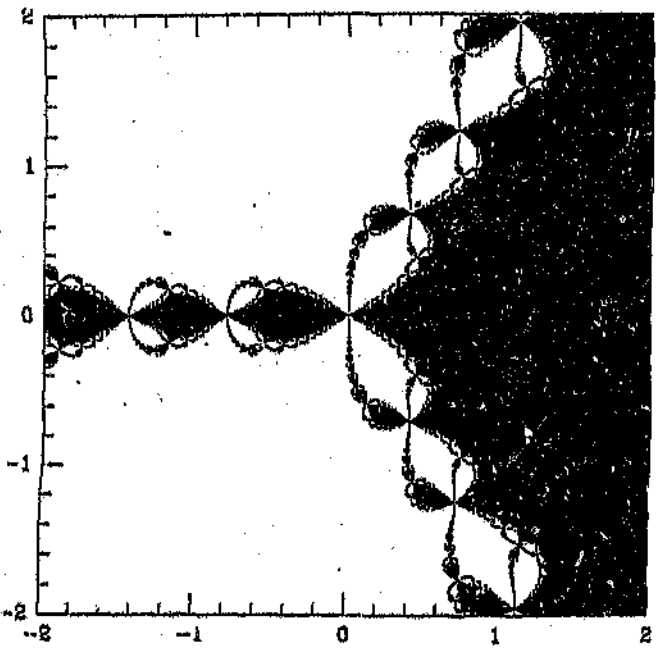

The region coloured black shows the values that converge to the root at z=1. The upper region shaded white shows the values that converge to the root at z=exp(2πi/3), and the lower region shaded white shows the values that converge to the root at z=exp(-2πi/3) (Press et al 1992, p.360)

the right, so it is forced deeper until the gradient of the misfit surface flattens out and then it is drawn into the minimum at a horizontal position of 700km.

The misfit at the two trajectory starting positions used differed by only 2%, and the local gradient of the misfit surface at those positions is shown on the lower right of figure 4.9 .

Note that model parameters can only possess fractal regions in parameter space that converge to a particular parameter value if the model response to those parameters is non-linear, since a linear parameter will converge to the optimum value in one iteration from any starting value.

The inversion process was repeated using both the Pascal real type and double precision type for arithmetic operations, to see if any of the behaviour of the trajectories was the result of numerical instabilities in the computations. Changing to double precision was found not to alter the results described above. As a further check, matrix inversions from sample points on a trajectory were performed both with the Turbo Pascal routines and with Matlab 5.1(MathWorks, 1997) and the same results were achieved.

The inversion process uses the local gradient to calculate and improve the value of the parameters, and is therefore similar to the Newton-Raphson method of finding roots of equations. Figure 4.10a shows the principle behind the Newton-Raphson method. It requires an initial guess for the value of the root, and assumes

Figure 4.9 : Behaviour of Inversion Trajectories

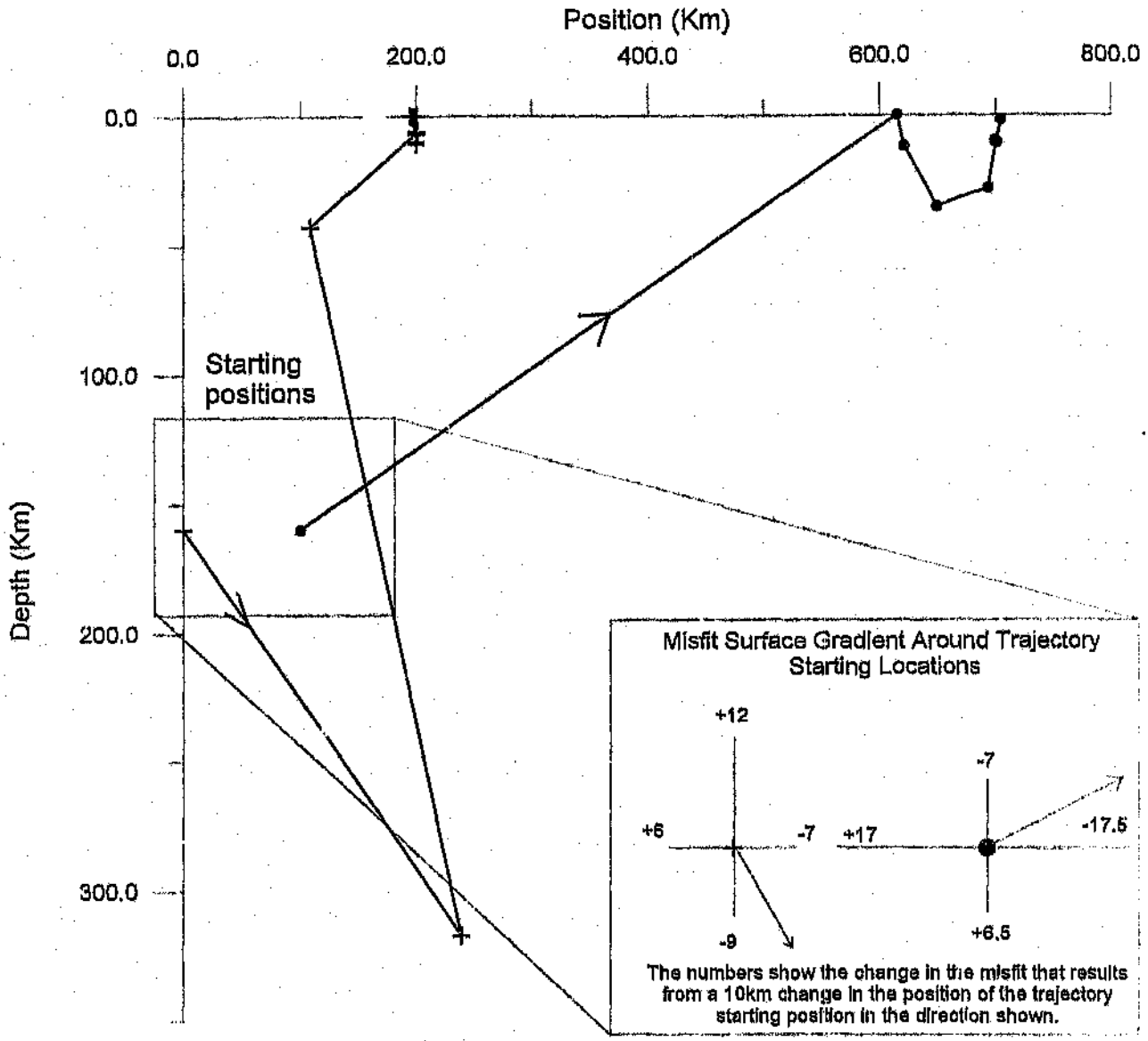

Figure 4.8 : Estimation of the Fractal Dimension of Basin of Convergence for the Model in Figure 4.1

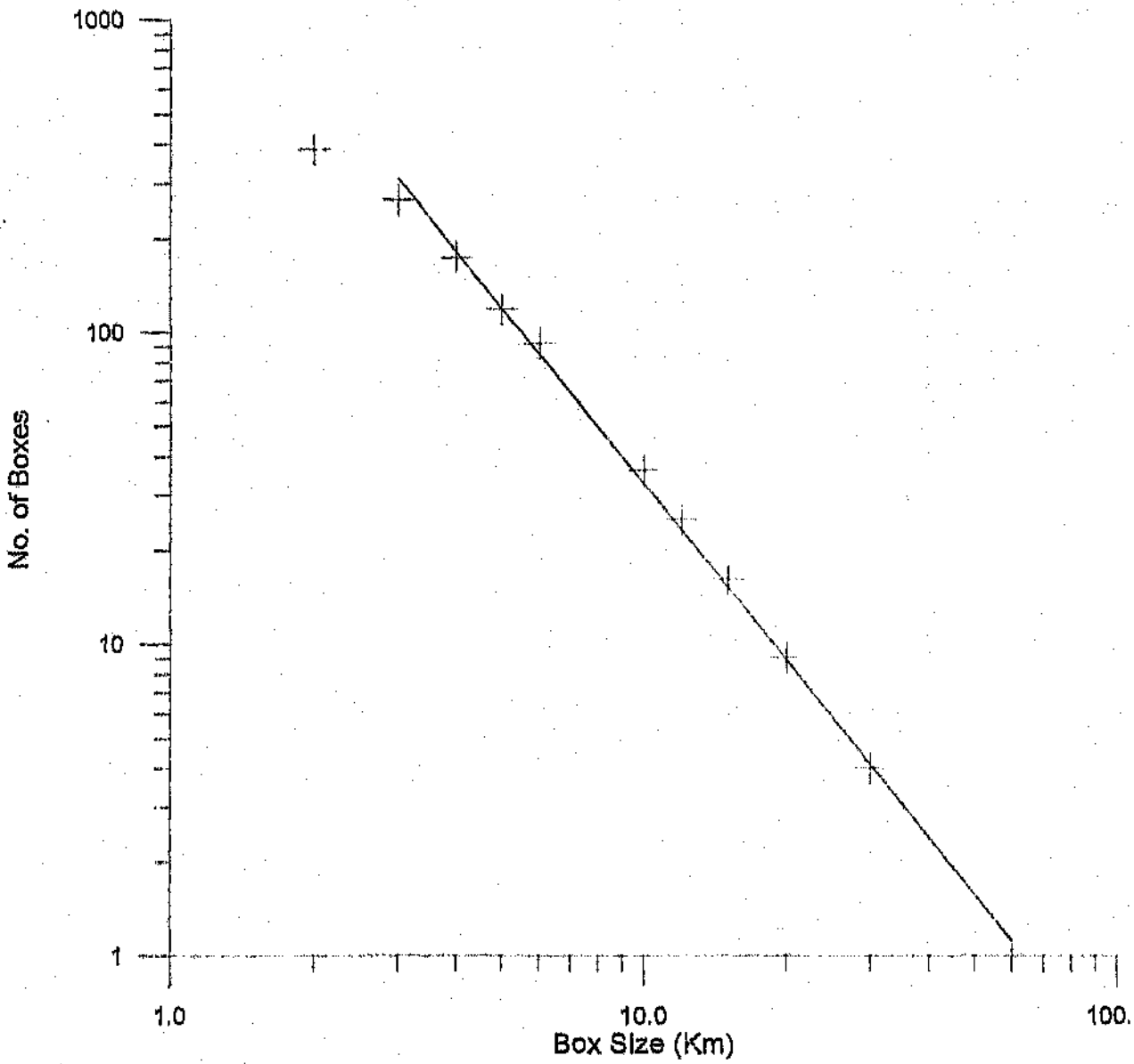

The fitted line indicates a fractal dimension of 1.8 +/- 0.1 for the basin of convergence.

fractal characteristics, namely self-similarity and complexity. The grid of starting points used was 15km apart. To calculate the fractal dimension, the box counting method described in 4.2.3 was used, which yielded a fractal dimension of 1.8 ± 0.1 for the magnetic model (see Figure 4.8).

Why does the fractal pattern exist ? The sensitivity of the inversion solution to the initial model parameters chosen occurs because neighbouring paths over the misfit surface are controlled at each iteration by the local gradient. Nearby points will have similar gradients, but over many iterations the differences between trajectories will acculmulate and the result will be convergence to a different solution. Figure 4.9 shows two inversion trajectories from nearby starting points that converge to different minima. The first trajectory (shown as a sequence of + symbols), which starts at a horizontal position of 0.0km, initially moves deeper and to the right. This is because the misfit increases if the body moves a small distance upward, and moving the body downward reduces the anomaly amplitude and hence also the misfit. The body is then almost vertically below the minimum at a horizontal position of 200km, to which it moves in the next few iterations. The second trajectory (shown as a sequence of dots), starts at the same depth as the first, but 100km further to the right. The body initially moves up and to the right to bring it closer to the minimum at 200km, but because the misfit surface is almost flat there (compared to positions closer to the minimum) the reduction in the misfit is relatively insensitive to the direction in which the body moves (compared to when the body is closer to the surface). The body overshoots the minimum at 200km and ends up at a horizontal position of 615km. At this position the misfit will increase if the body moves a small distance further to

Figure 4.7a : The Cantor Set

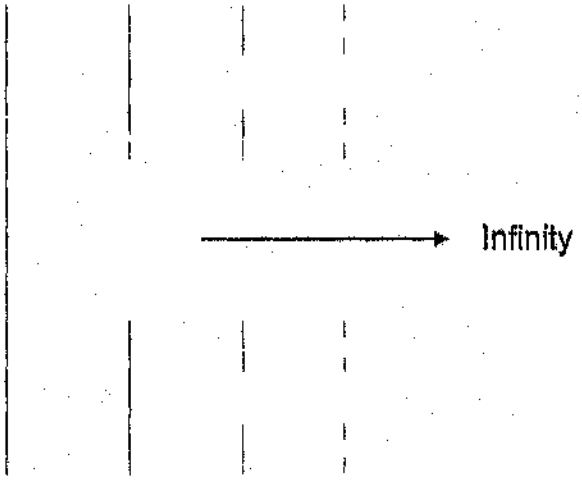

Stage	0	1	2	3
No. of segments	1	2	4	8

Figure 4.7b : The Mandelbrot Set

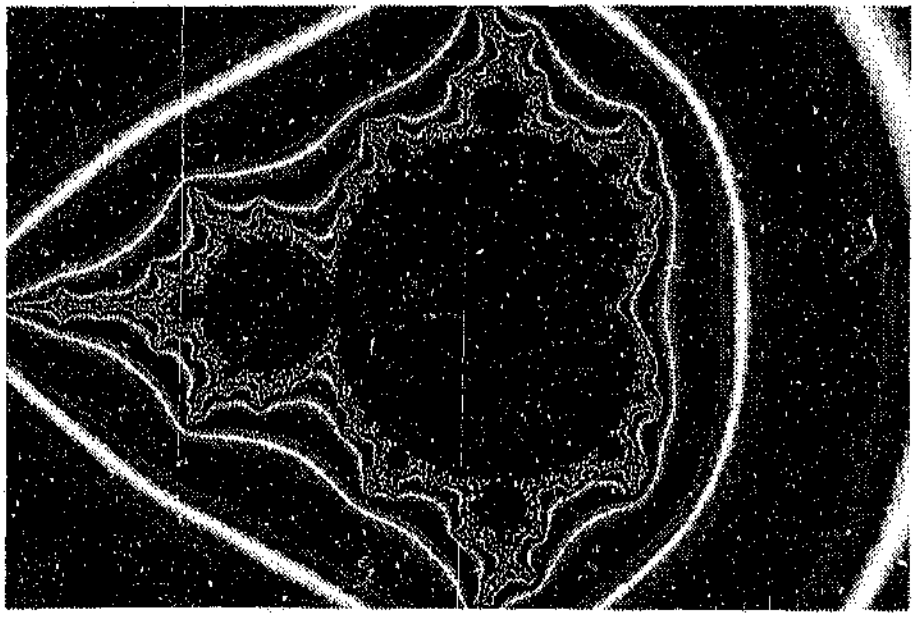

when measured in this way (Kaye, 1989 p.39). This is known as the 'box-counting' dimension. Many other aspects of nature have fractal attributes, such as some ferns and trees (Barnsley, 1986), gold colloid aggregates (Weisz and Oliveira, 1984), lunar dust particles (Kaye and Clark, 1985). Turcotte (1997) describes a wide range of geological and geophysical phenoma that have fractal characteristics.

Fractals can be constructed mathematically, such as the Cantor set, which is generated by iterati 'y removing the middle third from a line segment (see Figure 4.7a). The initial line segment is one unit long, and after one iteration the two remaining segments are 1/3 unit in length. The fractal dimension of the remainder after an infinite number of such iterations have been performed is (log 2)/(log 3) = 0.6309... (Hilborn, 1994, p.397). Another such entity is the Mandelbrot set, which is constructed by iterating the function (Hilborn, 1994, p.406) :

$$z_{n+1} = z^2_n + c \qquad (4.2)$$

Where z and c are complex numbers and $z_0 = (0.0,0.0)$. If repeated iterations of this function yield a value that increases towards infinity, then the value of c lies outside the Mandelbrot set, otherwise the point is inside the set. This simple equation produces an incredibly complex structure, as shown in Figure 4.7b . The Mandelbrot set is self-similar - enlargements of small portions look much like the whole set.

4.2.4 Fractals and Inversion

The set of positions from which the model converges to a given minimum - the *basin of attraction* (Hilborn, 1994 p.22) for that minimum - appears to have

Figure 4.6a : A Portion of Figure 4.5 Shown in More Detail

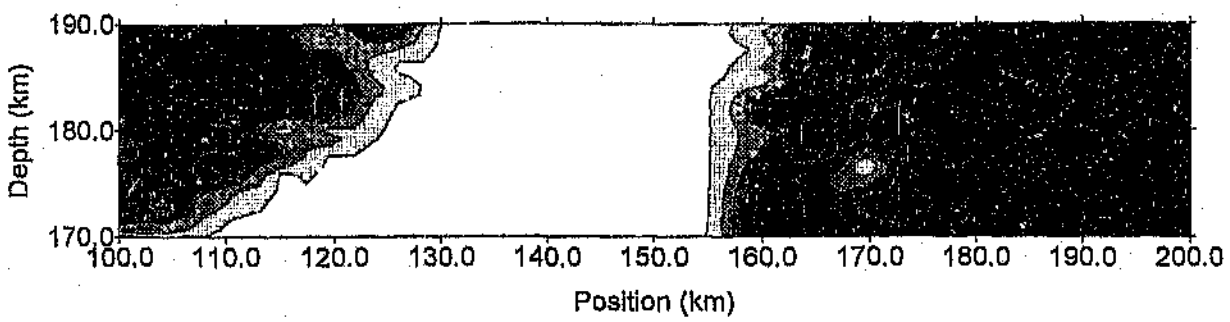

Black indicates that the body converged to the minimum at a position of 200Km, and white indicates that it converged to the minimum at a position of 700Km. Intermediate shades are interpolated between the two.

Figure 4.6b : A Portion of Figure 4.6a Shown in More Detail

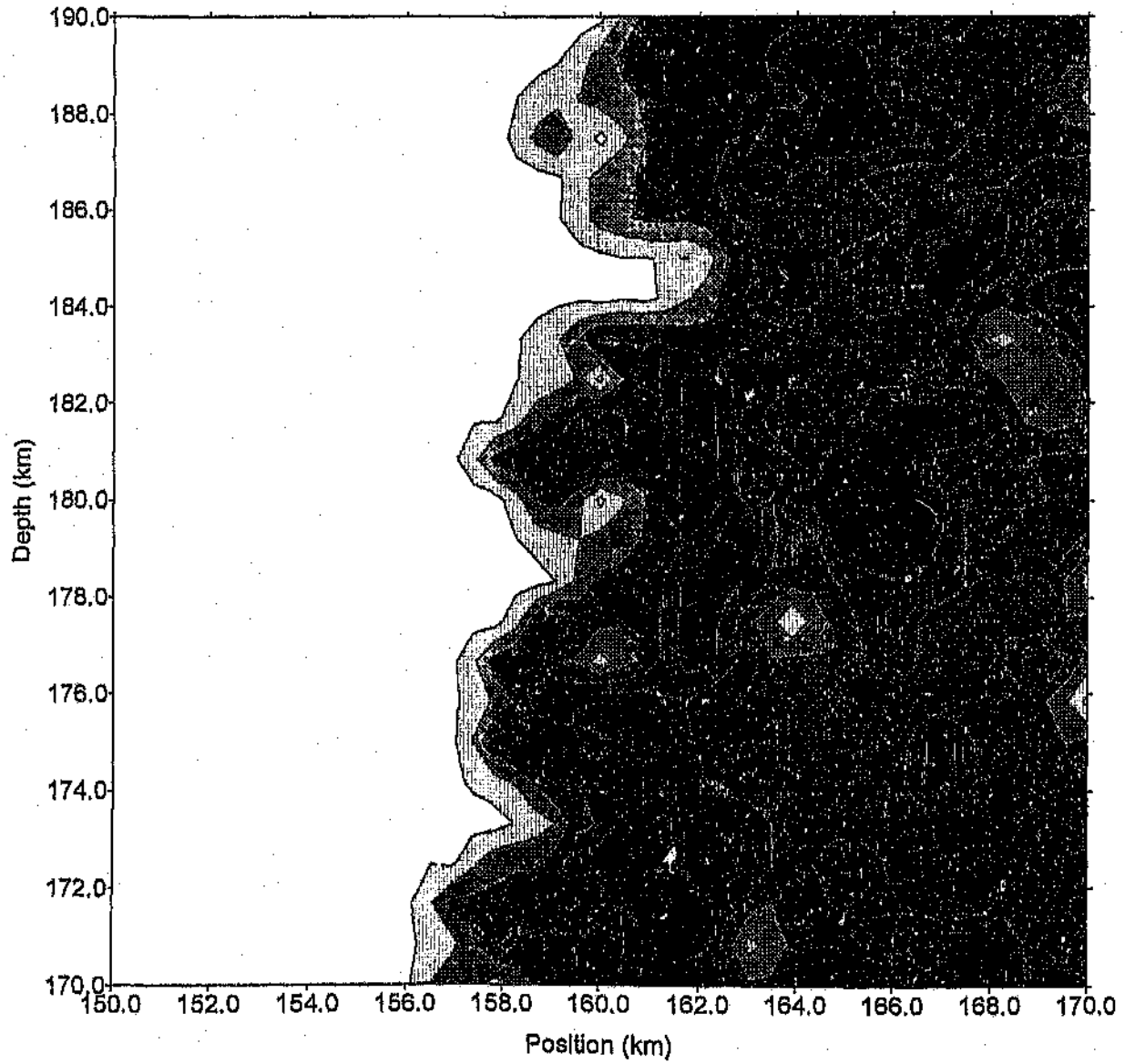

Figure 4.4 : Misfit as a function of Body Position for the Model in Figure 4.1

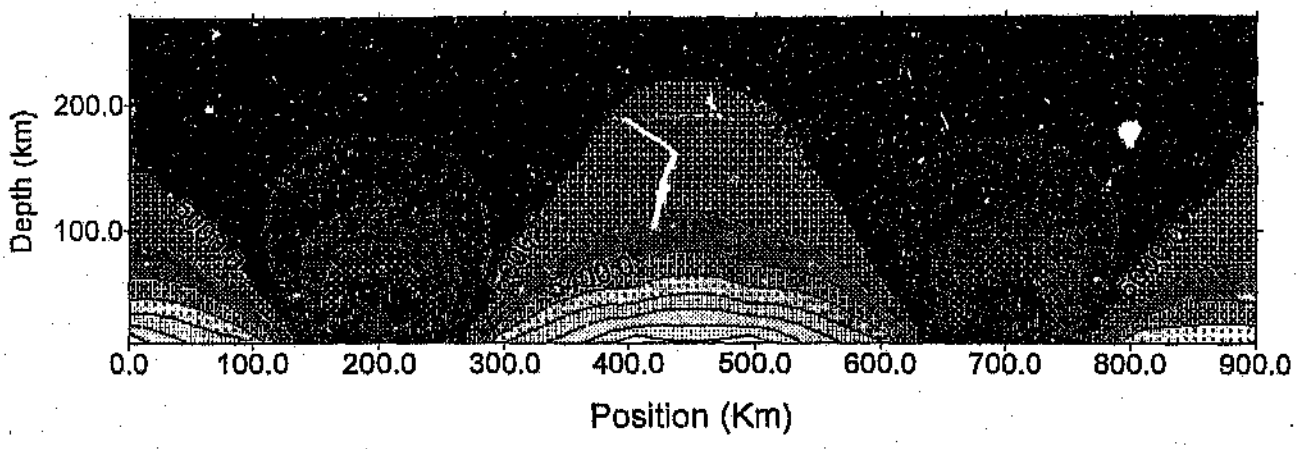

Figure 4.5 : Result of Inverting the Model in Figure 4.1 from a Grid of Different Starting Positions

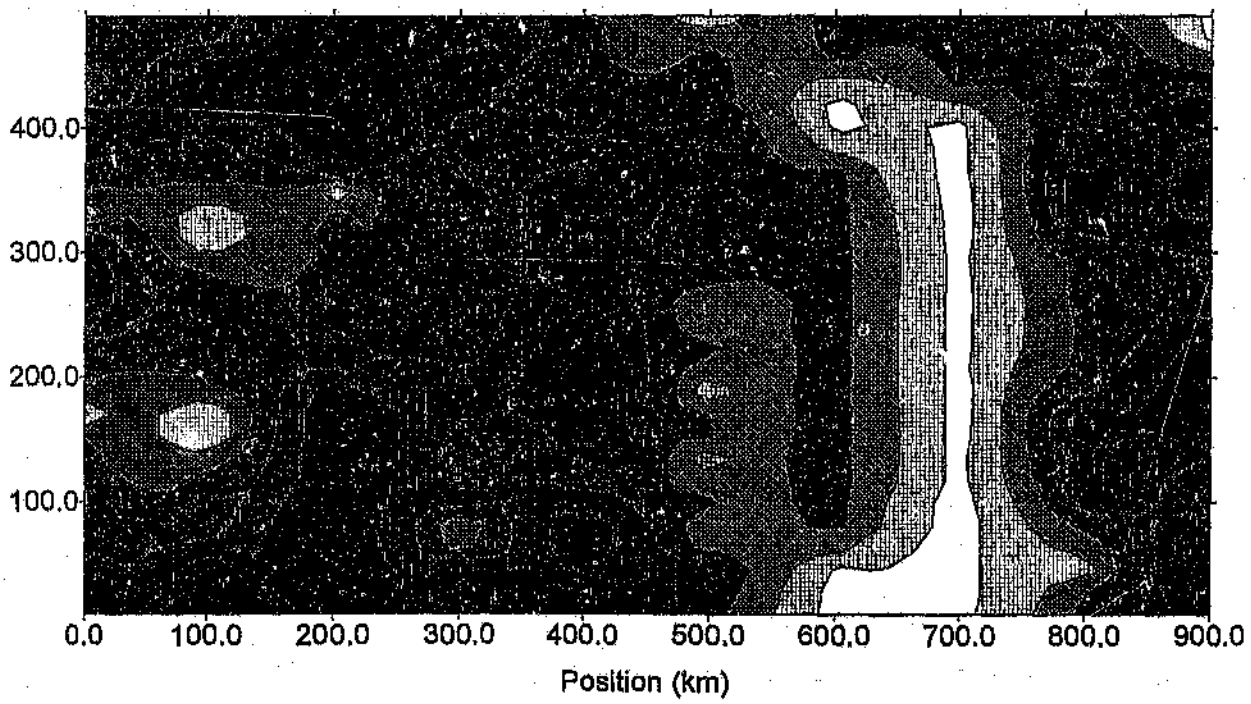

Black indicates that the body converged to the minima at a position of 200Km, and white indicates that it converged to the minima at a position of 700Km. Intermediate shades are interpolated between the two.

Hence the body encounters different conditions at each end of the profile.

4.2.3 Fractals

The set of initial models that converge upon a particular minimum shown in Figures 4.5 and 4.6 suggests a *fractal* i.e. an an entity which is a subset of $\Re^N$ who's Hausdorff-Besicovitch dimension exceeds its topological dimension (Mandelbrot, 1982 p.31). Fractals are mathematical models for very irregular, very detailed sets (Stoyan and Stoyan, 1994 p.3). They are characterised by self-similarity over a range of length scales. The coastline of the U.K. is an example. It's length depends upon how it is measured. If a NOAA (National Oceanic and Atmospheric Administration) satellite image (Richards, 1993 p.8) of resolution 1.1 km is used to map the country, and all the pixels that make up the coastline are counted, then a certain length will be obtained. If however the same procedure is repeated using LandSat data of resolution 30m then a greater length will be obtained. This is because the higher resolution pixels of LandSat will map the twists and turns of bays and coves that are missed by the larger NOAA pixels. If data of higher resolution were available then a greater length again would be measured. If the number of pixels required to cover the coastline was N_i when a pixel size of r_i was used, then (see Turcotte 1997, p.16)

$$N_i = C / r_i^D \qquad (4.1)$$

Where D is termed the fractal dimension, and C is a constant of proportionality. A plot of log N against log r should be a straight line (for a range of values of r) of gradient -D. The coastline of the UK has a fractal dimension of 1.25

Figure 4.3 : Convergence as a Function of Body Initial Horizontal Position for the Model Shown in Figure 4.1

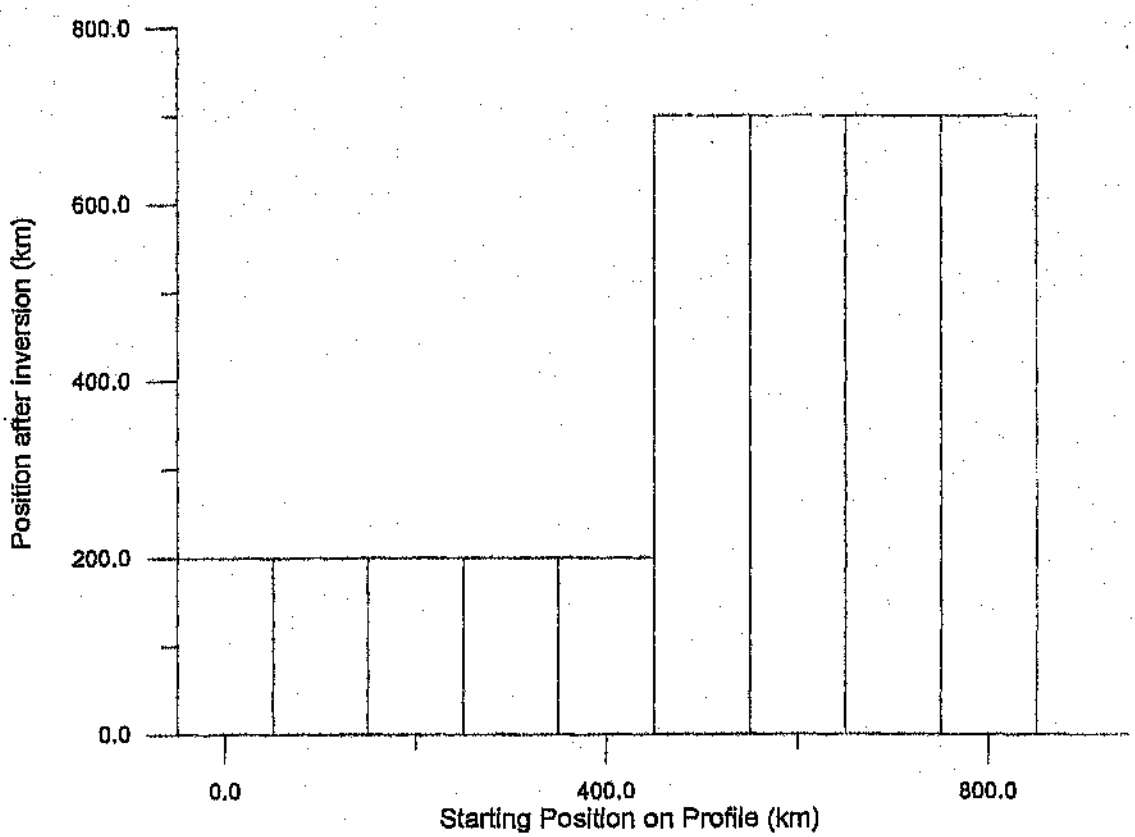

A value of 200 means that the body converged upon the minimum at a position of 200Km, and a value of 700 means that the body converged upon the minimum at a position of 700Km.

4.2.2 Inversion of Two Model Parameters

If the depth of the body in the model shown in Figure 4.1 is inverted as well as its horizontal position, then the misfit surface becomes a contour map, which is shown in Figure 4.4 . A dark tone indicates a small misfit and a lighter tone indicates a larger misfit. As can be seen, there are minima around the locations of the two anomalies.

The initial guess of the model parameters i.e. the body starting loca[illegible] now varied across a grid of positions and depths, then the model inverted and the resultant body position recorded. The possibilities were a) that it would converge to the anomaly at a position of 200km, b) it would converge to the anomaly at a position of 700km, or c) it would converge to neither. If case a) occurred then the result was given a value of 0. If case b) occurred then a value of 100 was assigned. If case c) ocurred then a value of 50 was assigned. The values are arbitrary, but enable the results of the inversion to be clearly seen. The values were contoured and displayed in Figure 4.5 .

As expected, the body converged to the closest anomaly in general, but the pattern is complex and certainly not smooth. Zooming into portions of the subsurface shows more detail, as is shown in Figures 4.6a and 4.6b. The pattern is not completely symmetrical with respect to the locations of the two minima because of the conditions at the edges of the profile were not identical for the two anomalies shown i.e. the anomaly on the left has a negative value at the left side of the profile, while the anomaly on the right has a positive anomaly on the right side of the profile.

the behaviour of the system until Γ=2.5. At this point the body did not settle down to any single position, but alternated between two different positions repeatedly. As Γ was increased further the distance between the positions increased. Figure 5.4a shows a plot of the misfit as a function of iteration for Γ=4.0, and the iteration scheme for this situation is shown in Figure 5.4b. When Γ reached 4.42 the body began oscillating between four positions, and when Γ became 4.6 the body never returned to the same position again, but kept moving back and forth between different positions. Figure 5.5a shows a plot of the misfit against iteration when Γ=5.0, and Figure 5.5b shows the iteration scheme.

5.4.1 Bifurcations

The values of the misfit that the inversion converged upon were plotted against the parameter Γ in Figure 5.6a, and the body position was plotted in Figure 5.6b. When Γ was small only one point is shown on the graphs. This corresponds to the situation in Figure 5.1 wherein a satisfactory fit to the data was achieved. At Γ=2.48 there are now two points on the graph ; a period-doubling bifurcation has occurred (Marek and Schreiber, 1991 p.59, Tan et al. 1995). Because of the symmetry of the shape of the gravity anomaly in Figure 5.1 there are points on each side of the anomaly peak that have similar values (because the anomaly was calculated at discrete positions 1km apart, the gravity values are not identical). The horizontal positions that the body oscillates between are on opposite sides of the peak, hence the bifurcations are of greater magnitude when plotted as a function of body position rather than misfit. As Γ is increased, more and more points are plotted as the the body oscillates between more and more different positions, then finally becomes chaotic.

Figure 5.3a : Misfit against Inversion Iteration for the Model in Figure 5.1 (Γ = 1.0)

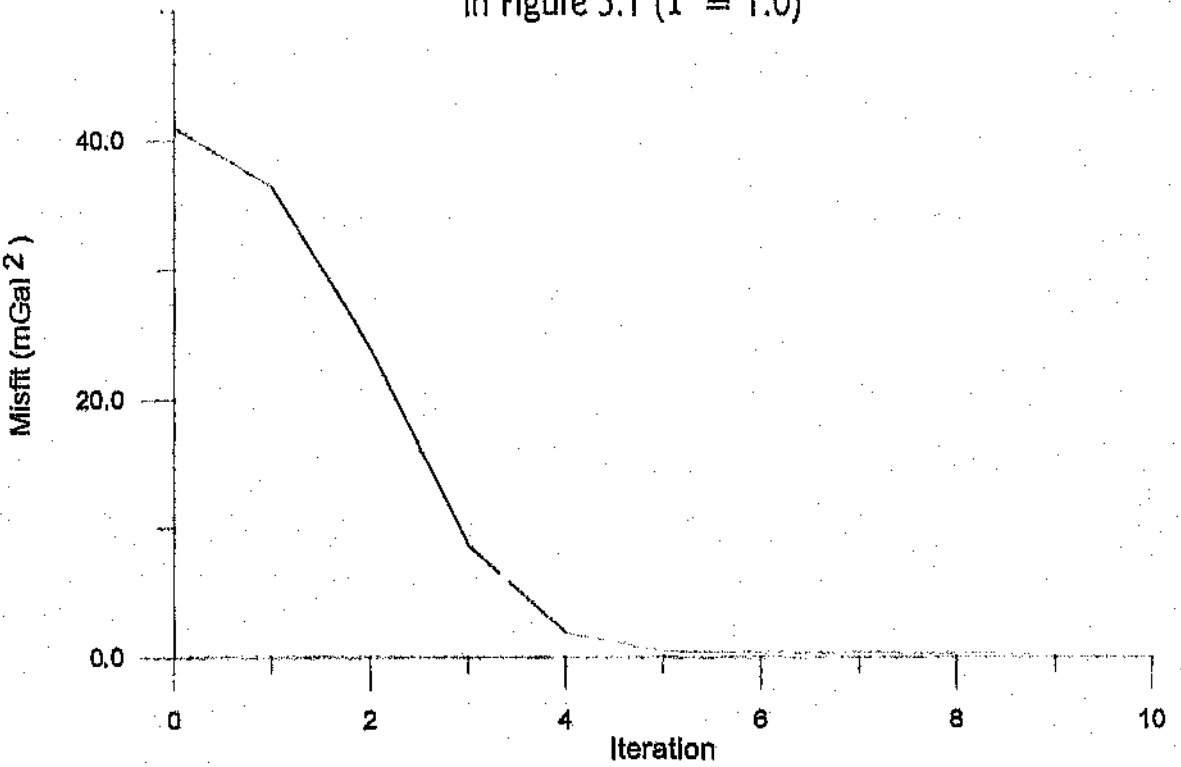

Figure 5.3b : Iteration Scheme for the Case when Γ= 1.0

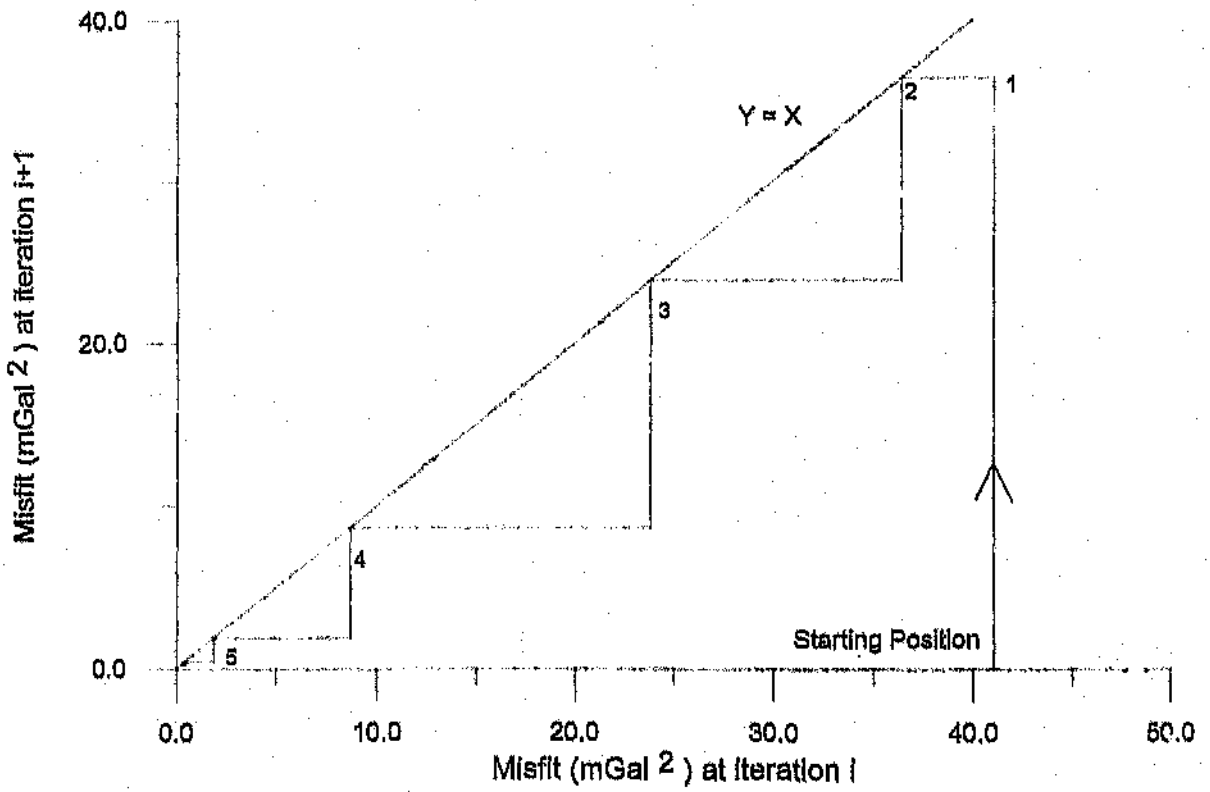

The numbers 1,2,3,4,5 on the plot refer to the inversion iteration.

Figure 5.2 : Misfit Surface for Inversion of the Model in Figure 5.1 with respect to Body Horizontal Position

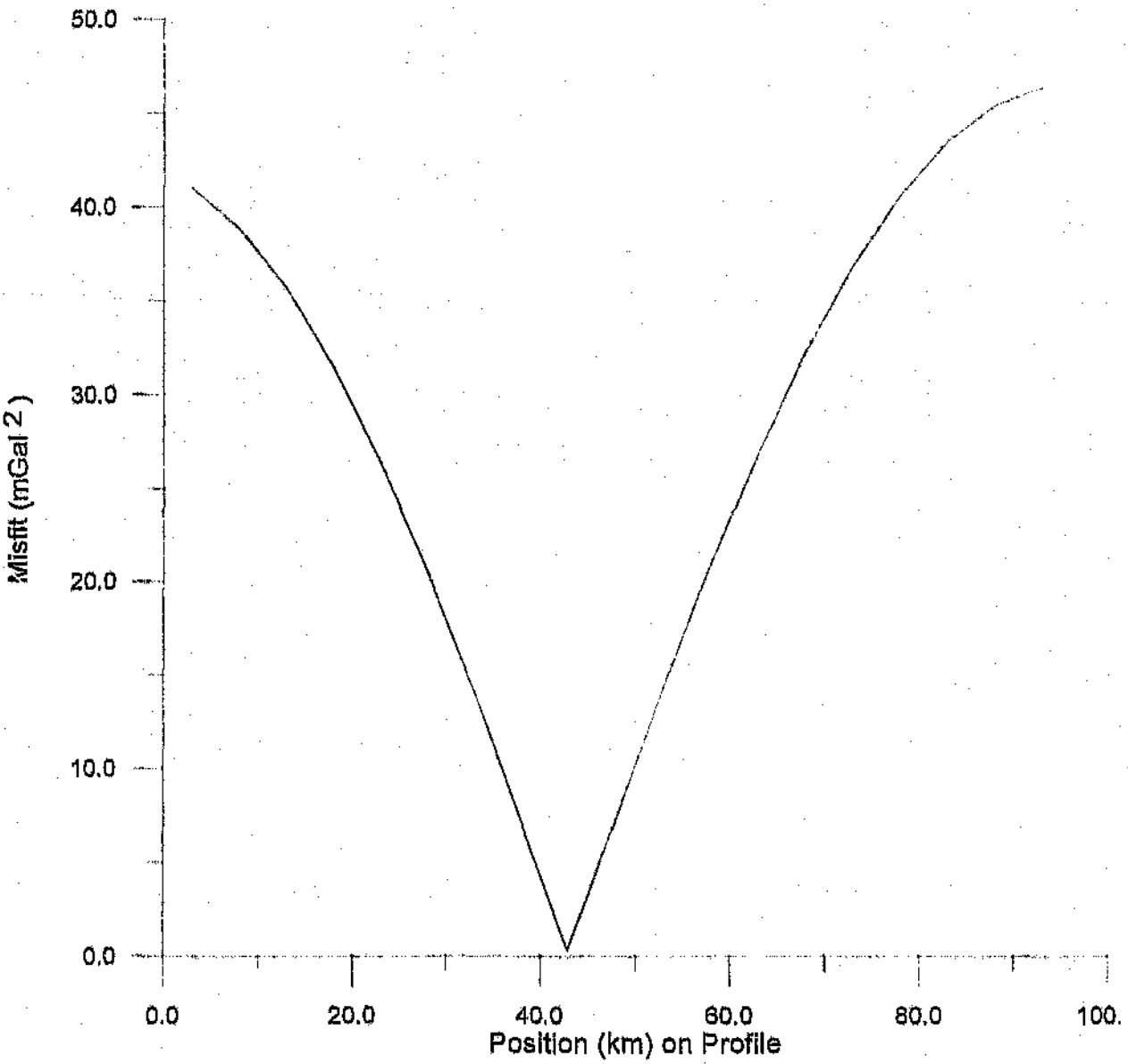

where all terms are as given in chapter 1, except C , which is an m point diagonal matrix given by ;

$$C = \Gamma I \tag{5.2}$$

where Γ is a scalar constant. The result of using the matrix C is to cause chaotic behaviour in the system (depending on the value of Γ), as is shown below.

5.4 Inversion of the Horizontal Position of the Body

The gravity model shown in Figure 5.1a had its horizontal position inverted using the software described in section 2. The body had the correct depth, shape, and density contrast, and was in the horizontal position shown. Figure 5.1b shows the position of the body that minimised the least-squares misfit. Figure 5.2 shows a plot of the misfit surface for this situation. When $\Gamma = 1.0$ the body moved steadily towards the optimum position and the misfit decreased smoothly. Figure 5.3a shows a plot of the misfit against the inversion iteration. The iteration scheme for these conditions is plotted in Figure 5.3b, along with the line $F(x) = x$. The value on each axis is the misfit, and each iteration can be seen as a step. The misfit at each iteration is plotted against the value at the next iteration. The trajectory starts with a large misfit value which decreases to a minimum value. As the minimum is reached, the improvement in the misfit becomes less at each iteration, and the trajectory converges to the line $F(x) = x$.

The model in Figure 5.1a was then reloaded, Γ was increased in increments of 0.1 and the inversion process was repeated. There was no change in the character of

Figure 5.1 : Gravity Model Used to Demonstrate Chaotic Inversion

a) Initial Model

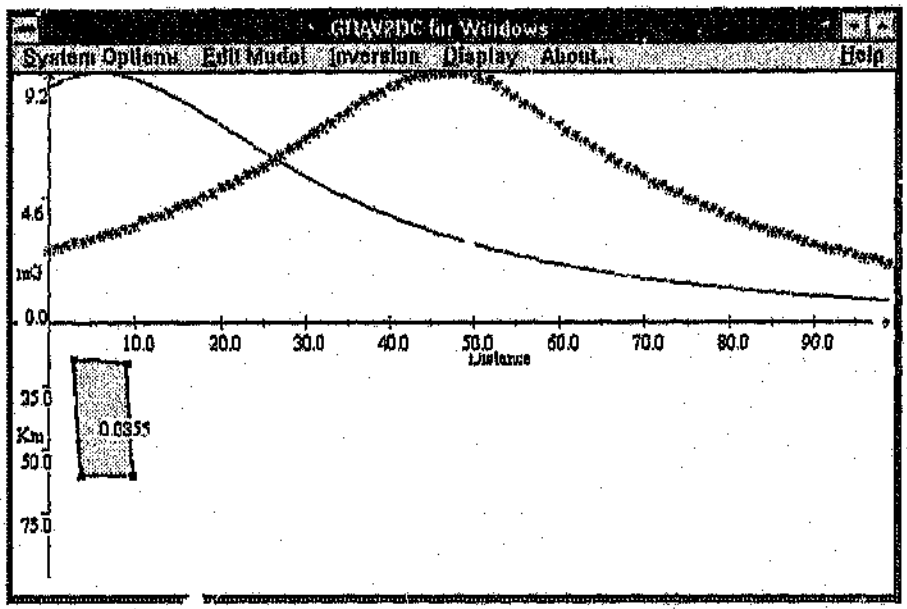

b) Model which Minimises the Misfit

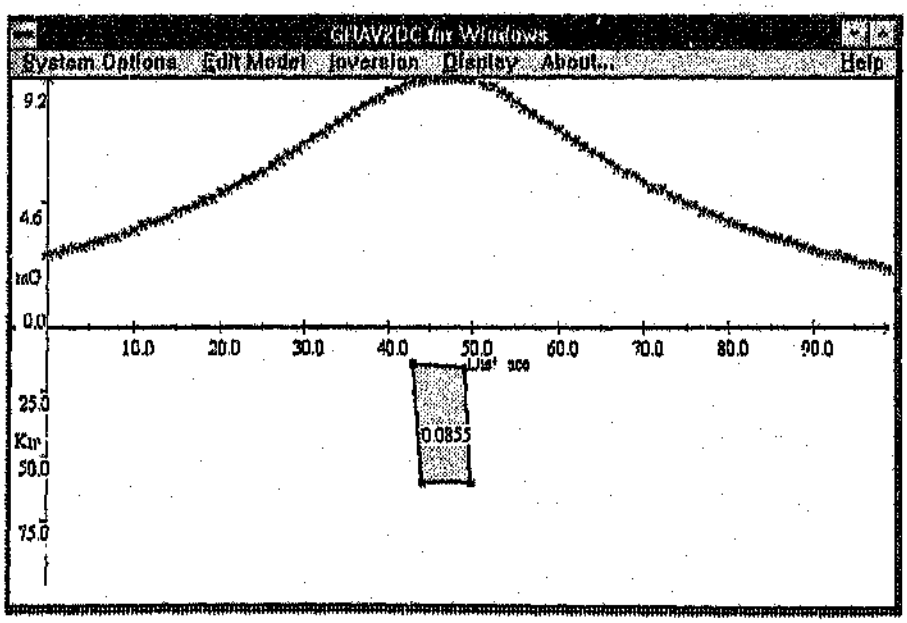

been achieved otherwise.

5.2 Chaotic Dynamics and Inversion

There are many similarities between inverse theory and chaos theory. Some parameter of the system, not necessarily one of the parameters under inversion, can be plotted as a function of the inversion iteration to give a trajectory (Cooper, 1995). This trajectory will hopefully converge on to a position corresponding to a minimum of the misfit surface, which can be considered as an attractor. The region of model parameters that invert to a particular minimum form the basin of attraction (which may be fractal in nature, as discussed in chapter 4) for that minimum.

If the dynamics of the inversion process can be made chaotic, and the chaos can be controlled, then this can prove advantageous. The chaos can be used to ensure that the inversion process samples a large amount of the space of possible model parameters, thus reducing the likelihood of the inversion becoming trapped in a local minimum of the misfit surface. In addition, if the inversion does become so trapped, then chaos can be used to force the trajectory out of the local minimum.

5.3 Generation of Chaotic Inversion

The gravity modelling program described in chapter 2 was used to perform least-squares inversion, in an overdetermined situation. The inversion process used equation 5.1 below :

$$dP = (A^TA + kI)^{-1}A^Te\ C \qquad (5.1)$$

CHAPTER 5 : ASPECTS OF CHAOTIC DYNAMICS IN THE INVERSION OF GEOPHYSICAL DATA

5.1 Introduction

The time evolution of many systems can be described by sets of differential equations which cannot be solved explicitly. The behaviour of such systems can be analysed by finite difference methods, given a set of initial conditions. In many cases, small differences in the initial conditions can give rise to large differences in the subsequent behaviour of the system. This is not due to the accumulation of round-off errors in the computer calculations, but is an inherent property of the system that is caused by the presence of non-linearities in the differential equations. As a parameter of the system is varied, the behaviour of the system can move from a steady state to a periodic state. Further changes to the parameter can cause the system to act in an apparently random manner. However, analysis of this motion shows that there is 'hidden' order within it. There are many examples of such systems, which are termed *chaotic*, including turbulence (Bergé, Pomeau, and Vidal, 1984 p.4), chemical reactions (Scott, 1992), population dynamics (May, 1974 ; May and Oster, 1976), the motion of the pendulum (Tritton, 1986) and electrical circuits (Madan and Wu, 1993). Even the value of shares on the stock market can be analysed in this manner (Beresford, 1996 ; Savit, 1988).

This chapter looks at parallels between chaos theory and the dynamics of the inversion process, and suggests a method for exploiting chaos to reach better solutions (in the sense that they have a smaller least-squares misfit) than would have

Figure 4.13 : Convergence to Minima as a Function of Position for Magnetics (Maximum X change allowed per iteration = 100km, Y change allowed 50km)

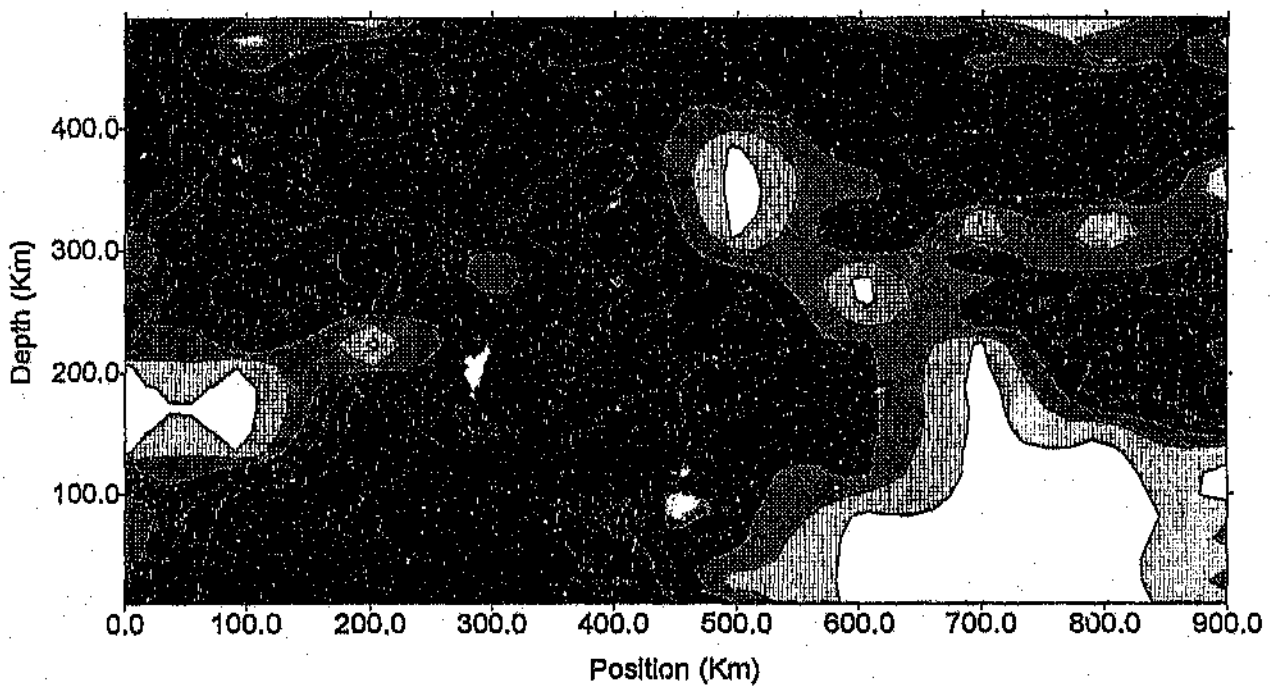

Black indicates that the body converged to the minima at a position of 200Km, and white indicates that it converged to the minima at a position of 700Km. Intermediate shades indicate convergence to neither.

starting positions left of the position midway between the two anomalies (i.e. 450km) would converge to the minimum at 200km. Figure 4.12b shows the percentage of inversion starting points as a function of k for which this was true. This is only 20.9% when k is 0.1, but rises to 92.9% when k was increased to 10.0 (recall that trajectories can also converge upon the minima at the very edges of the profile in addition to those at 200km and 700km - see Figure 4.2).

An alternative method of damping is to limit the amount that the parameters can change by at each iteration. The result of limiting the change in position per iteration to 100m and the change in depth to 50m (with k=1.0) is shown in Figure 4.13. The fractal pattern can still be seen. Obviously the allowed parameter change cannot be made too small at each iteration or the inversion will take a large number of iterations to converge.

4.4 Conclusions

The set of initial models that converge to a particular solution using the Gauss-Newton method of inversion is a fractal, providing that there are at least two parameters under inversion for which the model response is non-linear. Since this is undesirable, because it makes the selection of the initial model parameters difficult, two ways of controlling the inversion behaviour were examined. Increasing the damping coefficient k proved effective in reducing the fractal dimension of the set of models that converged to a particular solution, but restricting the parameter change allowed per inversion iteration did not.

Figure 4.12a : Fractal Dimension as a Function of Damping Coefficient

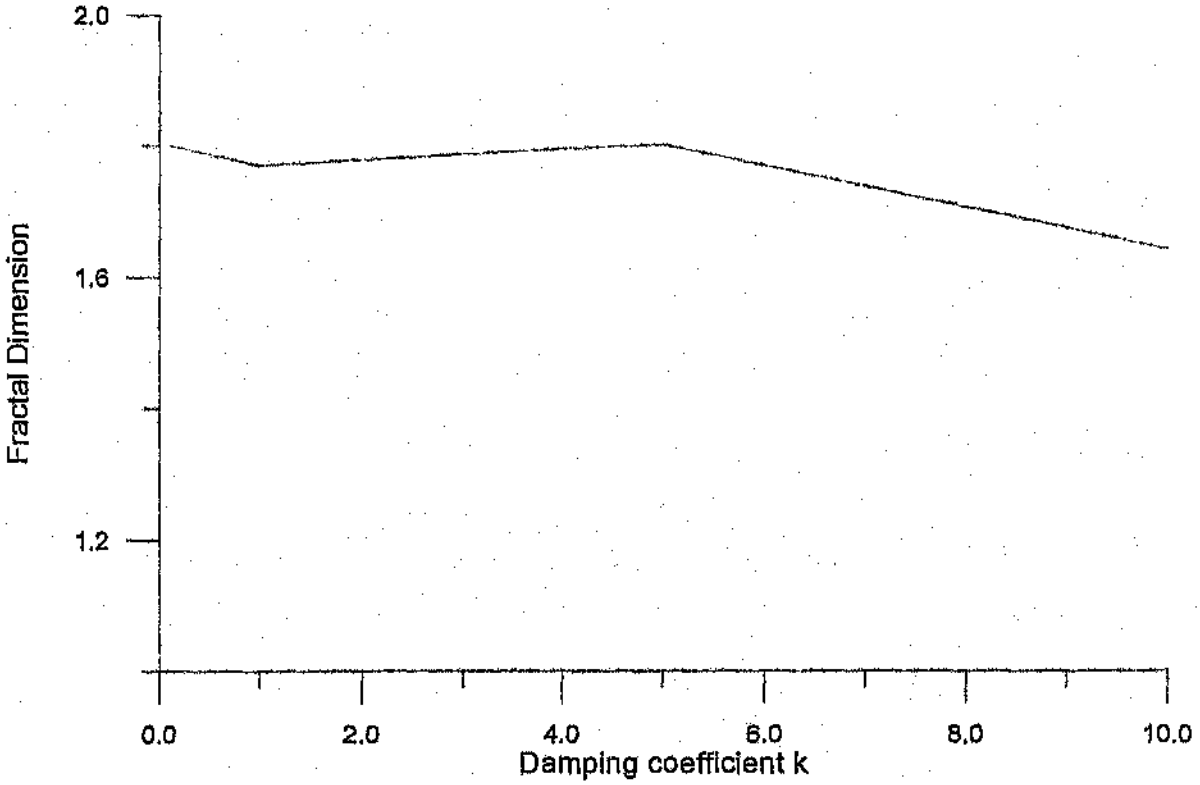

Figure 4.12b : Percentage of Starting Positions for Inversion that Converge to the Minimum on the Same Side of the Profile as They Started Upon

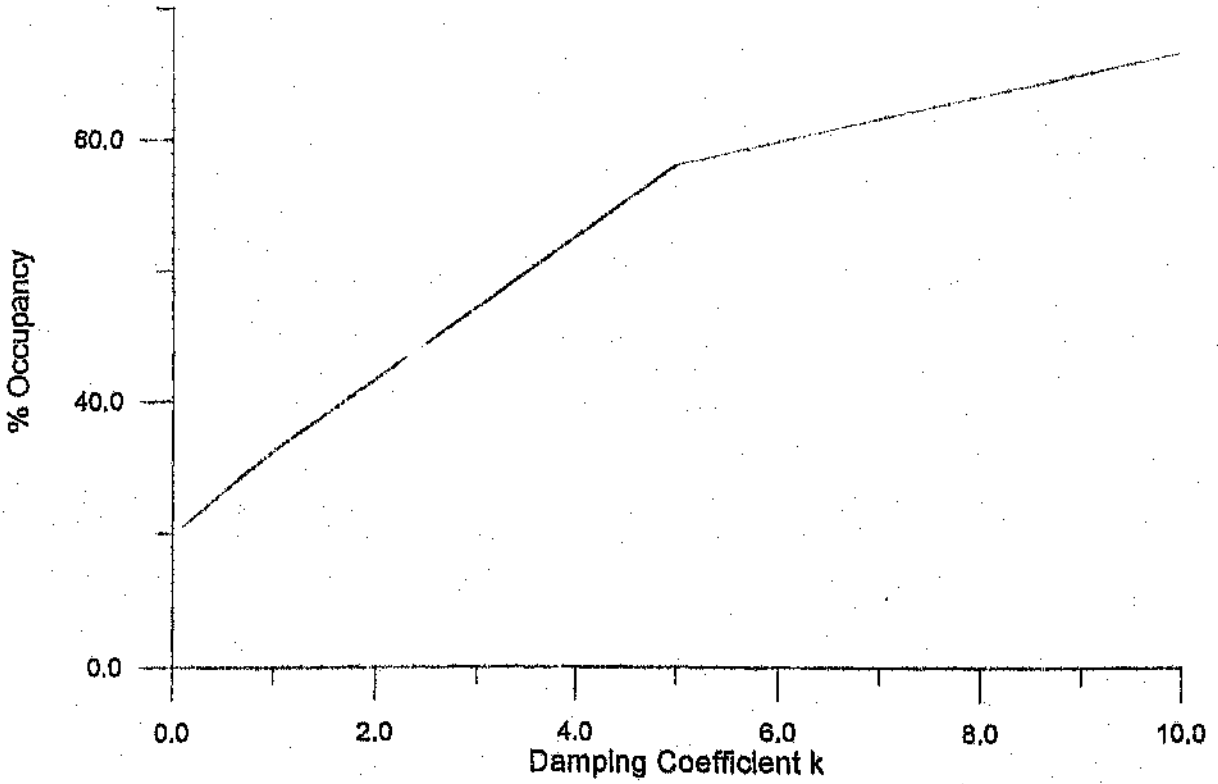

Figure 4.11 : Convergence to Minima as a Function of Position for Magnetics (Damping Factor k = 10.0)

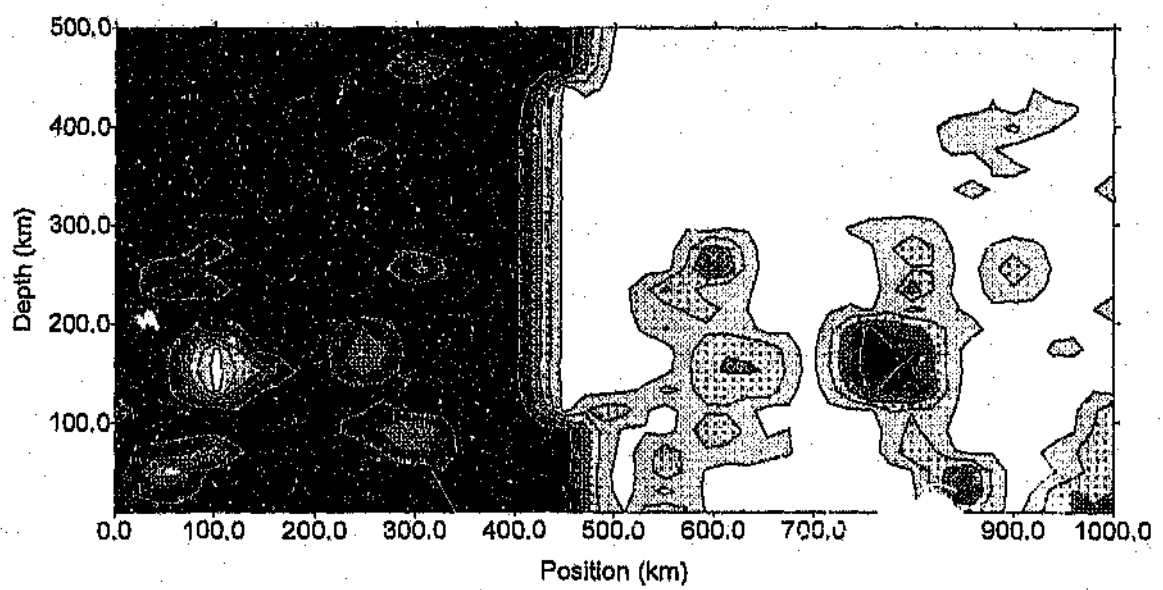

Black indicates that the body converged to the minima at a position of 200Km, and white indicates that it converged to the minima at a position of 700Km.

that it is dealing with a linear function. When it is not (the usual case) it provides an improved value for the root, and the process then proceeds iteratively until the root is found within the required limits of error. However, when multiple roots exist, the set of initial guesses that converge to a particular root can have a fractal nature. Consider the equation ;

$$z^3 - 1 = 0 \qquad (4.3)$$

This has three roots ; ', $e^{-2\pi i/3}$, and $e^{2\pi i/3}$. The set of which starting guesses in the complex plane converge to which of the three possible roots is a fractal (Press et al 1992, p.360), and is shown in Figure 4.10b.

4.3 Effect of Damping the Inversion

The damping of the inverse process is controlled by the factor k in equation 4.4 below ;

$$dP = (A^TA + kI)^{-1}A^Te \qquad (4.4)$$

where all terms have the same meanings as defined in chapter 1. Figure 4.11 shows the convergence plot for the magnetic model in Figure 4.1 with the value of k increased from 0.1 (the value used previously) to 10.0. It can be seen that the effect of increasing the damping has been to smooth the basin of convergence. The fractal dimension has been reduced to 1.6. Figure 4.12a shows the fractal dimension as a function of k, and it can be seen that (as expected) the fractal dimension decreases as the damping is increased. Intuitively it might have been expected that all inversion

Figure 5.7 : A Period - Doubling Bifurcation Event in Phase Space

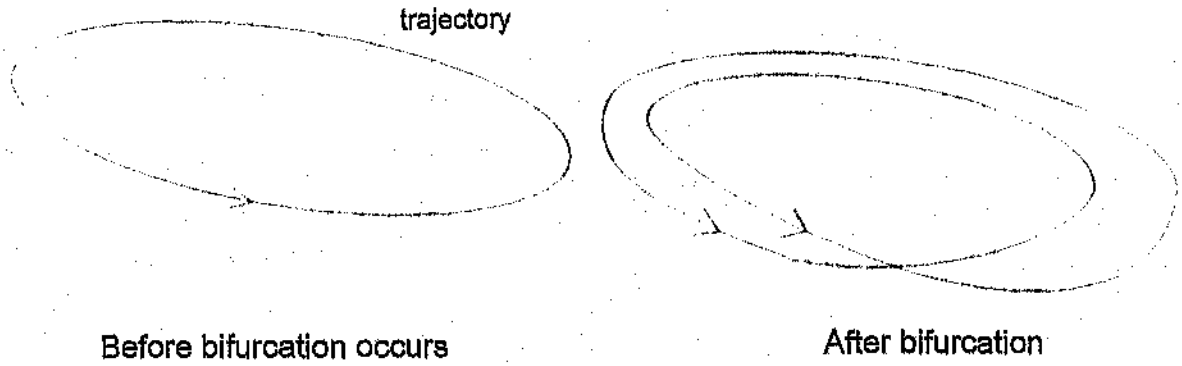

Figure 5.8 : The Feigenbaum Constants

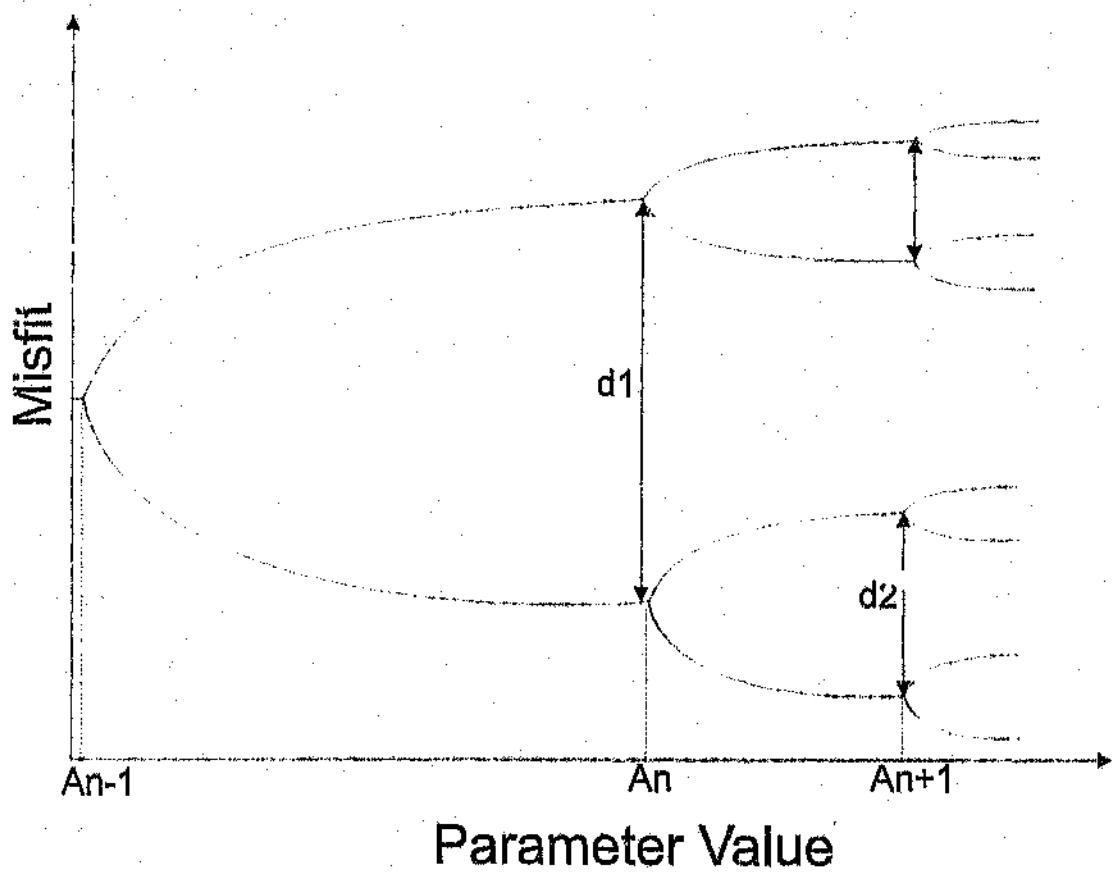

Figure 5.11a : Divergence of Nearby Trajectories During Chaotic Motion
(Γ= 5.0)

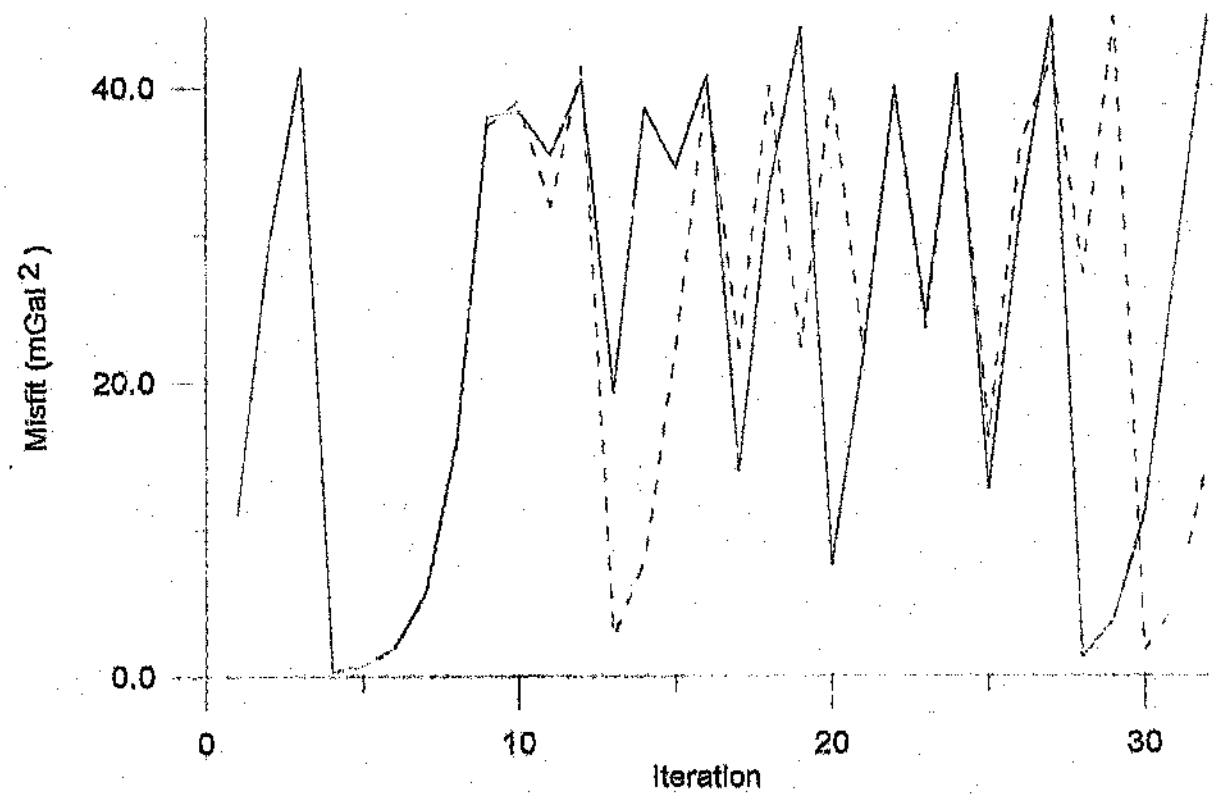

Figure 5.11b : Example Calculation of Lyapunov Exponent

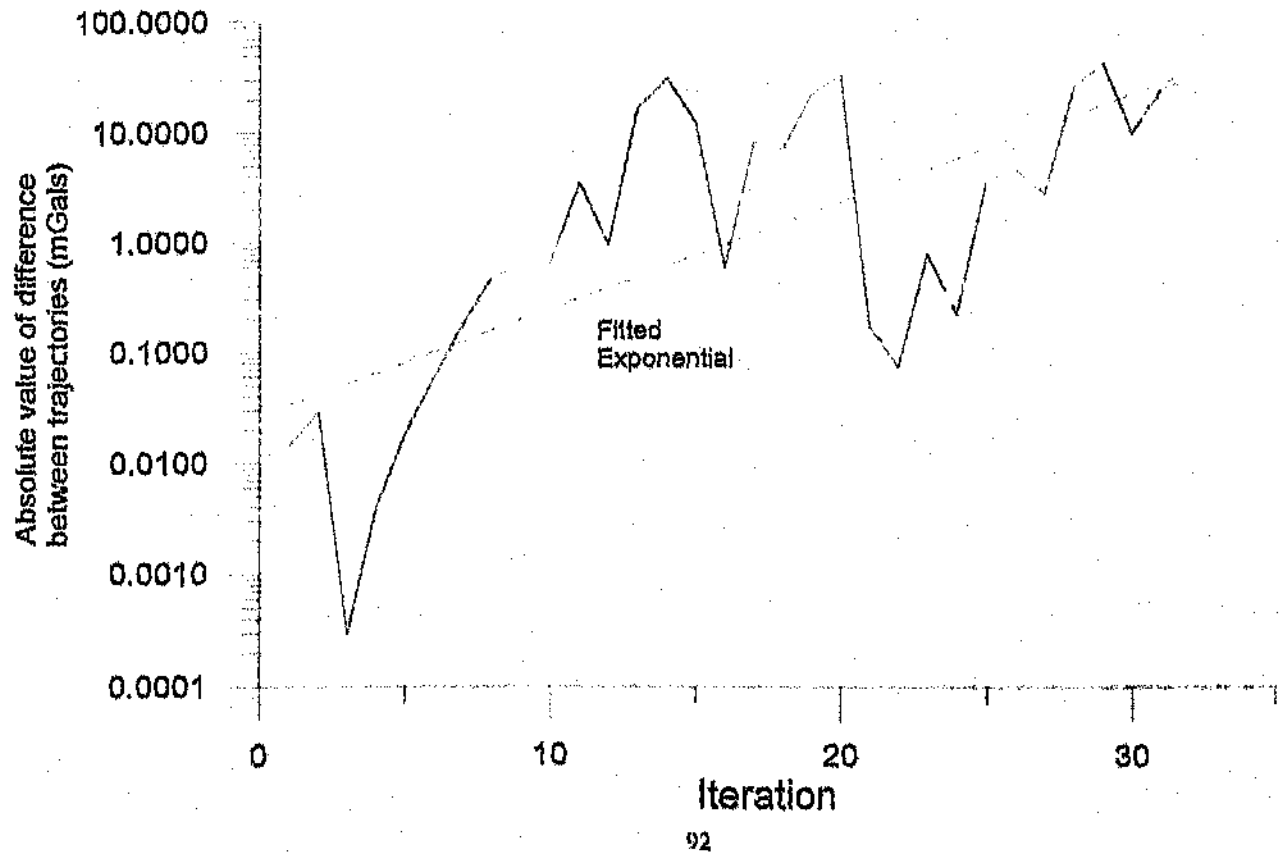

5.4.4 Lyapunov Exponents

The presence of chaos can be tested for by checking for the divergence of nearby trajectories (Hilborn 1994, p.27). The extreme sensitivity of chaotic systems to initial conditions is termed the 'butterfly effect' (Gleick, 1987 p.20) The difference between the trajectories should (on the average) diverge exponentially, and the rate of the divergence is given by the Lyapunov exponent λ, which is defined from (La Salle and Lefschetz, 1964) :

$$V = e^{\lambda t} V(x_0) \qquad (5.9)$$

Where the arbitrary function V is measured as a continuous function of time t, and has initial parameters x_0 . The misfit was measured at discrete intervals, so a discrete form of equation 5.7 was used (Hilborn 1994, p. 372) ;

$$\lambda = (1 / n) \ln (d_n/d_0) \qquad (5.10)$$

where d_0 is the absolute value of the difference between two points on nearby trajectories, and d_n is the difference n iterations away. The number of iterations used to estimate λ must not be too large because there is a maximum value of the misfit possible. Hence the situation must be avoided where the difference between the trajectories is of similar size to this maximum possible misfit. If the system is displaying periodic motion then λ is zero, since the trajectory will return to the same points at regular intervals.

Figure 5.10 : Power Spectrum of Data from a Chaotic Trajectory (Γ= 5.0)
Horizontal Body Position Inversion

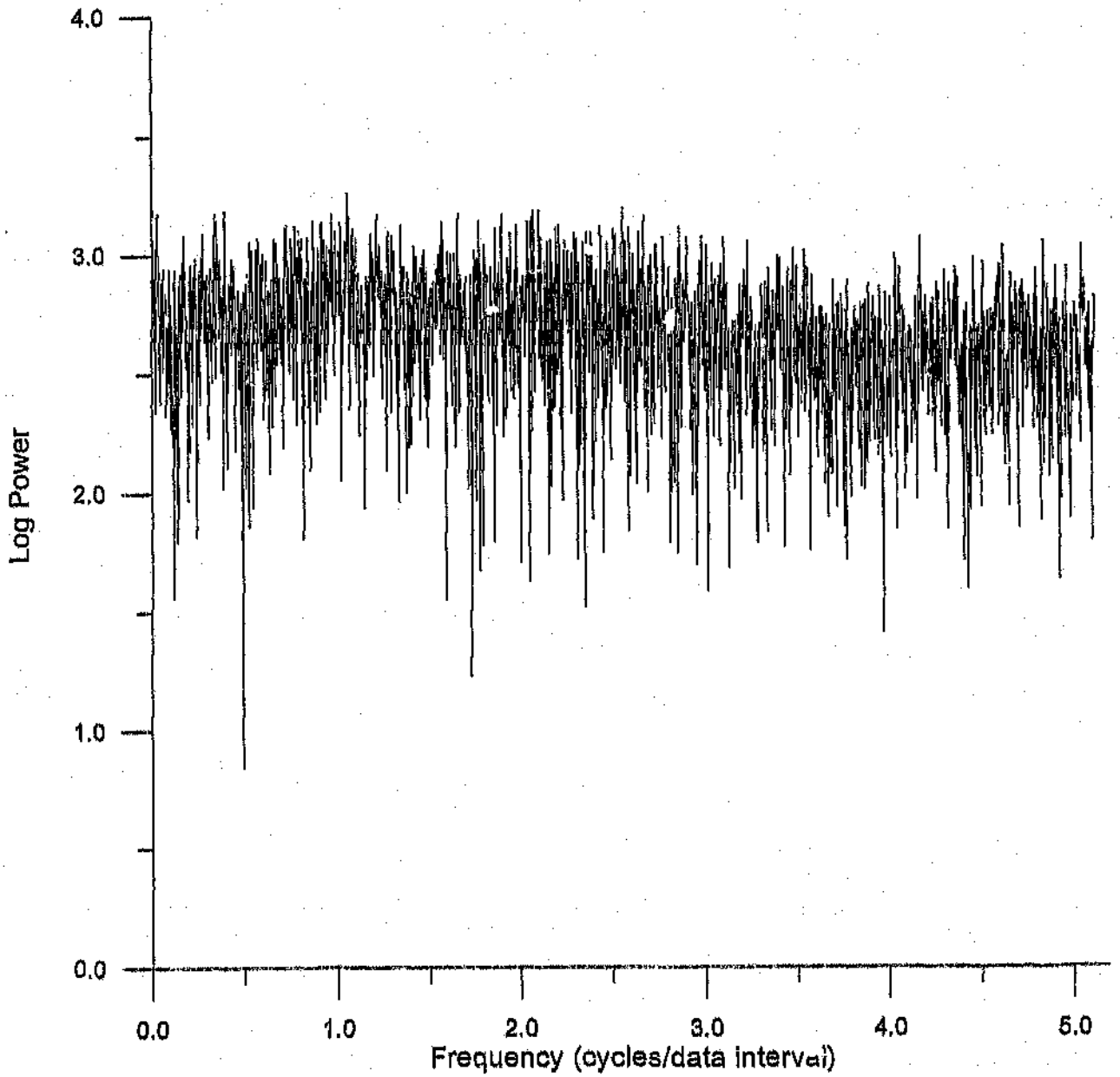

settling down to a periodic motion. This lengthening of the period of transient behaviour serves as an indication that a change in the behaviour of the system is about to occur.

5.4.3 Fourier Analysis of the Motion

Analysis of the power spectrum of the data from a trajectory can be useful in showing the presence of any periodic motions. The Fourier transform F(f) of a dataset F(x) is given by (Blakely, 1995 p.262) ;

$$F(f) = \int_{-\infty}^{\infty} f(x)\ e^{-ik'x}\,dx \qquad (5.7)$$

Where $k' = 2\pi/\lambda'$ is the wavenumber, and λ' is a wavelength present in the data. The power spectrum shows the amount of energy P(f) present at a given frequency f, and is given by :

$$P(f) = \sqrt{(R(f)^2 + I(f)^2)} \qquad (5.8)$$

Where R(f) and I(f) are the real and imaginary parts of the complex amplitude F at a given frequency f. A fast Fourier transform algorithm (Press et al 1992, p.501) was applied to 8192 points from a trajectory corresponding to Γ=5.0 and k=0.5 of the body horizontal position data, then the power spectrum was then calculated from equation 5.8 . The power spectrum is shown in Figure 5.10, and it can be seen that there are no well defined peaks corresponding to a motion dominated by a few frequencies. Fourier analysis cannot discriminate between random and chaotic motion however, and other methods must be applied to achieve this.

Figure 5.9a : Transient Behaviour Near a Bifurcation Point

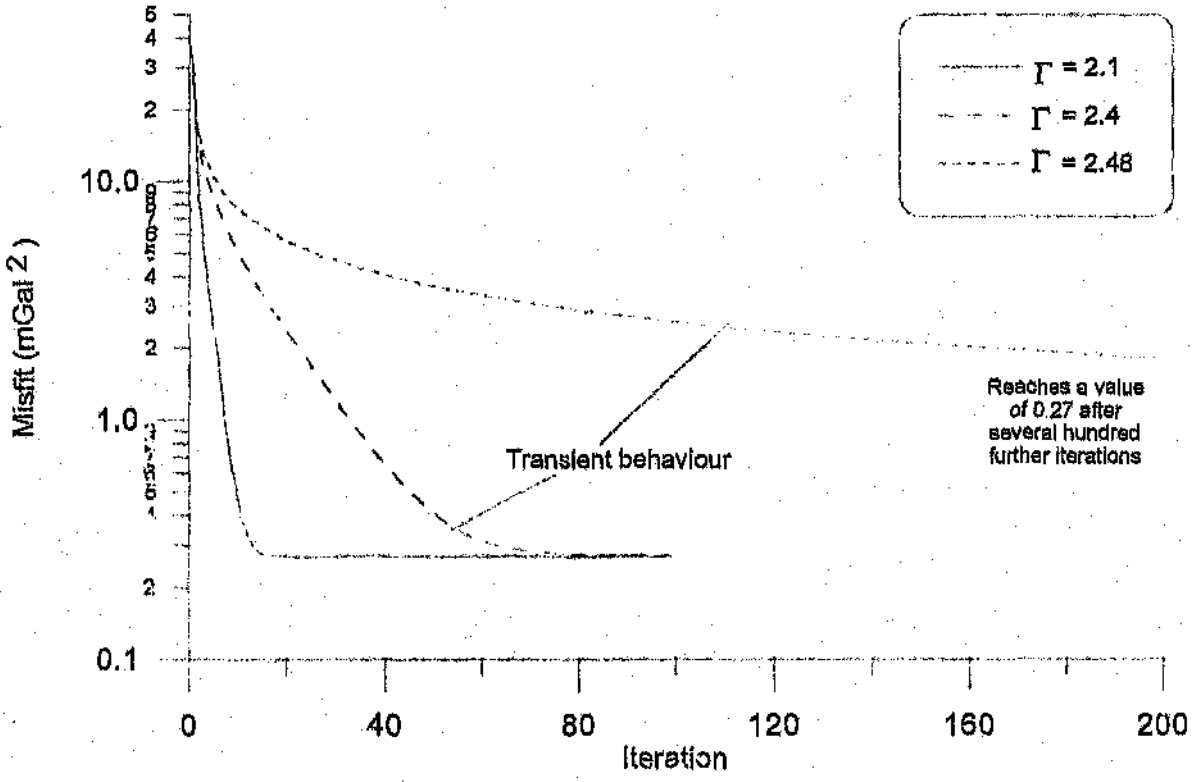

Figure 5.9b : Number of Iterations Required for Convergence against Distance from a Bifurcation Event

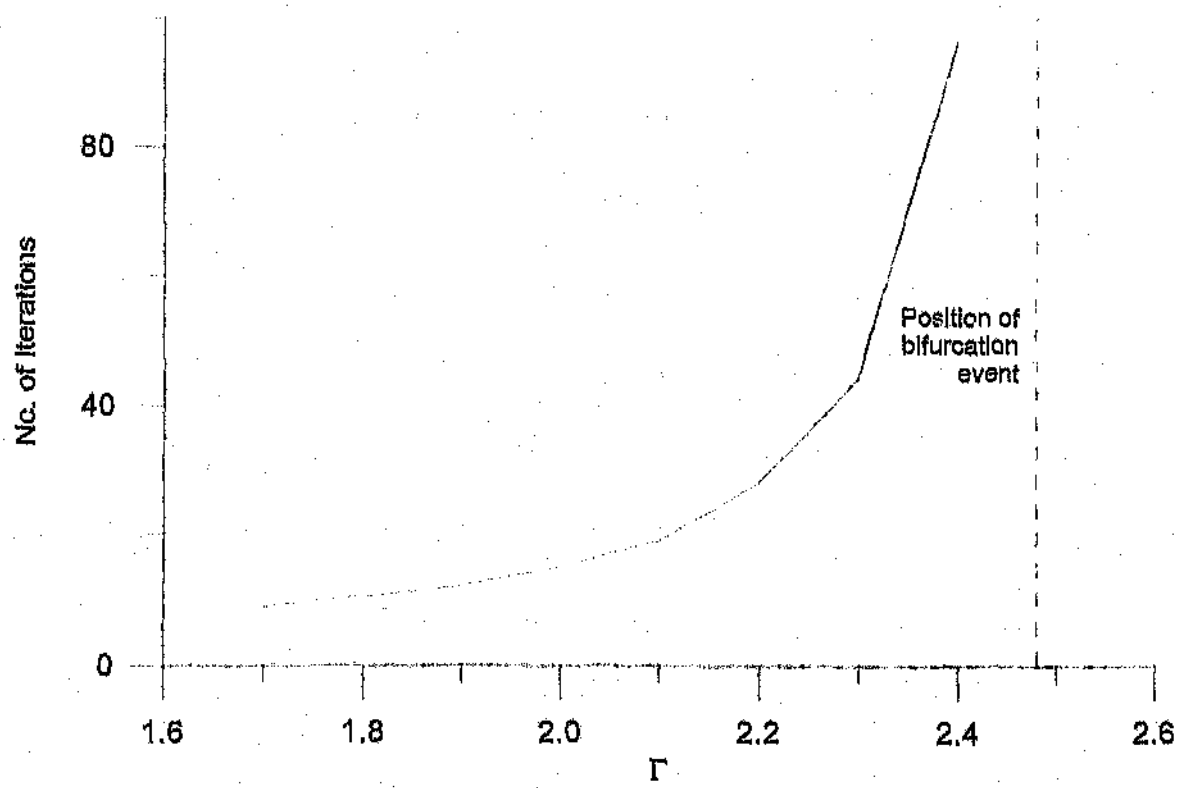

$$-\alpha\,(-\alpha + 1) = \delta \qquad (5.5)$$

Substituting for α=2.9 in equation 5.5 gives a value of δ of 5.5, which is higher than that measured. However the relation is only approximate, since using α=2.5029 gives δ as 3.76, lower than the expected value of 4.66.

The Feigenbaum numbers are only applicable to unimodal functions that are quadratic in form near their maximum, as mentioned above. The values of α and δ vary according to the form of the function near its maximum. For functions of the form :

$$f(x) = 1 - a\,|x|^z \qquad (5.6)$$

they vary smoothly with z , with α decreasing toward 1.27 and δ increasing linearly as z becomes large (Hilborn 1994, p.221).

5.4.2 Transient Behaviour

The duration of the transient behaviour that occurs before the model settles down to periodic motion varies considerably. The nearer the periodic behaviour is to a value of Γ corresponding to a bifurcation, the longer the transient behaviour exists. This is shown in Figure 5.9a. Figure 5.9b shows the misfit plotted against iteration for several values of Γ close to a period doubling bifurcation event. As Γ approaches the value at which period-2 behaviour is seen, the system displays almost periodic oscillations whose amplitude gradually decreases to zero. Similarly, if chaos is soon to appear, then the model will display apparently chaotic behaviour for a while before

behaviour, but returns to period-2 behaviour for $4.44 < \Gamma < 4.53$. In addition, as Γ was increased from 2.48 the amplitude of the oscillation of the body position increased also, until Γ reached 4.0, when the lower limb of the bifurcation diagram turned upwards suddenly (see Figure 5.6b). The gradient of the upper limb also changed at this point. The overall pattern of the bifurcation diagram is consistent with a bifurcation occurring at $\Gamma = 3.9$, which would yield $\delta = 3.62$. This is in reasonable agreement with the asymptotic value of 4.67.. stated above, which is only valid in the limit when $n = \infty$. However it implies that portions of the chaotic motion are unstable and are hence not seen. Sarkovskii's theorem states that there can be an infinite number of unstable periodic trajectories at given parameter value (Hilborn 1995, p.205).

The Feigenbaum α is the ratio between the size of the largest period-n segment to the size of the largest period-2n segment. It is given by (Hilborn 1994, p 54) :

$$\alpha = \lim_{n\to\infty} d_n/d_{n+1} = 2.5029... \qquad (5.4)$$

Figure 5.8 shows the parameters d_n, where $\alpha = d_1/d_2$. The period-2 behaviour and period-4 behaviour that occur from $2.5 < \Gamma < 4.5$ were examined, and although it was difficult to read the values accurately, a value for α of 2.9 was obtained for the inversion of the horizontal position of the body.

α and δ are related approximately by (Hilborn 1994, p 220) :

Figure 5.6a : Bifurcation Diagram for the Misfit in the Inversion of the Horizontal Position of the Model in Figure 5.1a

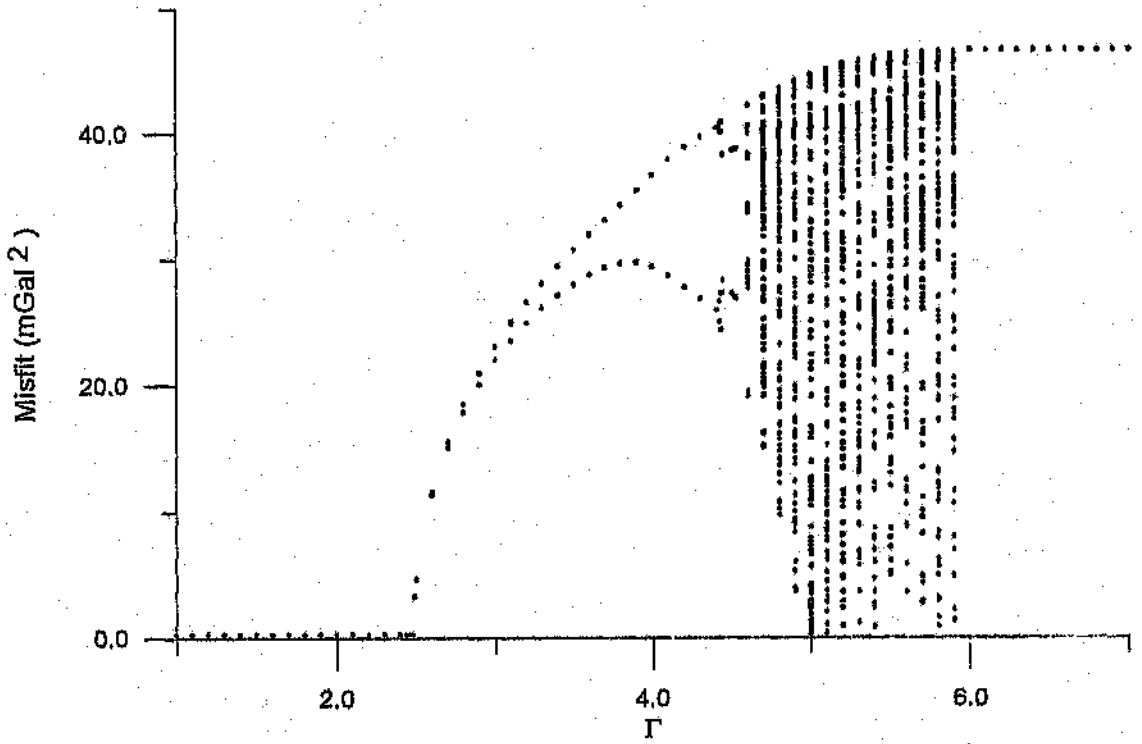

Figure 5.6b : Bifurcation Diagram for the Inversion of the Horizontal Position of the Model in Figure 5.1a

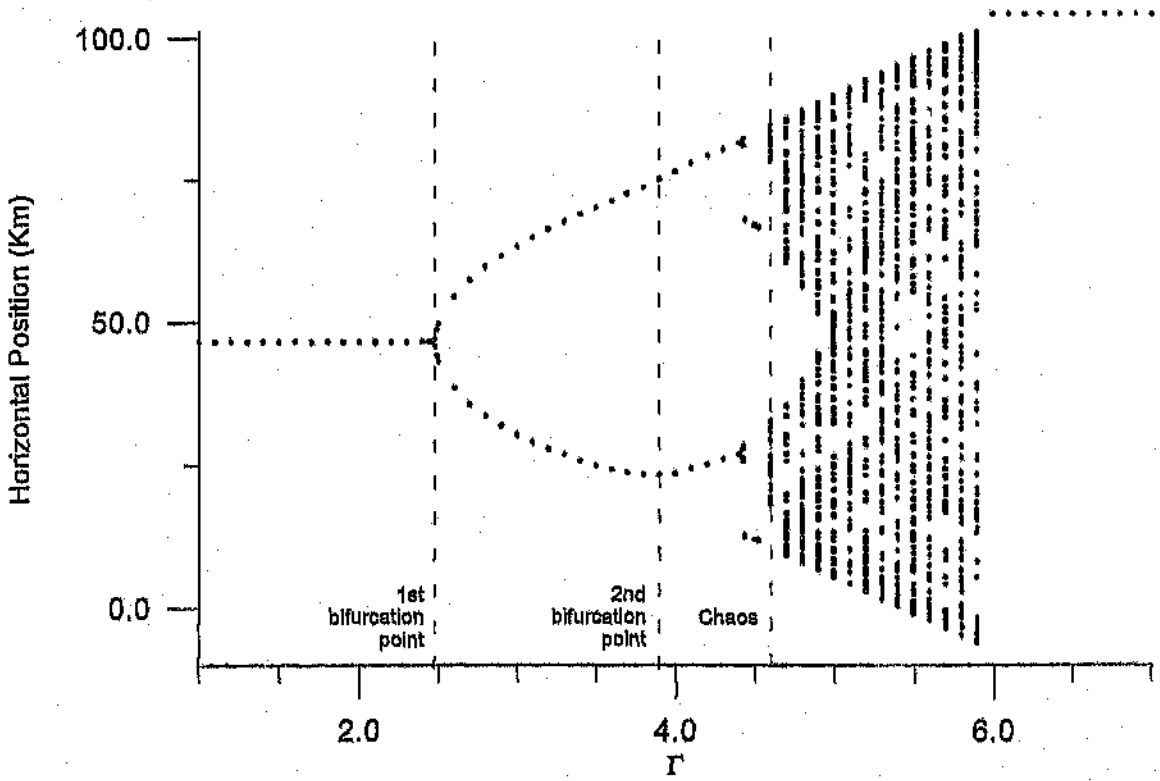

120 points are plotted in the chaotic regions.

At each bifurcation point, the current periodic motion becomes unstable and a frequency double the current frequency becomes stable. Figure 5.7 shows a schematic frequency doubling trajectory in state space. A state space plot depicts model parameters plotted against each other, and a set of points on the plot at different times make up a trajectory that shows the evolution of the system (Hilborn 1995, p.33).

The Feigenbaum δ characterises the ratio between the parameter values at which different bifurcation events occur in chaotic systems that are based upon a unimodal map function (i.e. a function that possesses a single maximum or minimum in the range of parameters used) of quadratic form, and is given by (Lauwerier 1986, p.44) :

$$\delta = \lim_{n\to\infty}(A_n - A_{n-1}) / (A_{n+1} - A_n) \qquad (5.3)$$

where A_n is the value of Γ at which a bifurcation occurs. A_{n+1} is the value of Γ at which the next bifurcation occurs, and A_{n-1} is the value of Γ at which the previous bifurcation occurred (see Figure 5.8). This ratio should be approximately the same for all values of n, and for large values of n it should approach a value of 4.66920161.. The first bifurcation event occurred at Γ = 2.48 (period-2) and the second at Γ = 4.42 (period-4). No period 8 behaviour was observed, but the system was behaving chaotically by Γ = 4.6 . Using these values gives δ = 10.7 (which will be an underestimate, since $A_n < A_\infty$). However the behaviour is more complicated than it first appears. The period-4 behaviour does not blend smoothly into the chaotic

Figure 5.5a : Misfit against Iteration for the Model in Figure 5.1a (Γ= 5.0)

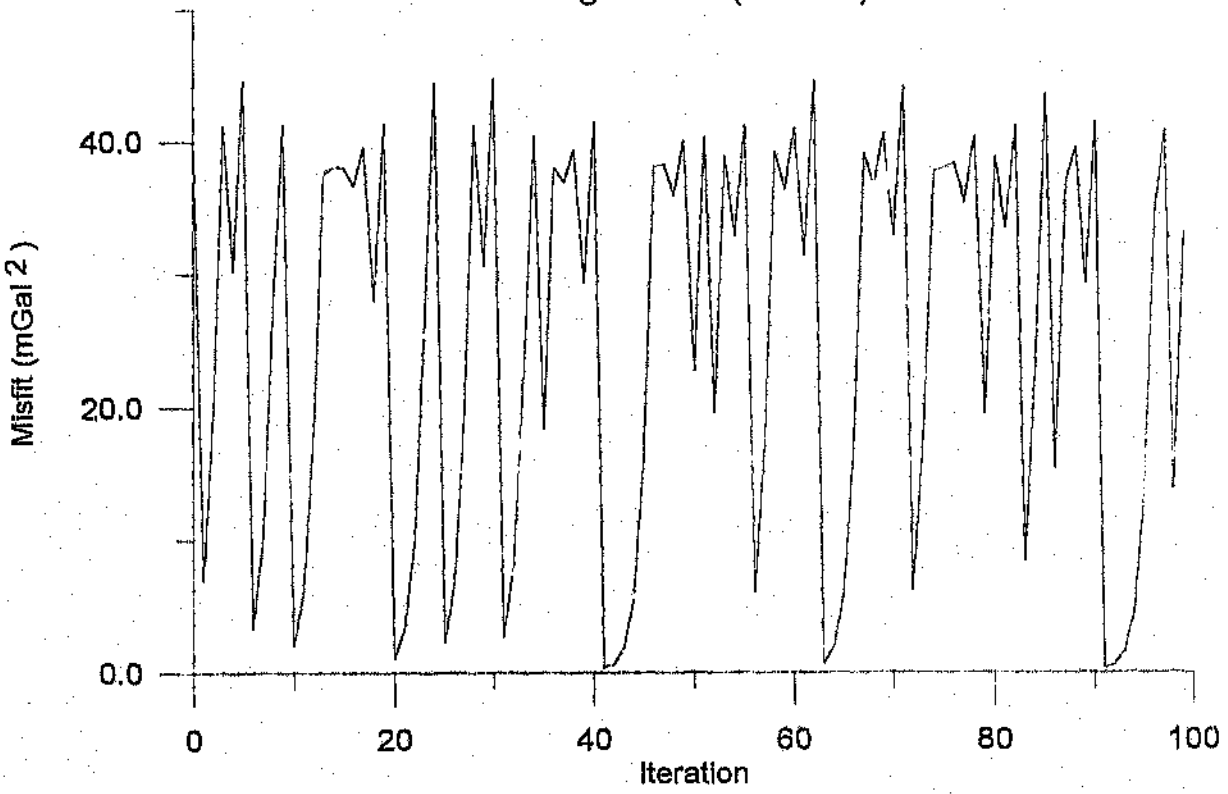

Figure 5.5b : Iteration Scheme for the Case when Γ= 5.0

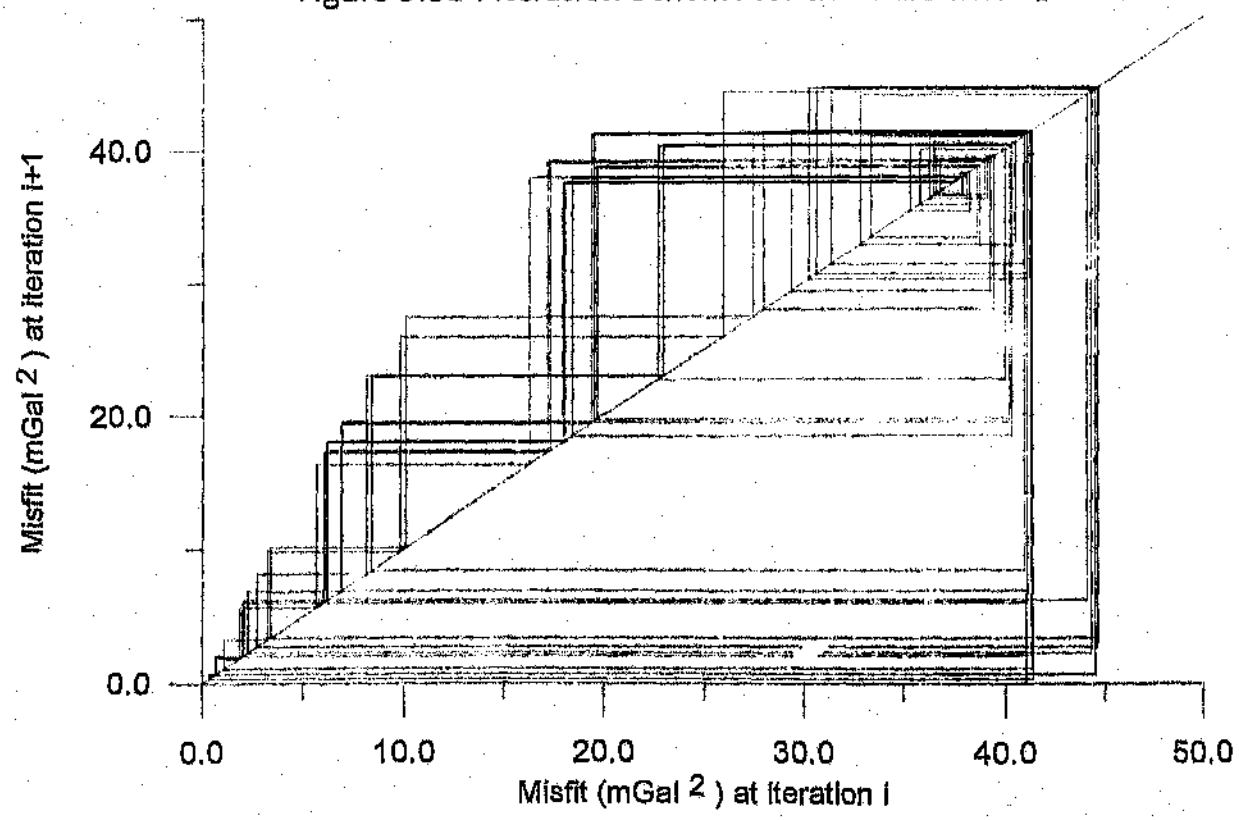

Figure 5.4a : Misfit against Iteration for the Model in Figure 5.1a (Γ= 4.0)

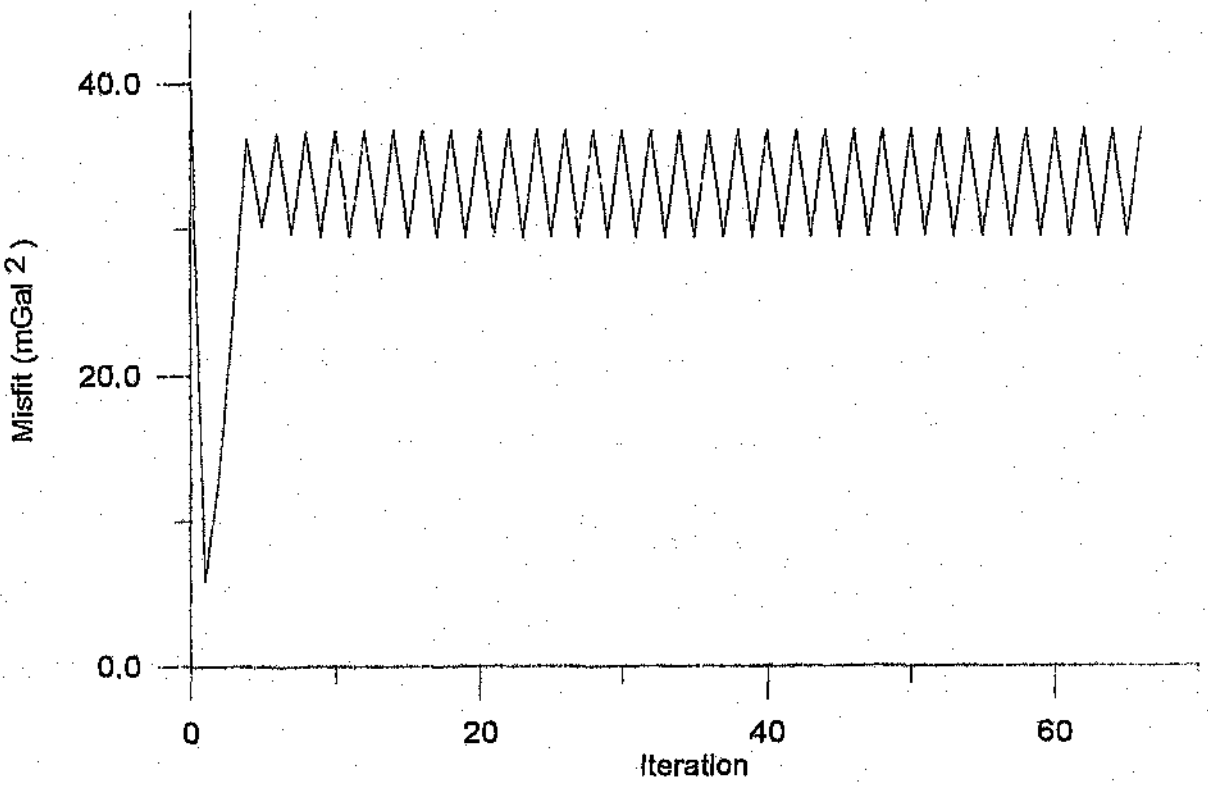

Figure 5.4b : Iteration Scheme for the Case when Γ = 4.0

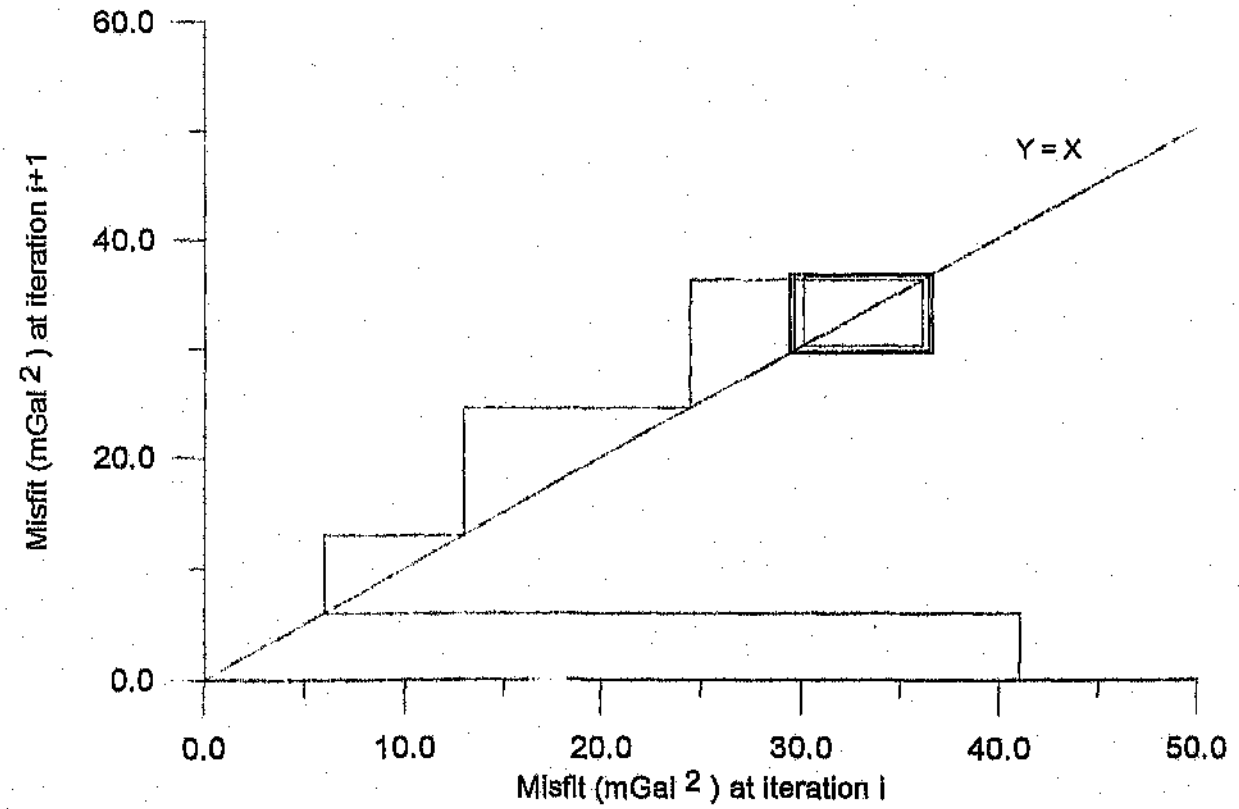

Figure 5.16 : Bifurcation Diagram for Horizontal Body Position Inversion with k = 2.5

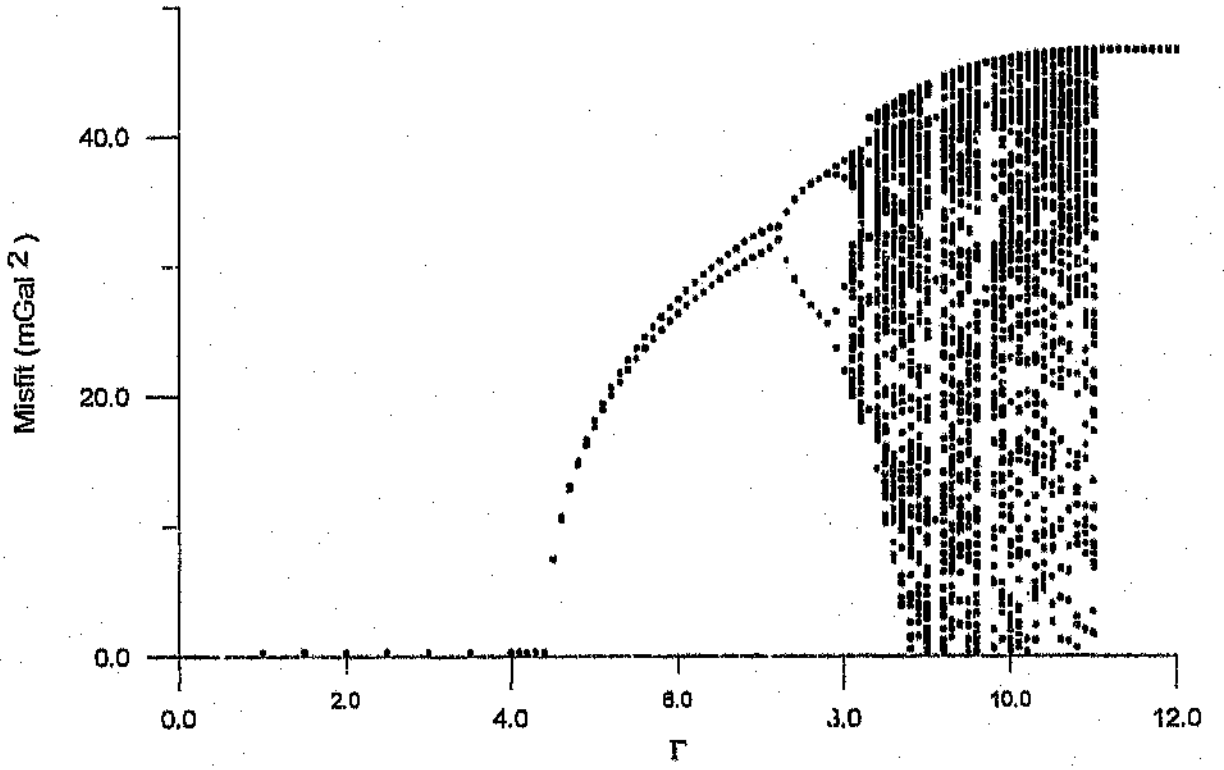

Figure 5.17 : Bifurcation Diagram for Horizontal Body Position Inversion for k = 5.0

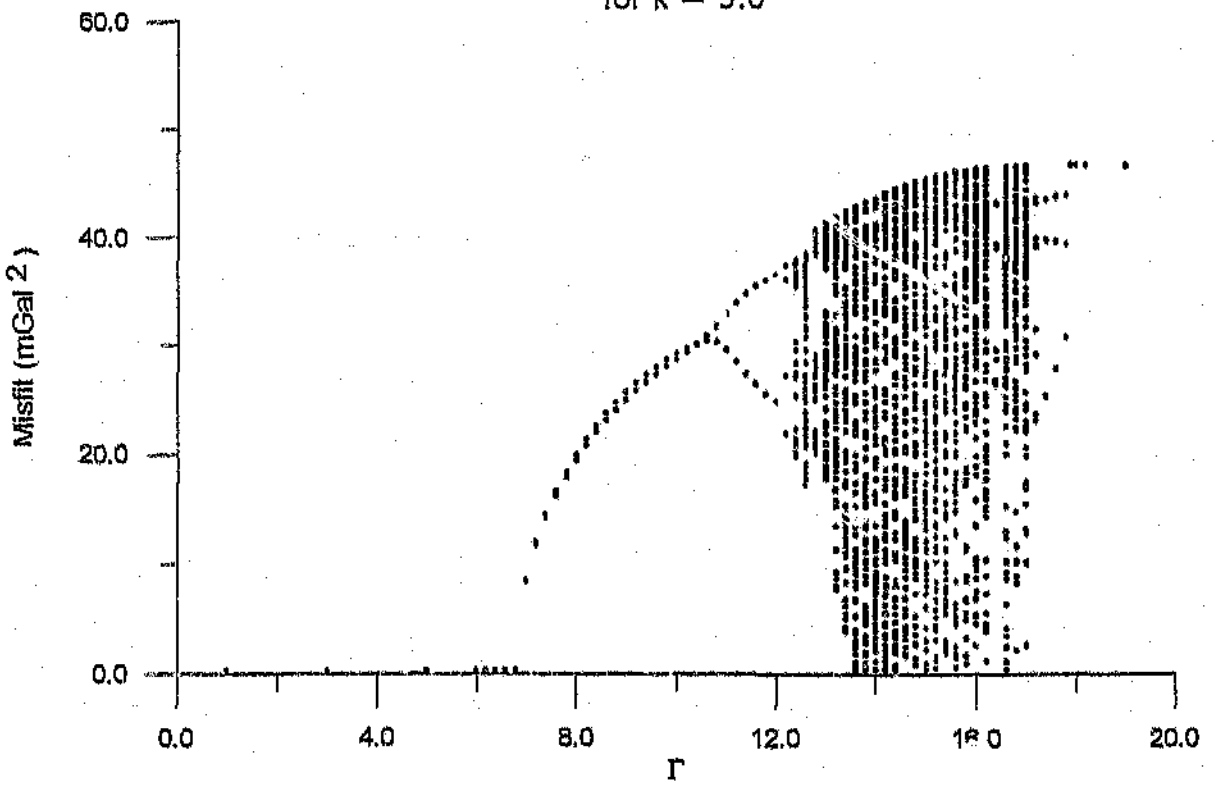

Figure 5.15 : Effect of Damping Upon Inversion Behaviour

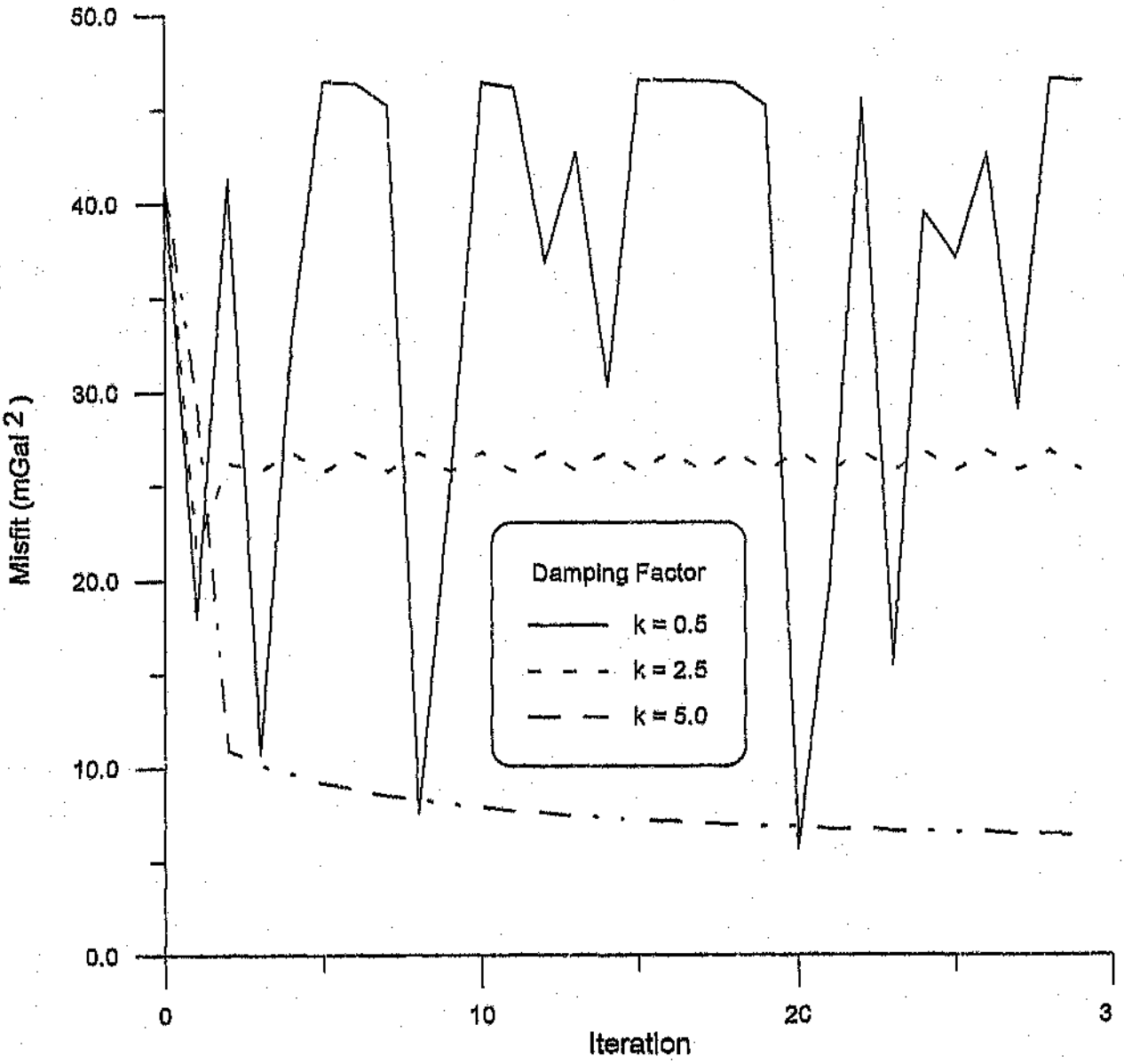

maximum global embedding dimension required to unfold the attractor, but the dimension actually required in this case is 5 (as determined from the FNN analysis above). (Abarbanel, 1996 p.46)

5.4.7 Damping

To demonstrate the effect of damping on the chaotic inversion process, the model was inverted with three different values of the damping parameter k (see equation 5.1) and Γ=6.9. Figure 5.15 shows 30 iterations of the misfit in the inversion process for each value. When k = 5.0 the inversion is heavily damped, and no signs of chaos are present. When k is decreased to 2.5 the inversion displays period 2 oscillatory behaviour. When k is decreased still further to 0.5 chaotic behaviour can be seen. Hence the damping can be used to control the nature of the behaviour of the system.

Two bifurcation diagrams are shown in Figures 5.16 and 5.17, and they can be compared with Figure 5.6a. The damping parameter k has values of 2.5, 5.0, and 0.5 in the three figures respectively. As expected, the higher the damping, the greater the value of Γ required to produce chaos. Figure 5.17 appears stretched out along the Γ axis compared to Figure 5.16. The windows of periodic behaviour that emerge from the chaos are present for larger ranges of Γ. The overall pattern, that is to say bifurcations, periodic behaviour, and chaos is the same for all three figures.

5.5 Inversion of the Angle of Rotation of the Body

The model shown in Figure 5.1a was used again, but this time the body was

against log R. Figure 5.14a shows the result of applying this technique. It is not possible to take the limit R→0 since the dataset consists of a finite number of datapoints, and so C(R) fails to scale with R as given in equation 5.18 for small values of R. The straight portion of the curve where R is large is known as the scaling region, and the slope here is used to estimate D_c. The scaling region can be difficult to estimate, since the curve may not be exactly straight anywhere. The uncertainty in the value of D_c can be estimated by varying the size of the scaling region.

The measured value of D_c is a function of the embedding dimension (Ruelle, 1992 p.80), because the trajectory will not be correctly unfolded unless the embedding dimension used is large enough. The upper curve of Figure 5.14a, wherein the data points making up the trajectory were used individually, corresponds to an embedding dimension of one. The problem of C(R) failing to scale with R for small values of R gets worse the higher the embedding dimension used, since the points on the trajectory are effectively scattered throughout a greater volume.

A plot of correlation dimension against embedding dimension is shown in Figure 5.14b. Takens (1981) has shown theoretically that if the state space of a system has d_s dimensions, then the embedding space needs $2d_s+1$ dimensions to describe the attractor adequately. However in practice it is often sufficient to use an embedding dimension that is about twice the dimension of the attractor. From Figure 5.14b it can be seen that the correlation dimension becomes independent of the embedding dimension when the latter reaches a value of about 8. The attractor dimension can then be seen to be approximately 3.9 . Note that the value of 8 is the

Figure 5.14a : Correlation Sum vs Distance R for Different Embedding Dimensions
Body Horizontal Position Inversion (Γ= 5.0)

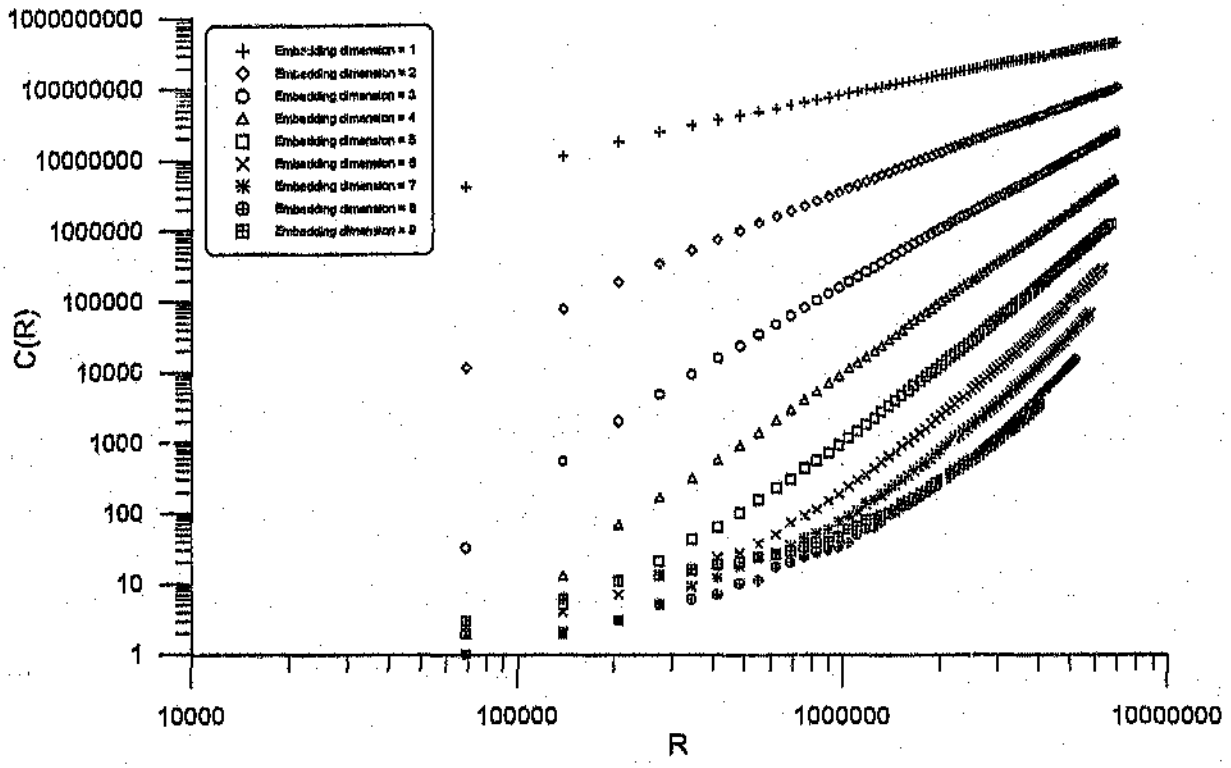

Figure 5.14b Correlation Dimension against Embedding Dimension
Body Horizontal Position Inversion (Γ= 5.0)

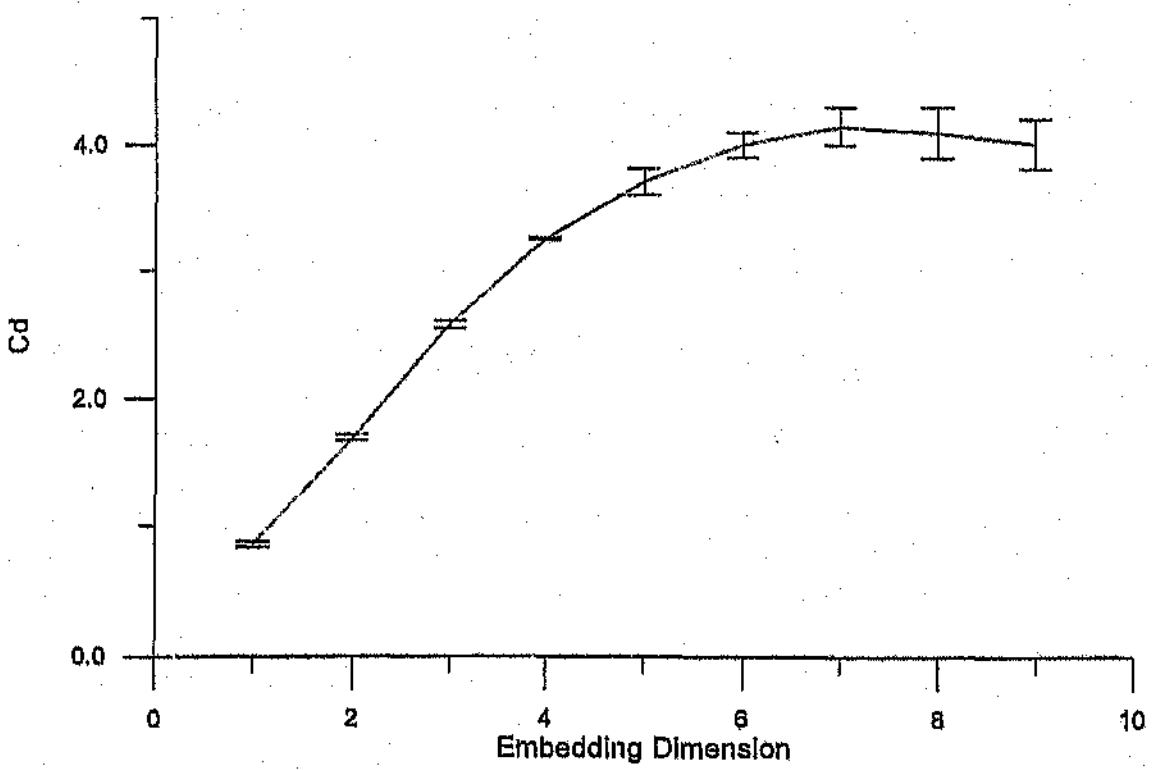

represent, but Figure 5.13a shows a plot of the trajectory in two dimensions alongside a similar plot for a random number sequence (Figure 5.13b). The structure in the former can clearly be seen, indicating its non-random nature.

5.4.6 Correlation Dimension

The fractal dimension of the chaotic attractor can be measured in different ways, such as the box-counting method (see section 4.2.3) or the ruler method (Turcotte, 1997 p.12). However a more suitable method computationally for measuring the dimension of an attractor that is scattered throughout a many dimensional space is the correlation sum method. This counts how many points on a trajectory in state space lie within a distance R of a particular point.

7000 Data points from the chaotic regime of body horizontal position inversion (Γ = 5.0) were analysed. The correlation sum is given by (Hilborn, 1994 pg. 409) ;

$$C(R) = 1/(N(N-1)) \sum_{i=1}^{N} \sum_{j=1, j\neq i}^{N} \Theta(R - |x_i - x_j|) \qquad (5.18)$$

Where x_i and x_j are data points on a trajectory which consists of N points, and Θ is the Heaviside step function. The correlation dimension D_c is then defined as (Ruelle, 1992 p.79) ;

$$D_c = \lim_{R\to 0} \log C(R)/\mathrm{Log}(R) \qquad (5.19)$$

The correlation dimension can then be estimated from a plot of log C(R)

Figure 5.13 : Embedding of Data in State Space

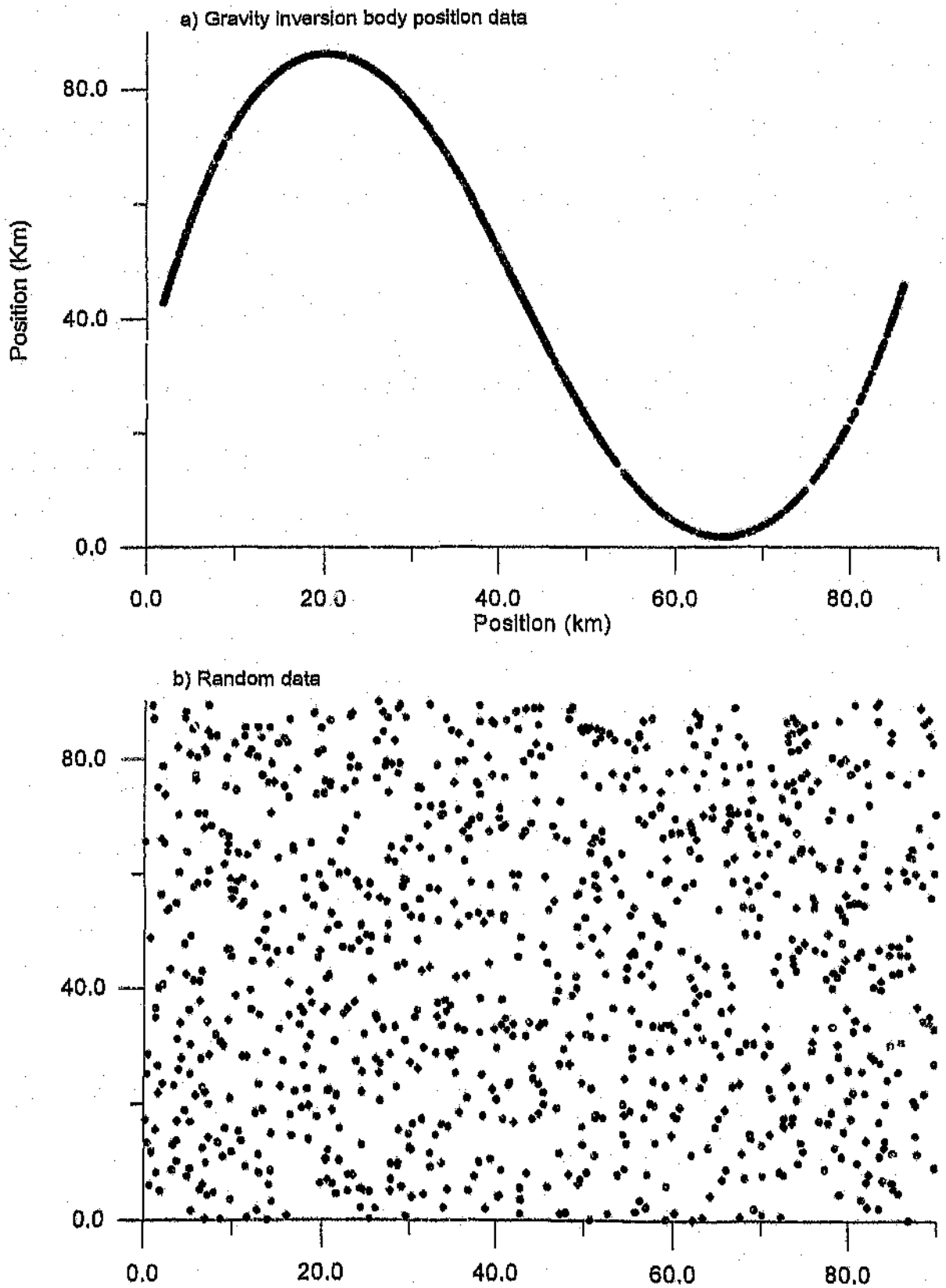

$$R_d(k)^2 = \sum_{m=1}^{d} [s(k+(m-1)T) - S^{NN}(k+(m-1)T]^2 \qquad (5.15)$$

and in dimension d+1 is (Abarbanel 1995, p.41) ;

$$R_{d+1}(k)^2 = \sum_{m=1}^{d+1} [s(k+(m-1)T) - S^{NN}(k+(m-1)T]^2$$

$$= R_d(k)^2 + |s(k+dT) - S^{NN}(k+dT)|^2 \qquad (5.16)$$

and hence the distance between points seen in dimension d+1 relative to that in dimension d is ;

$$\sqrt{\frac{R_{d+1}^2(k) - R_d(k)^2}{R_d(k)^2}} = \frac{|s(k+dT) - S^{NN}(k+dT)|}{R_d(k)} \qquad (5.17)$$

When this distance exceeds the empirically determined value of 15 the neighbour is taken to be false (Abarbanel 1995, p.41).

A plot of the percentage of false nearest neighbours (FNN) against dimension indicates what dimension should be used for the phase space embedding. When the number of FNN falls to zero the attractor is taken to be completely unfolded. Figure 5.12b shows the FNN analysis for the chaotic trajectory discussed above using a delay of 22 samples. The number of FNN's never falls to zero but has a minimum at d=5 and increases thereafter with the dimension. This behaviour is characteristic of the presence of a high dimensional signal ('noise') in the system (Abarbanel 1995, p.211). The analysis was repeated using a delay of 7 samples, and this produced an almost identical curve to that of Figure 5.12b, as expected.

A plot in five dimensions of the trajectory in phase space is difficult to

Figure 5.12 : Analysis of a Chaotic Body Horizontal Position Trajectory ($\Gamma = 5.0$)

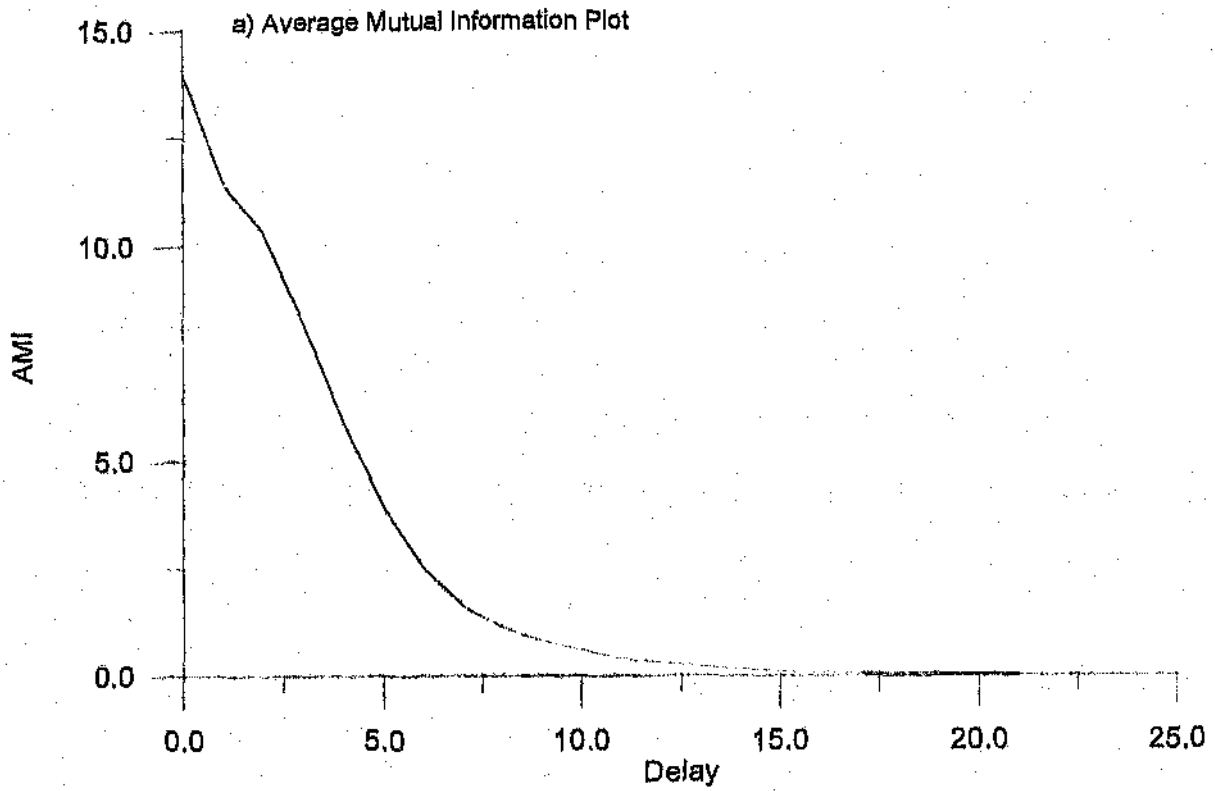

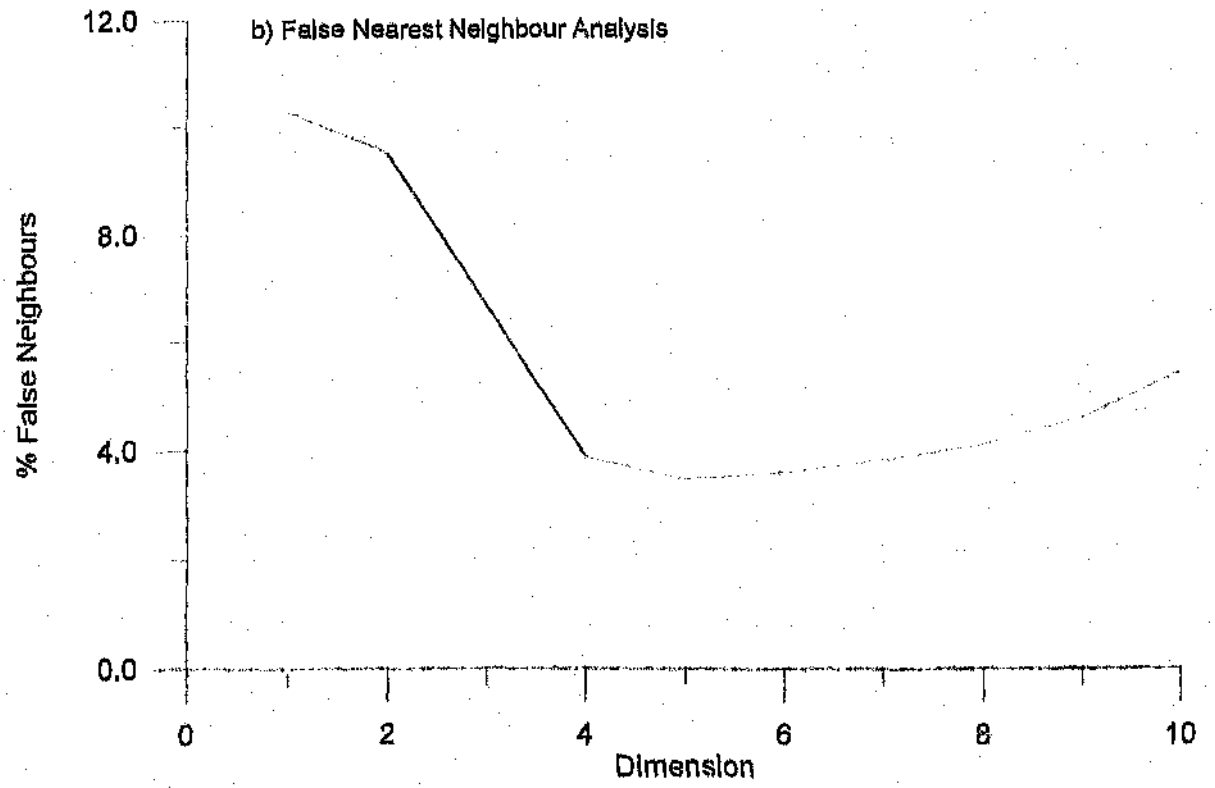

The first minimum of the AMI indicates which multiple T of τ_s is to be used. The AMI plot based on 70000 points of the body position from the trajectory when Γ=5.0 is shown in Figure 5.12a, and the first minimum value is at T=22, indicating that data points 22 samples apart are completely uncorrellated (the AMI can increase again at greater values of T due to the presence of random noise). However the curve decreases very slowly for delays greater than about 7, and the value of the AMI is already only about 10% of the initial value. This indicates that there is in practice little to be gained by using a delay greater than 7.

The number of dimensions to use when embedding the data is found by determining when the geometrical structure of the trajectory has been completely unfolded i.e. all points lie close to one another because of the dynamics of the trajectory, not because of the projection (Abarbanel, 1995 p.5). The data are analysed in dimensions of 1, 2, ..., N to determine which points neighbour which. A true neighbour will remain a neighbour regardless of the dimension that it is projected in, but a false neighbour will not. Consider a vector in a state space with d dimensions ;

$$y(k) = [\, s(k),\ s(k+T),\ \ldots,\ s(k+(d-1)T \,] \qquad (5.13)$$

where T is the time delay estimated from the AMI. Its nearest neighbour in this state space is then ;

$$y^{NN}(k) = [s^{NN}(k),\ s^{NN}(k+T),\ \ldots,\ s^{NN}(k+(d-1)T] \qquad (5.14)$$

The Euclidean distance squared between the nearest neighbour points as seen in dimension d is ;

be useful in revealing their structure (Savit, 1992). The one dimensional time series of misfit values contains sufficient information to allow the reconstruction of a d-dimensional vector space of trajectories because all the variables that describe a non-linear system are connected (Abarbanel, 1995 p.21). To enable the correct unfolding of the chaotic trajectory the average mutual information (AMI) and the number of dimensions in which to view the dataset, must be established. The AMI gives the amount of information (in bits) learned about a parameter $x(t + T\tau_s)$ at a time $T\tau_s$ from the measurement of $x(t + (T-1)\tau_s)$, where τ_s is the sampling interval of the data. The amount learned about a measurement b_j drawn from a set B from the measurement a_i from the set A is (Abarbanel, 1995 p.28) ;

$$Mutual\ Information = 1 \cdot \log_2 \frac{P_{AB}(a_i, b_j)}{P_A(a_i)\,P_B(b_j)} \qquad (5.11)$$

where $P_{AB}(a,b)$ is the joint probability density for measurements A and B resulting in values a and b. $P_A(a)$ and $P_B(b)$ are the individual probability densities for the measurements of A and B. The probabilities can be estimated from a histogram showing the variations of a_i and b_j. If the value a_i is independent of the value b_i then the mutual information is zero. The average of this measurement over A and B is the average mutual information ;

$$AMI = \sum_{a_i, b_j} P_{AB}(a_i, b_j) \quad \log_2 \frac{P_{AB}(a_i, b_j)}{P_A(a_i)\,P_B(b_j)} \qquad (5.12)$$

Figure 5.11a shows the misfit plotted against the inversion iteration for Γ = 5.0, which is in a region where chaos is apparently present. The two curves show the misfit for two trajectories whose initial values differ from each other by about 1%. The trajectories start off very close to one another, but diverge rapidly. After only about 14 iterations the two trajectories are over 34 mGal² apart.

Figure 5.11b shows an example Lyapunov exponent calculation. The log of the absolute value of the difference between the two trajectories shown in Figure 5.11a has been plotted, and an exponential function fitted to it. In this case the value of λ calculated was 0.2 ± 0.1 . A positive value of λ indicates the presence of chaos, since it indicates the exponential divergence of nearby trajectories. A negative value of λ would mean that trajectories would get closer together after each iteration. The value of λ depends slightly on which points are selected from the attractor, and the actual value of λ for the system is taken to be the average of many measurements throughout the system.

5.4.5 Phase Space Reconstruction

When the trajectory was not chaotic it either converged to a fixed point (Figure 5.6, $1.0 \leq \Gamma \leq 2.49$) or displayed periodic behaviour (for example, $2.5 \leq \Gamma \leq 4.5$). The chaotic behaviour of the misfit trajectory is caused by its attempts to converge to an attractor of non-integral dimension ; a strange attractor (Ruelle and Takens, 1971).

The viewing (or 'embedding') of chaotic systems in higher dimensions can often

many parameters, and selecting a suitable starting position in parameter space is more difficult. This model was chosen for its illustrative capabilities in demonstrating the principles involved.

The model is initially inverted using Γ=1.0, then when the decrease in the misfit stops or becomes unacceptedly low, Γ is steadily increased. Once escape from a local minima has been achieved, then Γ is reset to 1.0 again and further convergence can occur. This procedure can be repeated until no further improvement is seen. Figure 5.27 shows the misfit as a function of iteration for this problem. The misfit decreases rapidly at first, but then levels out at a value of 92.3 mGals^2 after 15 iterations. After another 15 iterations no further improvement has been achieved, so Γ was increased until the motion became chaotic. When the chaotic trajectory escaped the local minimum and a misfit less than 92.3 mGals^2 was measured Γ was set to 1.0 again and the body converged upon the global minimum in one further iteration. This procedure could be repeated as desired until no further minima were located.

5.10 Conclusions

A method of inducing chaos into the least-squares inversion method was introduced, and the chaos was studied and quantified. The presence of chaos during inversion can be a benefit rather than a drawback. Chaotic inversion can be used as an alternative to the Monte-Carlo technique, wherein the chaotic trajectory is used instead of a random number generator for calculating parameter values. It has the additional advantage that some parameters can be inverted using ridge-regression

Figure 5.25 : Misfit Surface as Reconstructed from a Chaotic Trajectory for the Inversion of Body Position and Angle of Rotation

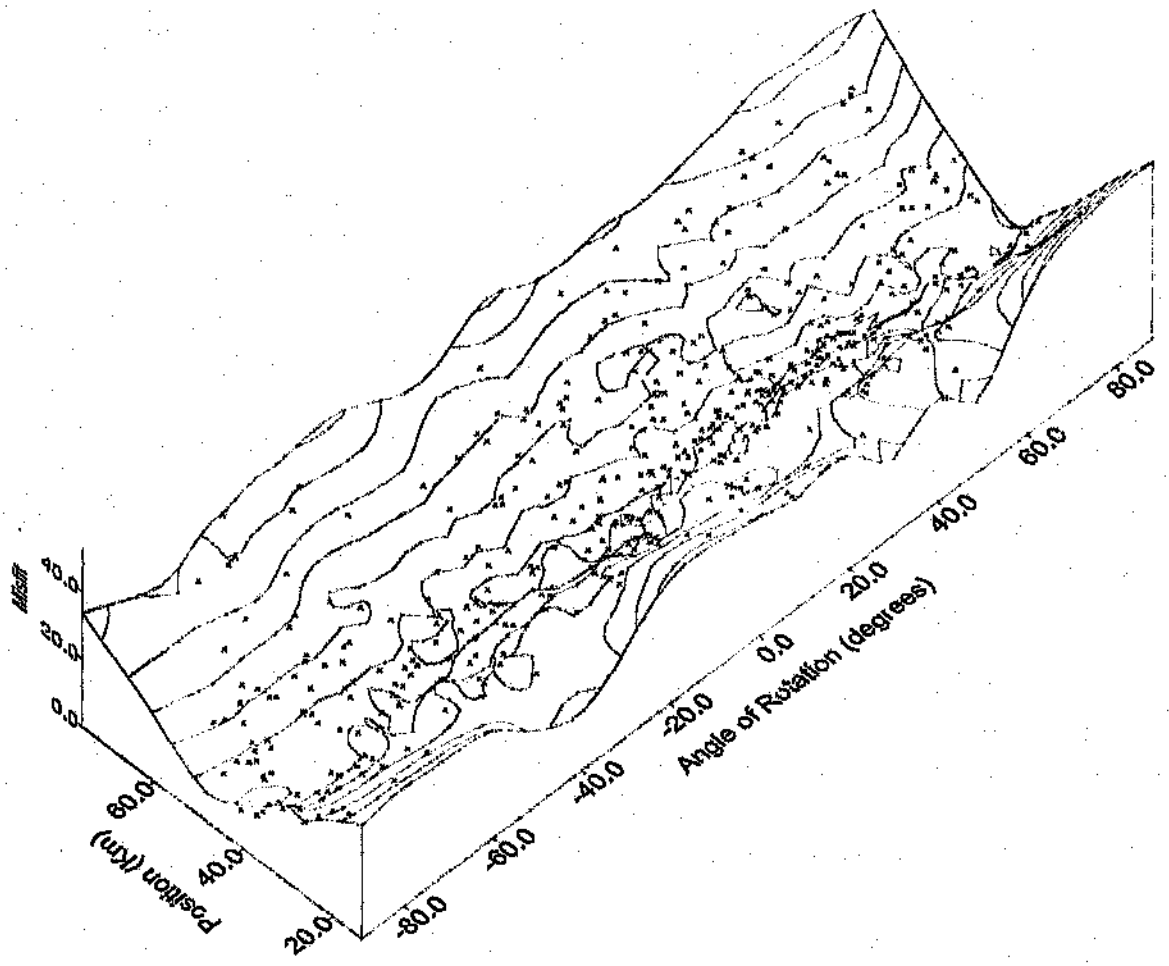

Each point on the trajectory is plotted as a + on the reconstructed misfit surface. The misfit can be seen to be much less sensitive to the angle of rotation of the body than to its position.

Figure 5.24 : Sample Trajectory from the Chaotic Inversion of Body Position and Body Angle for the Model in Figure 5.22

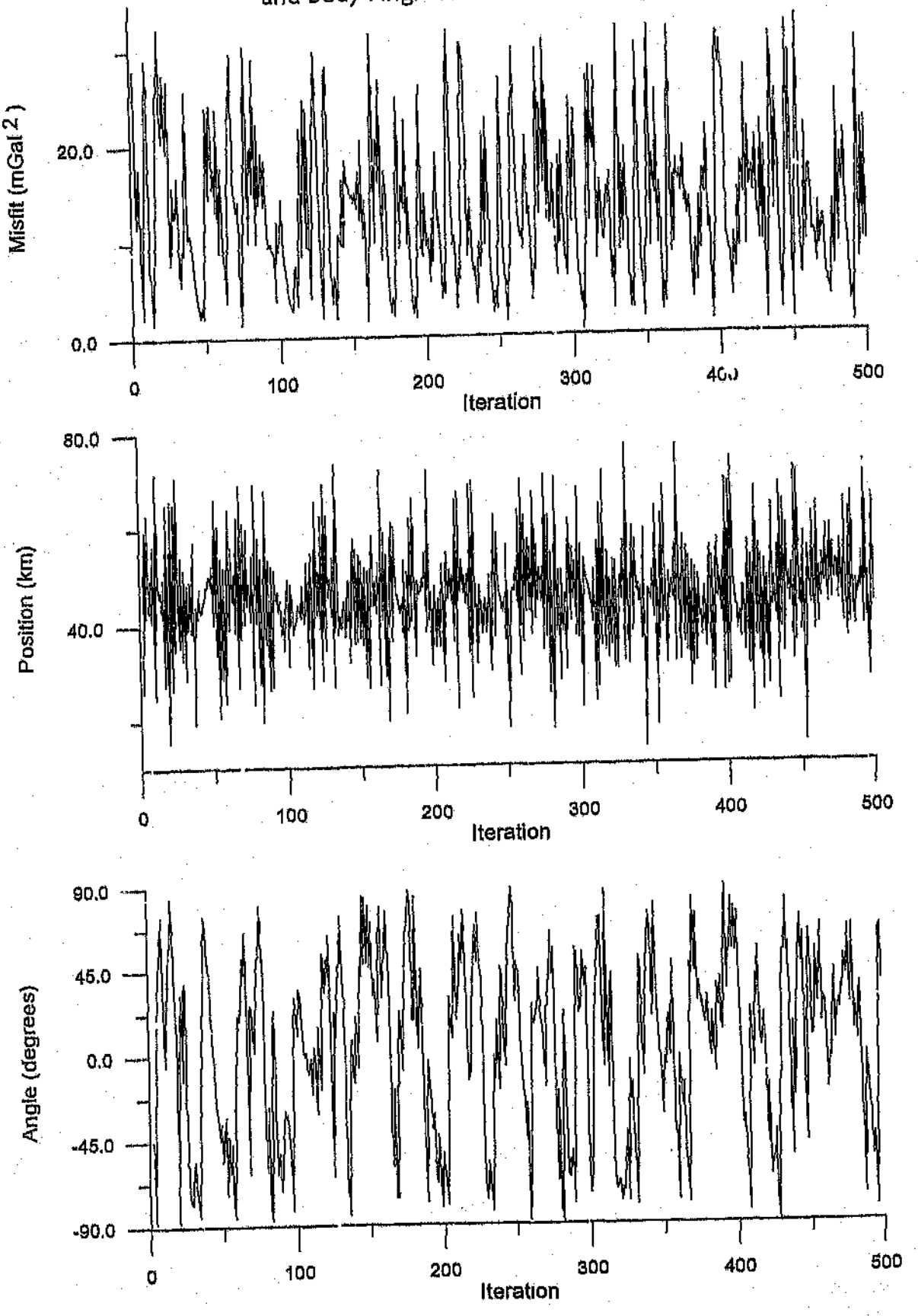

that parameter for some other reason, then Γ_i must be set to 1.0 .

5.9 Using Chaotic Inversion as an Alternative to the Monte Carlo Inversion Technique

Chaotic inversion can be used as an alternative to Monte Carlo inversion (see section 1.6), since the chaotic trajectories replace the random numbers used to determine the parameter values in that method. Figure 5.24 shows a chaotic trajectory from the model in Figure 5.22, and both model parameters can be seen to traverse roughly equivalent amounts of parameter space (due to the aforementioned scaling having been performed). Figure 5.25 shows a plot of the misfit of the points on the trajectory plotted against the parameter values. The misfit is much less sensitive to the angle of rotation of the body than it is to the position of the body. Note that when chaos is occurring both solutions with a very small and a very large misfit will be generated. The data quality does not affect the chaotic behaviour at all, but the larger the Gaussian noise present then the larger the minimum achievable misfit will be. This is true of ridge-regression also.

5.10 Using Chaotic Inversion to Escape Local Minima

The model shown in Figure 5.26 shows two gravity anomalies, one at a position of 300Km and another at 800km. The body shown will move to the anomaly at 300km when its horizontal position is inverted from the starting position of 100km shown. However a lower misfit would be achieved if it was at a position of 800km. One route to get around this problem is to induce chaos into the inversion. In this demonstration situation it would have been easy for the geophysicist to select an improved starting model compared to that shown. However real problems often have

Figure 5.23 : Bifurcation Diagram for the Inversion of Body Position and Angle of Rotation

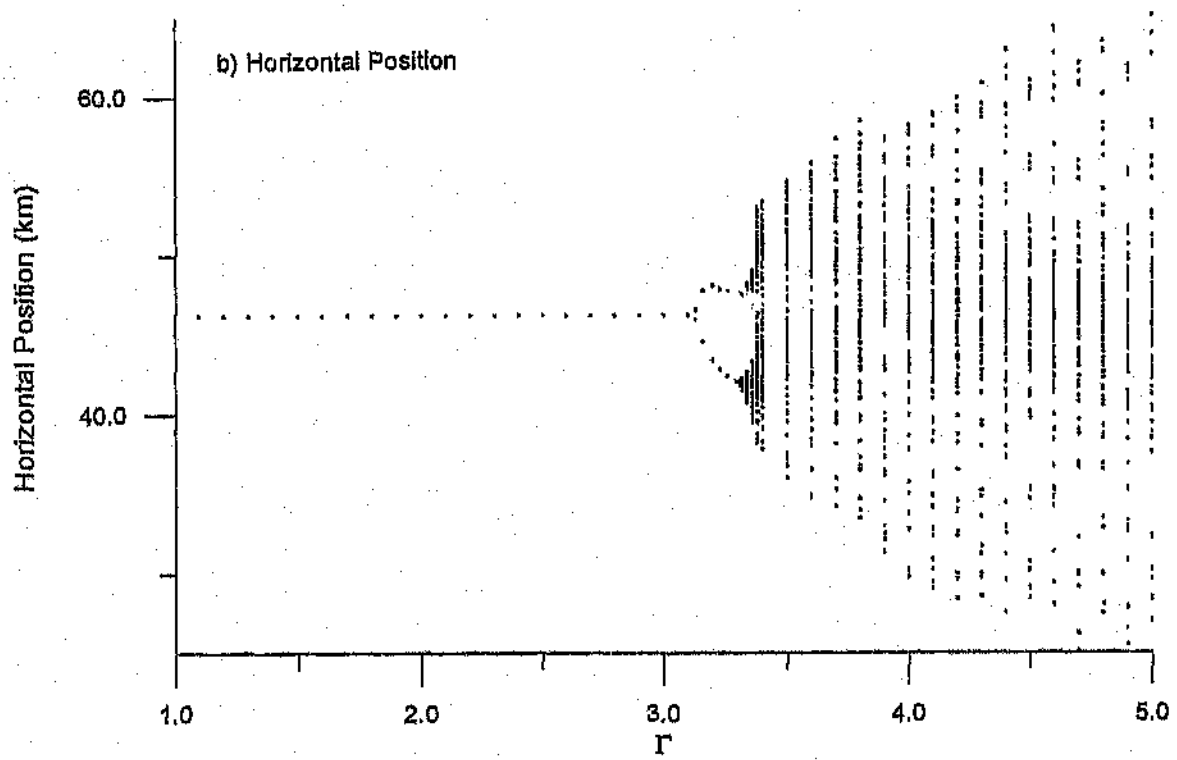

Figure 5.23 : Bifurcation Diagram for the Inversion of Body Position and Angle of Rotation

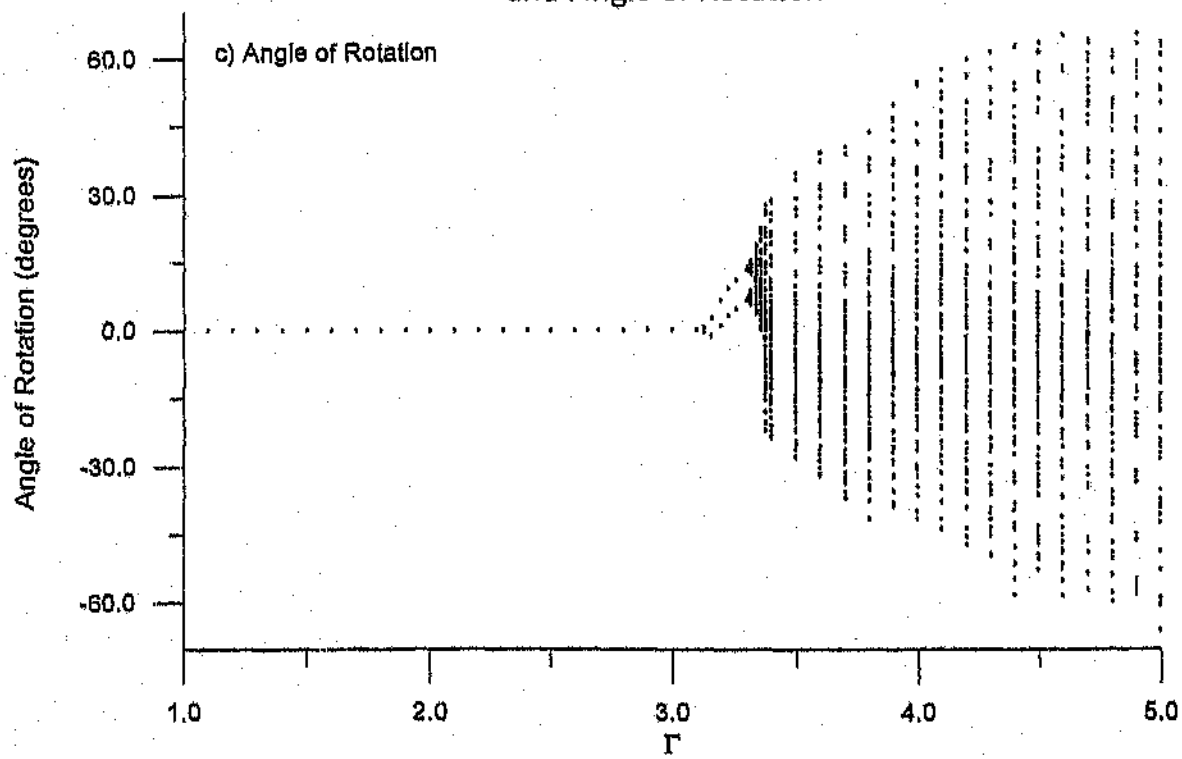

Values were calculated at intervals of $\Gamma = 0.1$, except in the region between $3.1 < \Gamma < 3.4$ where they were calculated at an interval of $\Gamma = 0.02$

Figure 5.22 : Model Used to Demonstrate Simultaneous Chaotic Inversion of Body Position and Angle of Rotation

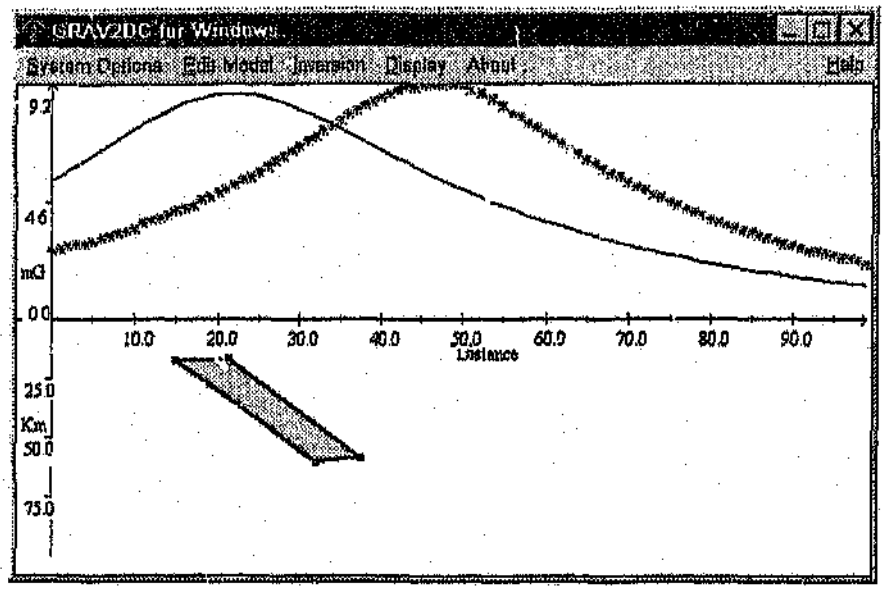

Figure 5.23 : Bifurcation Diagram for the Inversion of Body Position and Angle of Rotation

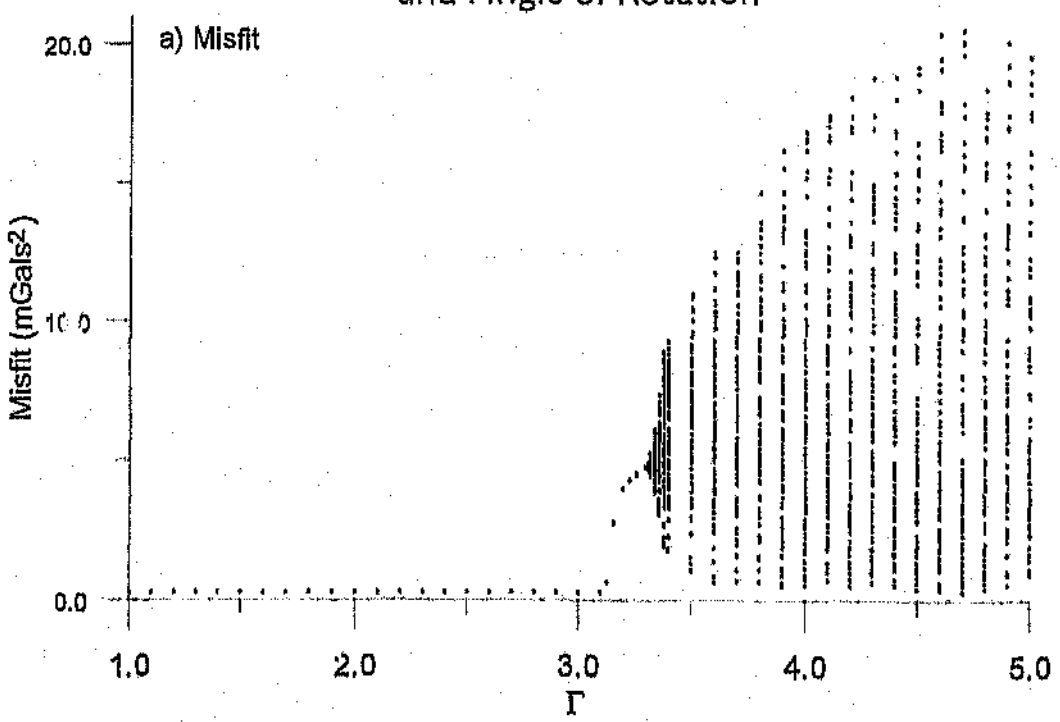

Misfit values were calculated at intervals of $\Gamma = 0.1$, except for the region between $3.1 < \Gamma < 3.4$ where they were calculated at interval of $\Gamma = 0.02$

p.53), which is a measure of the ill-posedness of the solution of the set of linear equations being solved (Dimri 1992, p.126). If the misfit function is much more sensitive to changes in one parameter than in another then the condition number will be large, and problems can occur if its reciprocal approaches the floating point precision of the computer performing the inversion. The scaling process introduces a scaling matrix S, such that :

$$dP_S = S\,dP \qquad (5.20)$$

where dP is the parameter change matrix (see equation 5.1). S can be calculated from :

$$S = diag[(\sum_{i=1}^{n} A_{i_1}^2)^{-1},\ (\sum_{i=1}^{n} A_{i_2}^2)^{-1}] \qquad (5.21)$$

and then the correct value of dP is recovered from the scaled value by (Gibowicz and Kijko 1994, p.56):

$$dP = S^{-1}\,dP_S \qquad (5.22)$$

The starting model shown in Figure 5.22 was inverted with respect to the body position and angle of rotation. Figure 5.23 shows the bifurcation diagram as a function of the body position, angle of rotation and misfit. The scaling has been successful in that bifurcations and chaos occur at almost exactly the same value of Γ for the three variables. Without it, it is possible that the body would (say) behave periodically with respect to body position while maintaining a fixed angle of rotation, or move between two positions of equal misfit on either side of the anomaly peak. If the model response to a parameter is linear, or it is not desired to induce chaos in

Figure 5.21a : Constrained Inversion of Body Horizontal Position

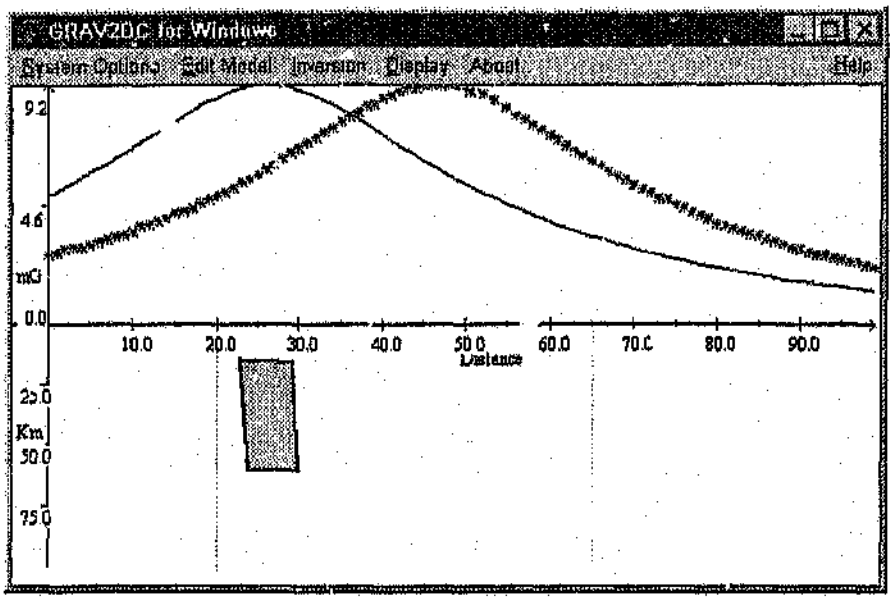

The horizontal position of the body is constrained to lie between the two dotted lines.

Figure 5.21b : Bifurcation Diagram for the Inversion of the Horizontal Position of the Body in the Model Shown in Figure 5.21a

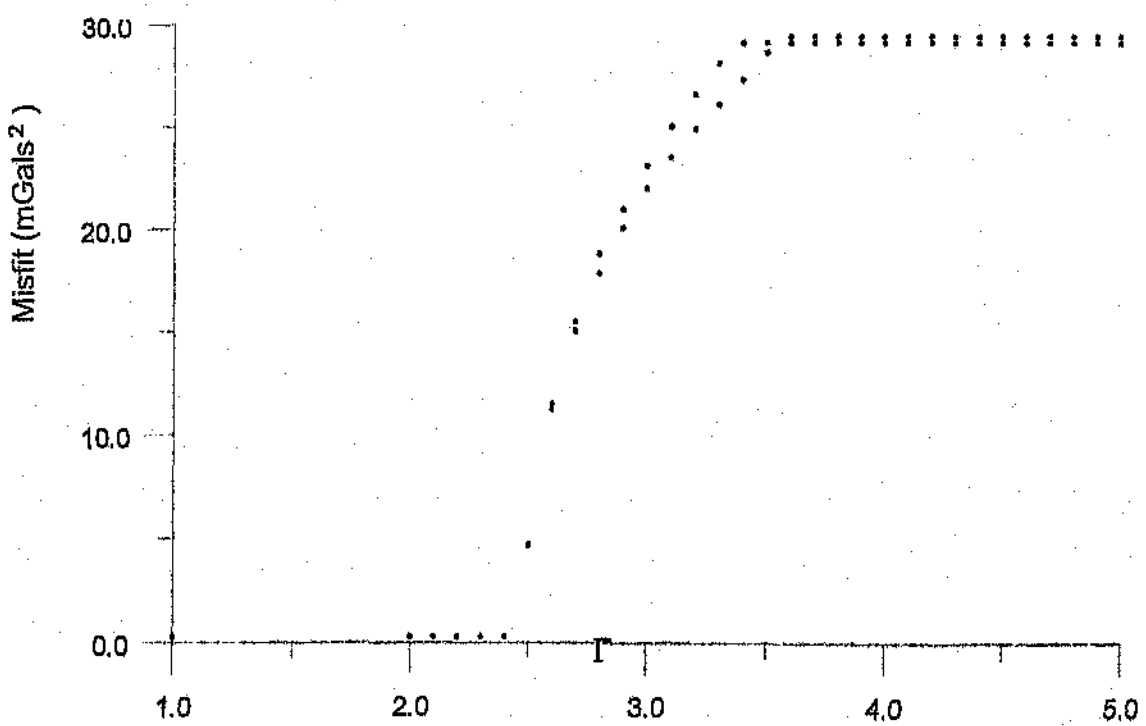

but was not allowed to exceed the limits shown by the dotted lines.

The effect of the constraints was to prevent the chaotic behaviour of the inversion. A plot of the misfit against Γ is shown in Figure 5.21L. As Γ was increased, period-2 behaviour occurred, but chaos was prevented and the body moved back and forth between the two limiting positions. If chaos is to be used to aid in the inversion process, then any constraints must be sufficiently relaxed to permit it to occur. The constraints can be reduced as the inversion proceeds ; if it is seen that chaos is not occurring and that the parameters being inverted are alternating between the upper and lower bounds set for them, then this indicates that the bounds must be changed. This could result in the bounds moving outside the geologically preferred constraints, but this is not a problem since any such solutions that are generated can simply be ignored.

5.8 Inversion of Multiple Parameters Simultaneously

When the horizontal position of the body alone was inverted, the first bifurcation event occurred at Γ=2.5, and chaos occurred when Γ=4.5 . However, when the angle of rotation of the body was inverted, the first bifurcation event only occurred at Γ=12.5, and chaos only when Γ=27.0 (both graphs were produced with the same value of the damping constant k - see equation 5.1). If it is desired to induce chaos simultaneously in a system of multiple parameters then the matrix A must first be centred and scaled correctly. Centering involves subtracting the mean value of each row of the matrix from each element of the row (Gibowicz and Kijko, 1994 p.55). Scaling can reduce the condition number of a matrix (Press et al 1992,

Figure 5.19 : Misfit Bifurcation Diagram for the Model in Figure 5.18
Body Angle of Rotation Being Inverted

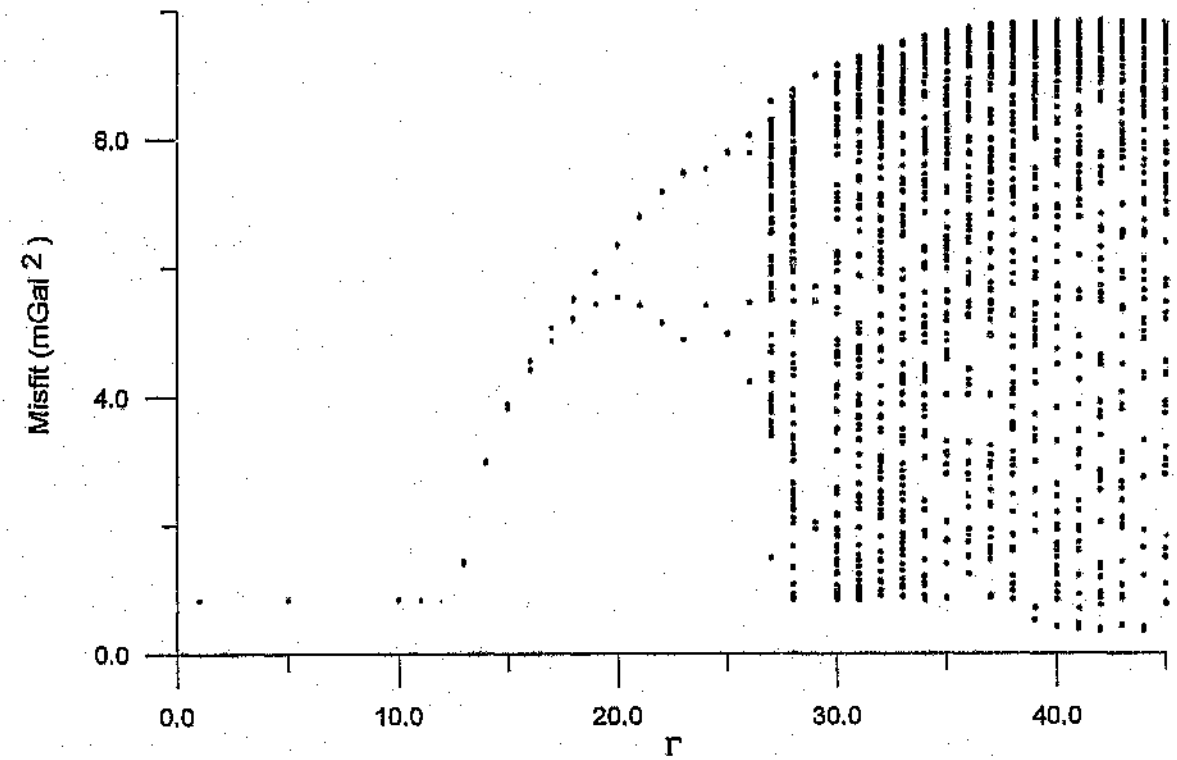

Figure 5.20 : Angle of Rotation Bifurcation Diagram for the Model in Figure 5.19

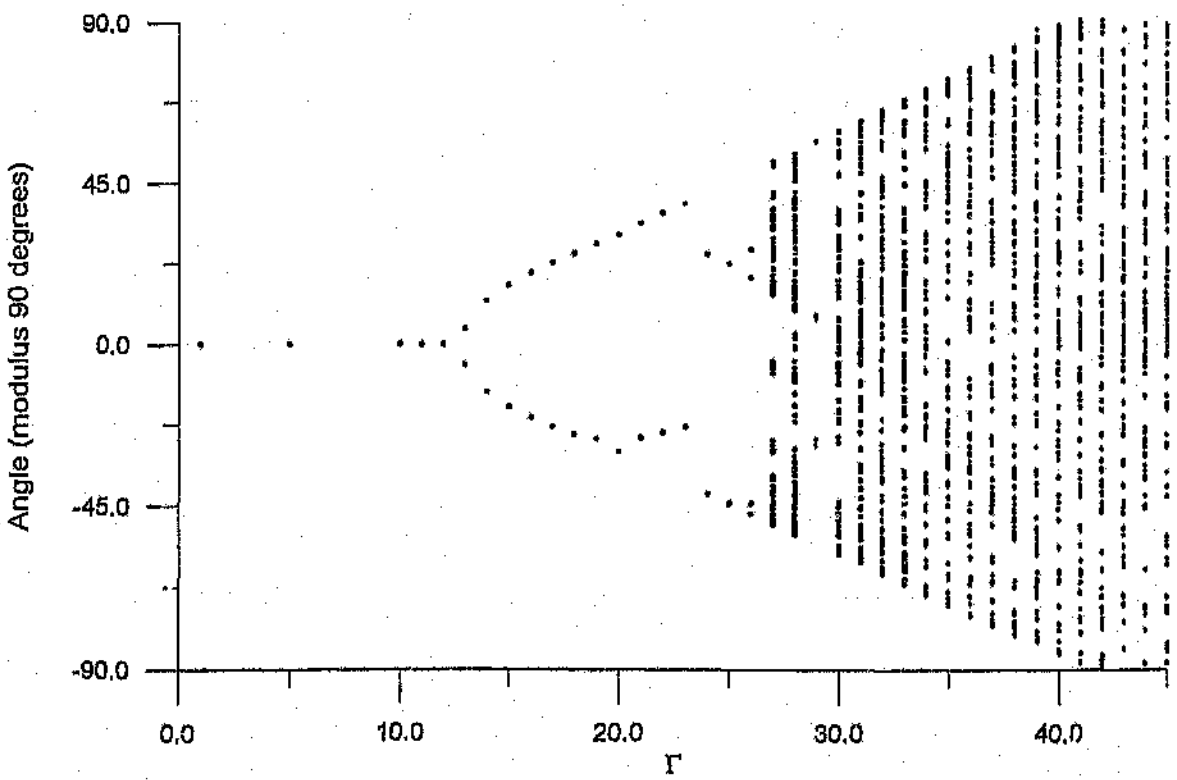

Figure 5.18 : Model Used for Body Rotation Inversion

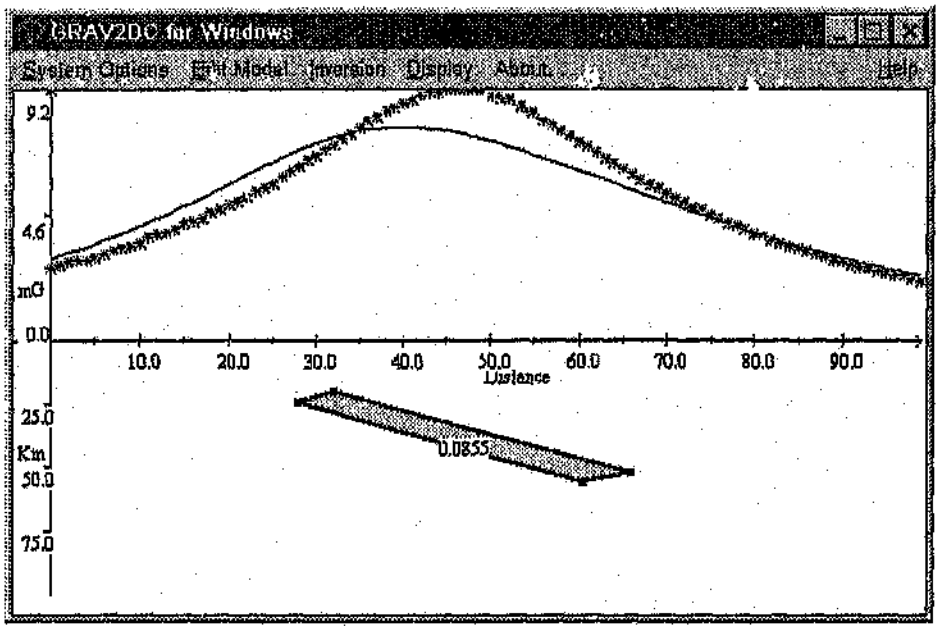

placed in the correct position on the profile and at the correct depth. The body was however rotated by 45 degrees from the correct orientation (as shown in Figure 5.18), and inversion was performed with respect to its angle of rotation (the damping coefficient k was set to 0.5). Bifurcations and chaotic behaviour were observed, and the bifurcation diagrams for both the misfit and the angle of rotation of the body are shown in Figure 5.19 and 5.20.

5.6 Inversion of the Density Contrast of the Body

The chaotic behaviour described above was possible because of the non-linearity of the geophysical response of the model with respect to the parameters under inversion. The density contrast of the body is a linear parameter (see equation 2.4), since doubling it will double the anomaly produced by the body at every point along the profile. Therefore inversion of the model in Figure 5.1b using equation 5.1, with respect to the density contrast, was not expected to produce chaos. The density contrast was set to an initial value of 0.01 $g.cm^{-3}$, which was lower than the correct value, then the inversion was performed. No bifurcations or chaotic behaviour were seen, and when $\Gamma \geq 2.0$ the misfit rose without limit at each iteration.

5.7 Placing Constraints on the Position of the Body

Normally there will be constraints placed on any inversion process by a priori information. In a geological/geophysical situation, the maximum and minimum depths for a body may be known, as might be its maximum and minimum lateral position. In the model used above the body parameters under inversion were not constrained at all. In the model of Figure 5.21a the horizontal position of the body was inverted

Consider the gravity model shown in Figure 6.5 . The application of this method after one inversion iteration of the horizontal position of the body produces an initial estimate for the body's optimum position of 376km compared to the correct position of 400km. Using the model of Figure 6.7 and inverting the body in a vertical plane from a depth of 200km produced an estimated depth of 38.7km compared to the correct depth of 44km. If P_1 and P_2 are close together (compared to the distance to the solution), and hence e_1 and e_2 are similar, then the accuracy of the estimates of a, b, and c will be reduced.

It can be seen that the knowledge of the form of the misfit function can greatly enhance the efficiency of the inversion process.

6.3.2 Effect of Noise

Any noise present will distort the misfit surface and will make the calculation of the correct quadratic function more difficult. However it will also affect the ridge-regression adversely. To test the sensitivity of both methods to noise, the model used above had 50% of uniformly distributed random noise added to each data point, which produced the model shown in Figure 6.8. The same starting positions were used as before, and a comparison of the efficiency of the two techniques is shown in Figure 6.9 for inversion in horizontal and vertical planes. As can be seen, the efficiency of the quadratic function method was unaffected by the noise, while the least-squares inversion took slightly more iterations to converge than in the noise-free case.

Fitting quadratic functions to portions of the misfit surface (rather than to the

the step size to choose. Given two points on the misfit surface and the gradient at one point, then there is a set of three simultaneous equations describing the quadratic function ;

$$\begin{aligned} e_1 &= aP^2_1 + bP_1 + c \\ e_2 &= aP^2_2 + bP_2 + c \\ de/dP\,|_{P_1} = d1 &= 2aP_1 + b \end{aligned} \qquad (6.2)$$

then a, b, and c can be found by solving the simultaneous equations in matrix form ;

$$\begin{vmatrix} P^2_1 & P_1 & 1 \\ P^2_2 & P_2 & 1 \\ 2P_1 & 1 & 0 \end{vmatrix} \begin{vmatrix} a \\ b \\ c \end{vmatrix} = \begin{vmatrix} e_1 \\ e_2 \\ d1 \end{vmatrix} \qquad (6.3)$$

Once a, b, and c are found then the quadratic equation can be solved to give the values of the parameters P for which the misfit e is zero. These are obtained from the familiar ;

$$P_{min} = \frac{-b \pm \sqrt{(b^2 - 4ac)}}{2a} \qquad (6.4)$$

If two iterations of ridge-regression inversion are performed then the gradient information need not be used, but this has a greater computational cost. Note that the misfit need never actually reach zero - the value P_{min} obtained will merely be used to provide an approximation to the actual P_{min}, and will be used in the quadratic inversion method described above. If the roots are complex then their real part will give the position of the minimum.

Figure 6.6 : Comparison of Parabolic Inversion and the Ridge-Regression Technique in the Inversion of Gravity Data

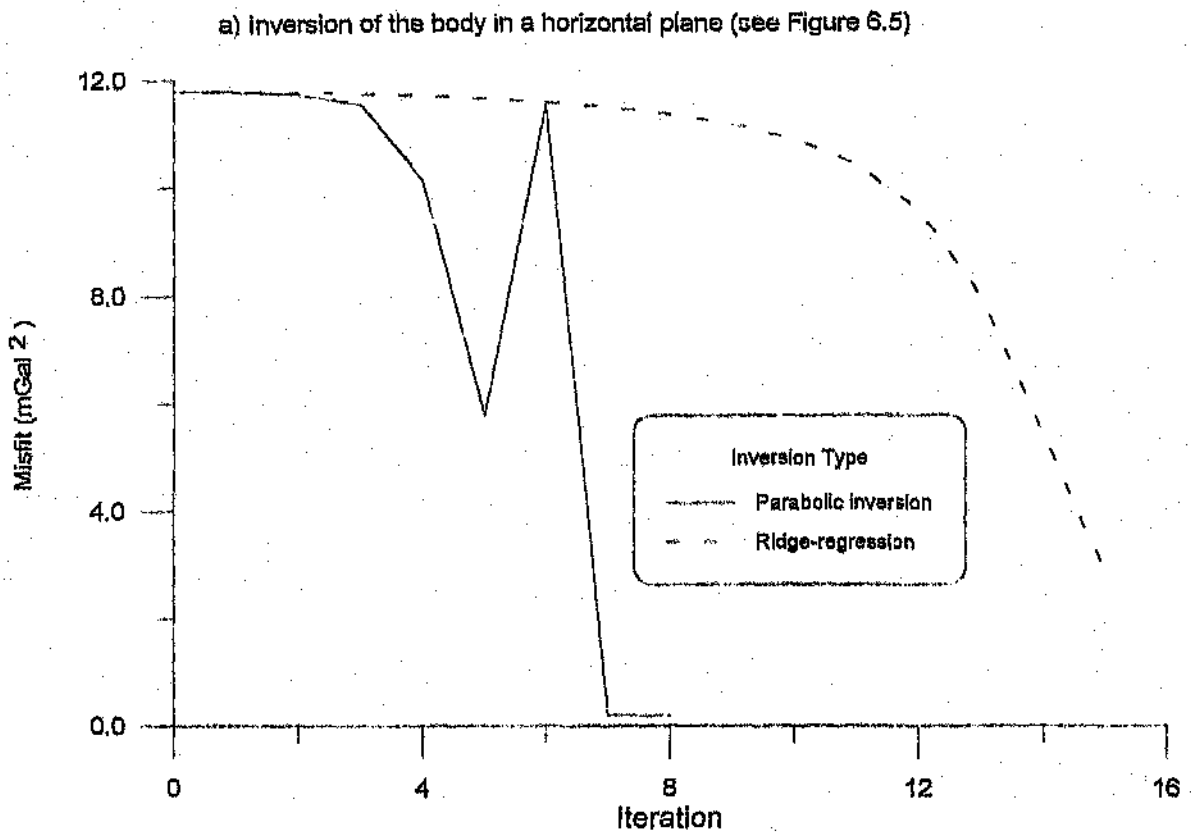

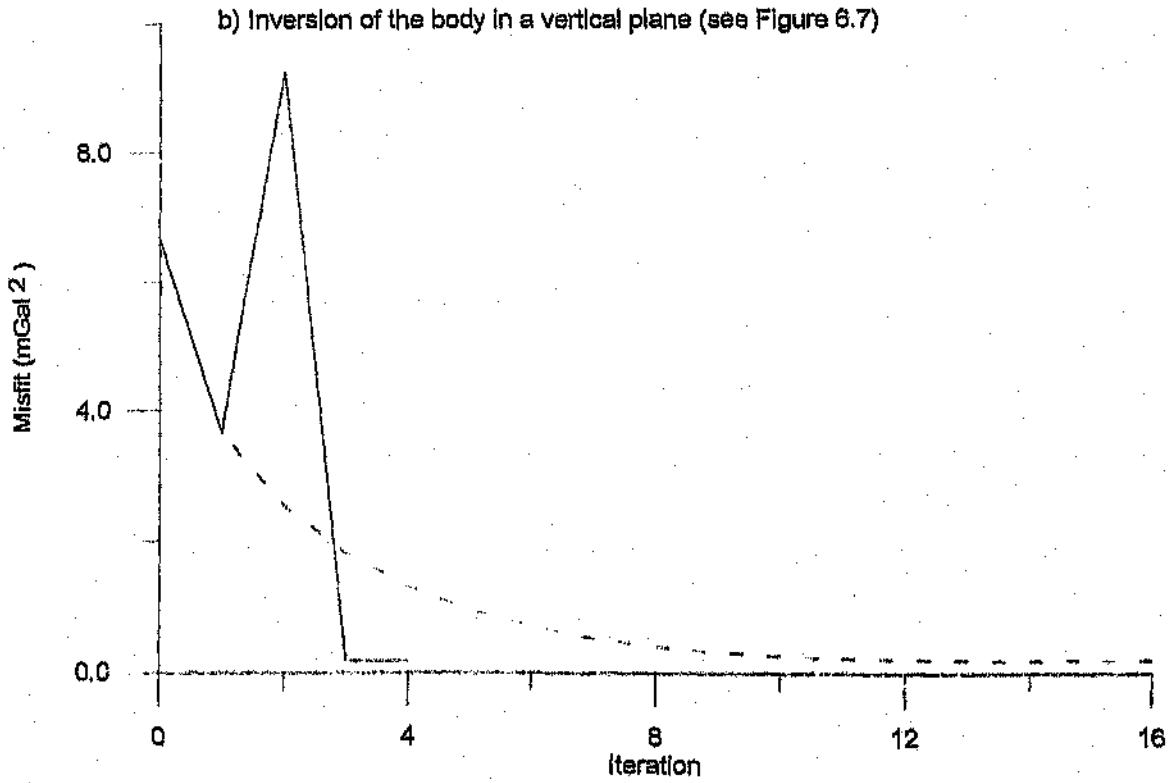

regression method and for the parabolic inversion for the inversion of the body in a horizontal plane. The superiority of the latter can be clearly seen, reaching the minimum in under half the number of iterations of the former. In addition, since all except the initial iteration require only a forward model to be run, the parabolic method is computationally much less demanding. Figure 6.6b shows a comparison of the quadratic approach and ridge-regression inversion when the same model was inverted in a vertical plane (Figure 6.7 shows the starting model used). Again, the quadratic method reached the minimum misfit in under half the number of iterations required by the ridge-regression approach.

6.3.1 Choosing a Step Size

As stated above, after the first least-squares inversion iteration the model parameters were changed by a multiple of the initial change. The size of the step to use can be determined by considering the range of values that the parameter is likely to have. For example, it may be known from borehole information that the depth of the body lies between two depths, or that it cannot lie outside a range of horizontal positions. The size of the step must be chosen such that the range of possible values is covered by sufficient points so as not to miss the minimum of the misfit surface. For the models used above, a step size doubling at each iteration was used. Since the step size is based on the parameter change at the first iteration, if several parameters are being inverted at once then the step sizes will be different for each parameter.

Alternatively, the fact that the flanks of the misfit surface are quadratic in nature can be used as a guide to both the position of the minimum and therefore of

calculated and the inversion uses this as the next improvement to the model. This process can be repeated using the new position on the misfit surface. If necessary, a final ridge-regression inversion iteration can be used to 'tidy up' the parameter value, since the assumption that the surface is of a quadratic form will not be completely accurate (particularly in the presence of noisy data).

To gain more information about the shape of the misfit surface, and to reduce further the computational effort required it is not necessary to perform a full inversion at each iteration. After the first iteration the parameter is changed by a multiple of the previous change, until the misfit increases. At this point the minimum has been overshot. The quadratic form can now be fitted to these data points. The technique is similar to the inverse parabolic interpolation approach used in the minimisation of functions, and will be termed parabolic inversion here. Given three points on the misfit surface, with $e_3 > e_2$ then the position of the minimum is given by (Press et al 1992, p.396) :

$$P_{min} = P_2 - \frac{(P_2 - P_1)^2 (e_2 - e_3) - (P_2 - P_3)^2 (e_2 - e_1)}{2 (P_2 - P_1) (e_2 - e_3) - (P_2 - P_3) (e_2 - e_1)} \quad (6.1)$$

Where there is a misfit e_i at a parameter value P_i.

Figure 6.5 shows a gravity model consisting of a single anomaly. The body has the correct shape and other parameters to fit the data but the horizontal position is incorrect. Figure 6.6a shows the misfit as a function of iteration for the ridge-

Figure 6.4 : Quadratic Fit to a Schematic Misfit Surface

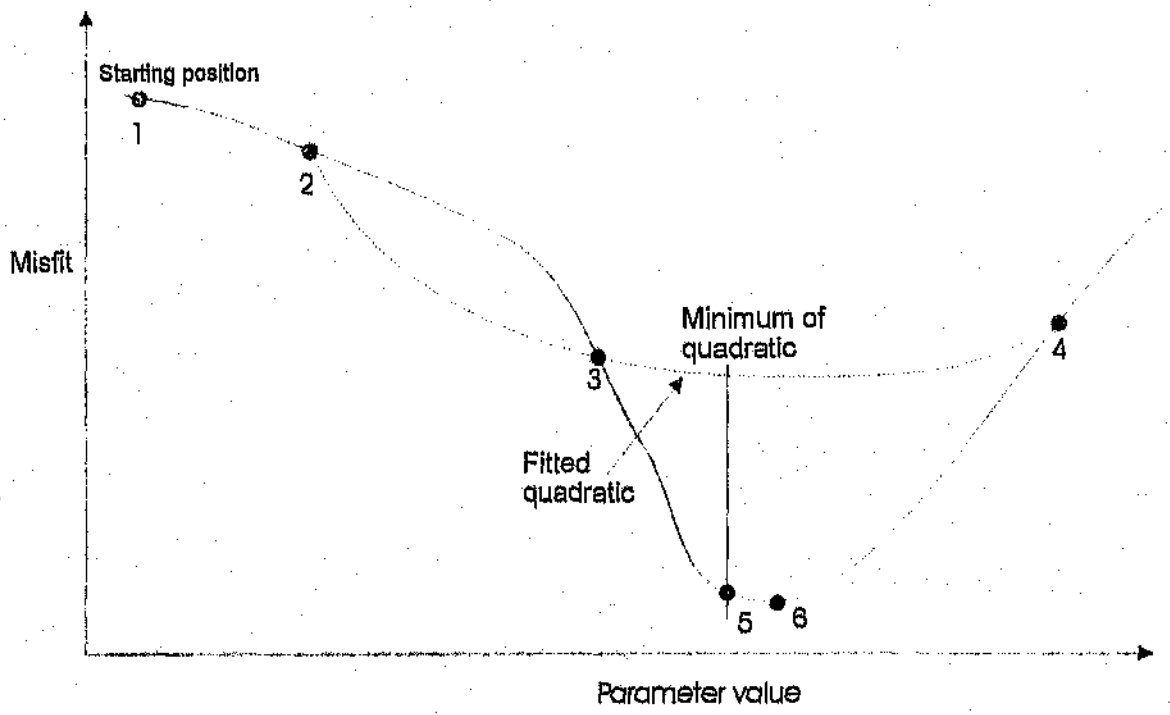

The inversion starts at point 1, then proceeds to point 2 by the use of ridge-regression inversion. The distance from point 2 to point 3 is a multiple of this initial move, as is point 4, which overshoots the minimum.

Point 5 is at the parameter value corresponding to the minimum of the quadratic generated from points 2, 3, and 4. Motion from point 5 to point 6 proceeds either via a another quadratic fit or a final ridge-regression inversion iteration.

Figure 6.5 : Gravity Model Used for Body Horizontal Position Inversion

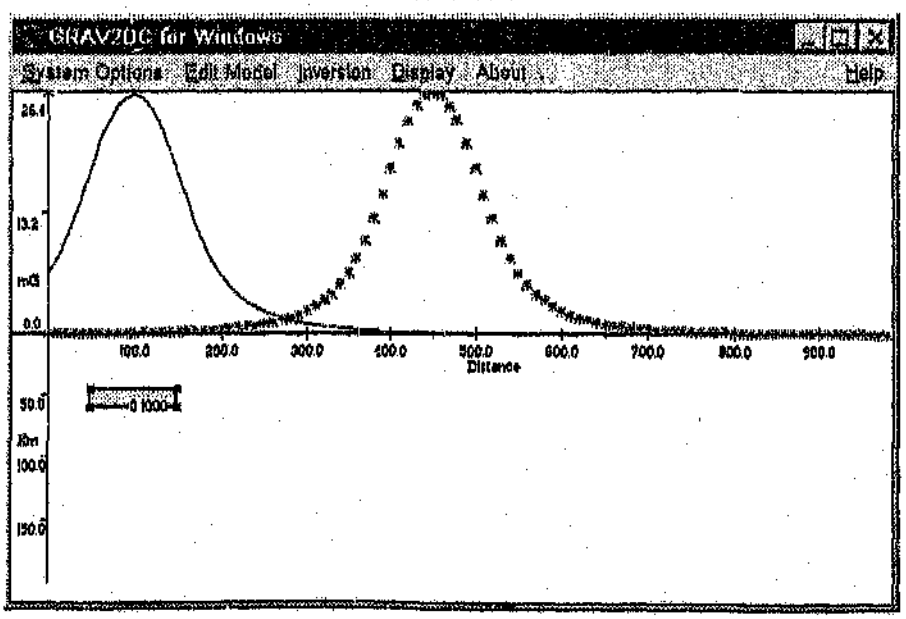

Figure 6.3 : Example Misfit Surfaces for Three Parameters in the Inversion of a Gravity Model

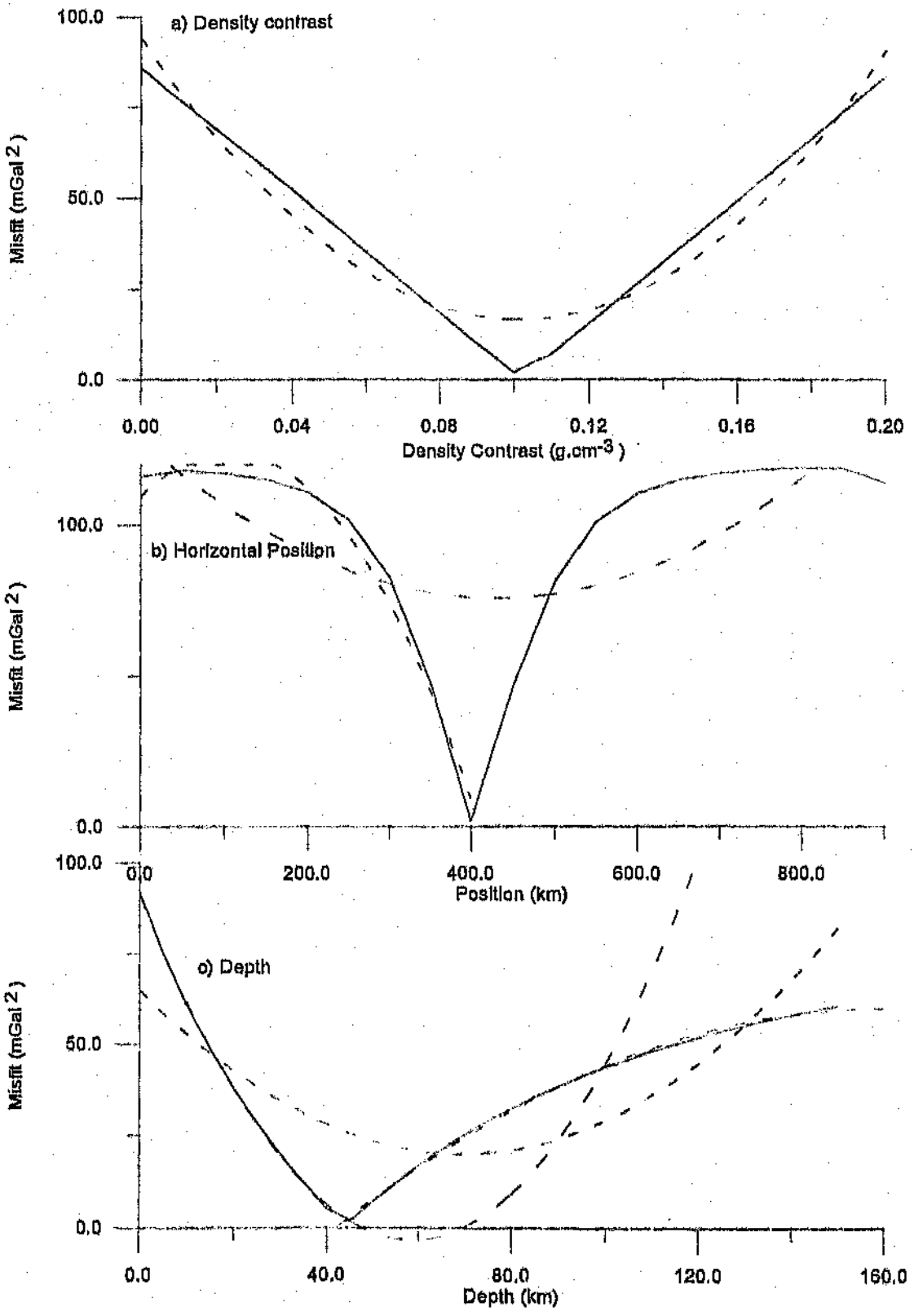

The dashed lines show quadratic functions that have been fitted to portions of the misfit surface, which is shown as a solid line.

quadratic fit, which, although matching the limbs of the misfit surface badly, nevertheless has a minimum in the same position as the surface does.

Figure 6.3b shows the misfit surface for the situation when the horizontal position of the body is being inverted. Quadratic functions have been fitted to the left limb of the curve and to the whole curve. The latter, while being a bad fit to the surface, again has a minimum in approximately the correct position on the profile. The former function is a good fit to the data (correlation coefficient R^2=0.98), and could therefore be used to estimate the position of the minimum, if it could be determined.

Figure 6.3c shows the misfit surface for the situation when the vertical position of the body is being inverted. Quadratic functions have been fitted to both limbs of the curve and to the curve as a whole. The latter, while again being a poor fit to the surface, again has a minimum close to the correct depth. The individual limbs of the surface are well approximated (R^2=0.999) by the quadratic functions.

6.3 Improving Convergence by Fitting Quadratic Functions to the Misfit Surface

Consider the inversion of a single model parameter, as shown in Figure 6.4 . If the inversion starts at the position shown then it will creep its way down the surface, eventually reaching the minimum after a number of iterations. However if the form of the surface was known then the position of the minimum could be found at once. Therefore the procedure is to use the information from each iteration - namely the value of the misfit for a given value of the parameter - to reconstruct the form of the surface. The parameter value that corresponds to the minimum is then

Figure 6.1 : Schematic Misfit Surface for the Case When Two Model Parameters are Inverted

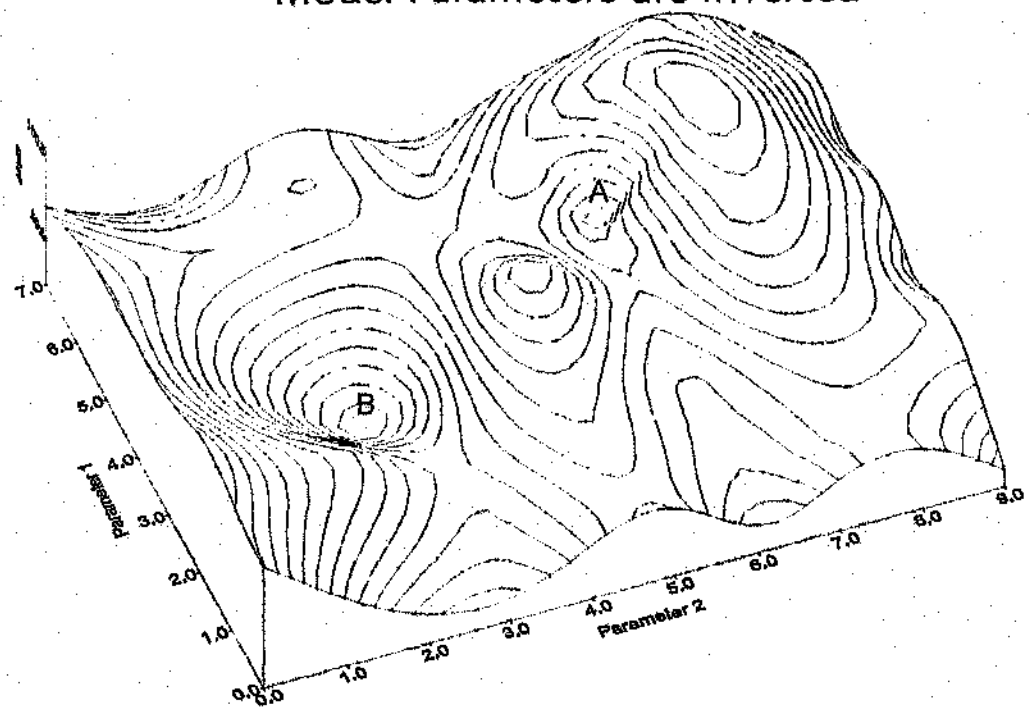

The inversion can get trapped in the minimum at A, but the minimum at B is deeper.

Figure 6.2 : Example Gravity Model

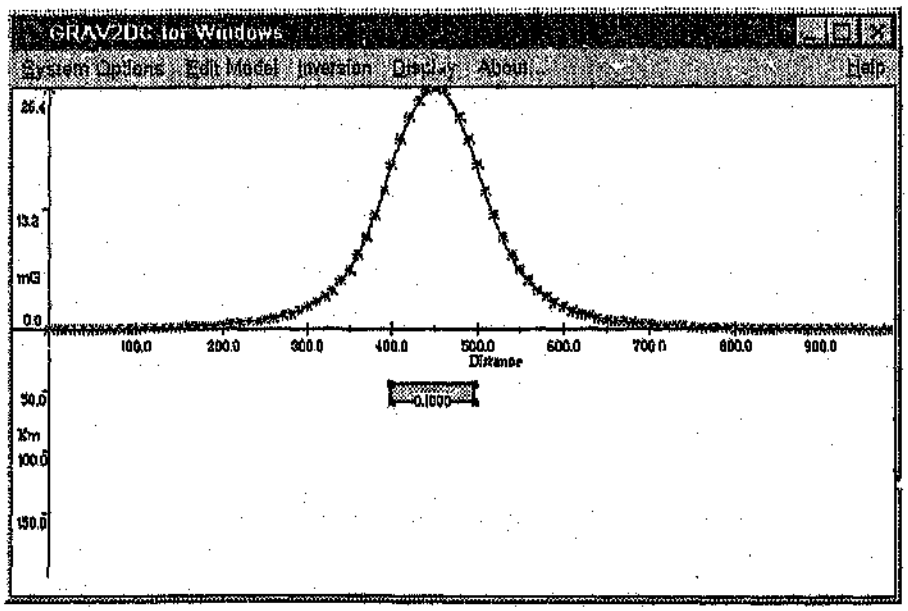

The rectangular body is shown in the lower half of the plot, and the calculated anomaly is the solid line in the upper half. The observed field data is the line of asterisks shown.

CHAPTER 6 : PROPERTIES OF THE MISFIT SURFACE

6.1 Introduction

The inversion methods described previously (such as Gauss-Newton and ridge-regression) seek to improve the model iteratively, given a parameter whose response is non-linear. The calculation improvement at each stage is based on the local gradient of the misfit surface (see equation 1.2), and uses no information at all from the previous iterations. This information can be extremely useful, however, since if the shape of the misfit surface was known then the inversion problem would be solved. While the misfit surface can be arbitrarily complicated, it can in practice be well approximated locally by a quadratic form, (Menke, 1989 p.154). When several parameters are being inverted then the surface as a whole can be approximated by a set of interconnected paraboloid regions. Figure 6.1 shows a schematic misfit surface for the situation when two model parameters are being inverted..

The aim of using information about the misfit surface was twofold ; firstly to improve the speed of convergence of the inversion, and secondly to determine whether there might be another minimum (possibly a deeper one) adjacent to the one that the inversion has just converged to.

6.2 Misfit Surfaces

The misfit surface for the gravity model shown in Figure 6.2 is shown in Figure 6.3a for the situation when the body density contrast is being inverted. The surface is seen to be almost linear, although Menke (1989, p.154) states that the misfit for the linear case is always a paraboloid. Superimposed on the misfit surface is a

while others are simultaneously in a chaotic state. This is accomplished by setting Γ_i = 1.0 for the former parameters and adjusting it to produce chaos for the latter parameters. This can be performed with one simple algorithm (equation 5.1), and does not require a complicated integration of equation 1.9 and a Monte-Carlo scheme.

Chaos can also be used to help solve local minima problems. Once ridge-regression has ceased to provide any further reduction in the misfit, the inversion can be made chaotic, thereby pushing it out of the minima. If it reaches a position in parameter space of lower misfit than that reached previously then Γ is set to the identity matrix and ridge-regression takes over again. This procedure can be repeated until no further improvement is achieved.

Figure 5.26 : A Local Minimum Problem

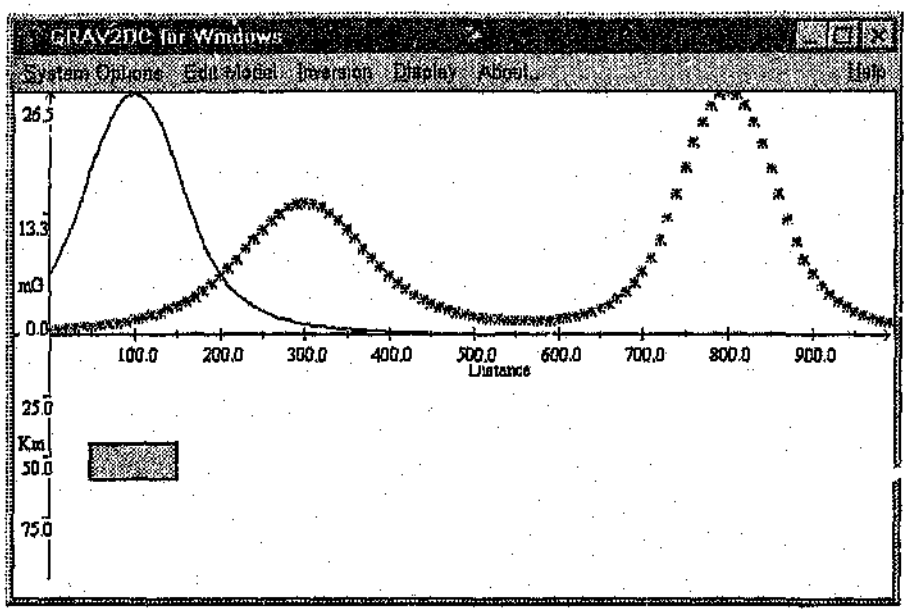

When the body's horizontal position is inverted from this starting position it will move to the minimum at 300Km rather than the deeper minimum at 800Km.

Figure 5.27 : Using Chaos to Escape a Local Minimum Problem (see Figure 5.26)

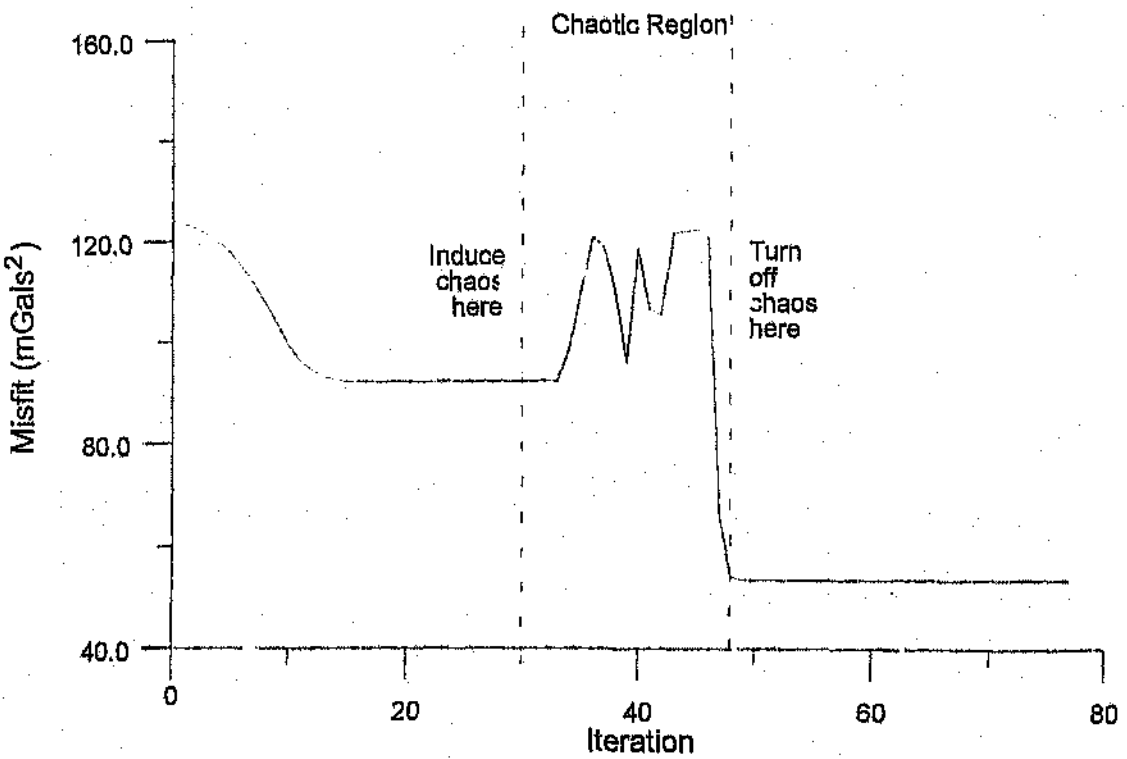

Figure 6.16 shows the solution of these equations for three data points and two gradients from the inversion of the model in Figure 6.13, and while the shape of the polynomial is not a completely accurate representation of the misfit surface, the presence of another minimum has been correctly predicted and an approximate location given (just over 600km). Since the misfit cannot be negative the position at which it becomes zero is used as an approximation to the position of the minimum. The inversion then converged from this point to the global minimum at a position of 750km. The points used and the fitted quartic are shown It was found beneficial to use the data points at the beginning, end, and at an intermediate point, together with gradients measured at both ends. However if the model starting position is too close to the position of the local minimum then the points on the misfit surface will contain little information on the other minimum, and any estimate of its position is likely to be inaccurate.

As a second example, the model shown in Figure 6.17 was used. All of the model parameters were correct except for the angle of rotation of the body. The misfit surface for the angle of rotation is shown in Figure 6.18, and it can be seen that there are two minima, one at 360.0 degrees and the other at 180.0 degrees. Due to the asymmetry in the shape of the body, the minima are not equally deep however. The body angle was inverted from a starting position of 260.0 degrees, from which it moved to the local minimum at 180.0 degrees. Three points (the beginning, the end, and an intermediate point) together with two gradients (measured at the beginning and the end) were used, and a quartic fitted through them. The fitted quartic had a predicted global minimum at 323.7 degrees. Ridge-regression inversion

Figure 6.14 : Misfit as a Function of Horizontal Position for the Model in Figure 6.13

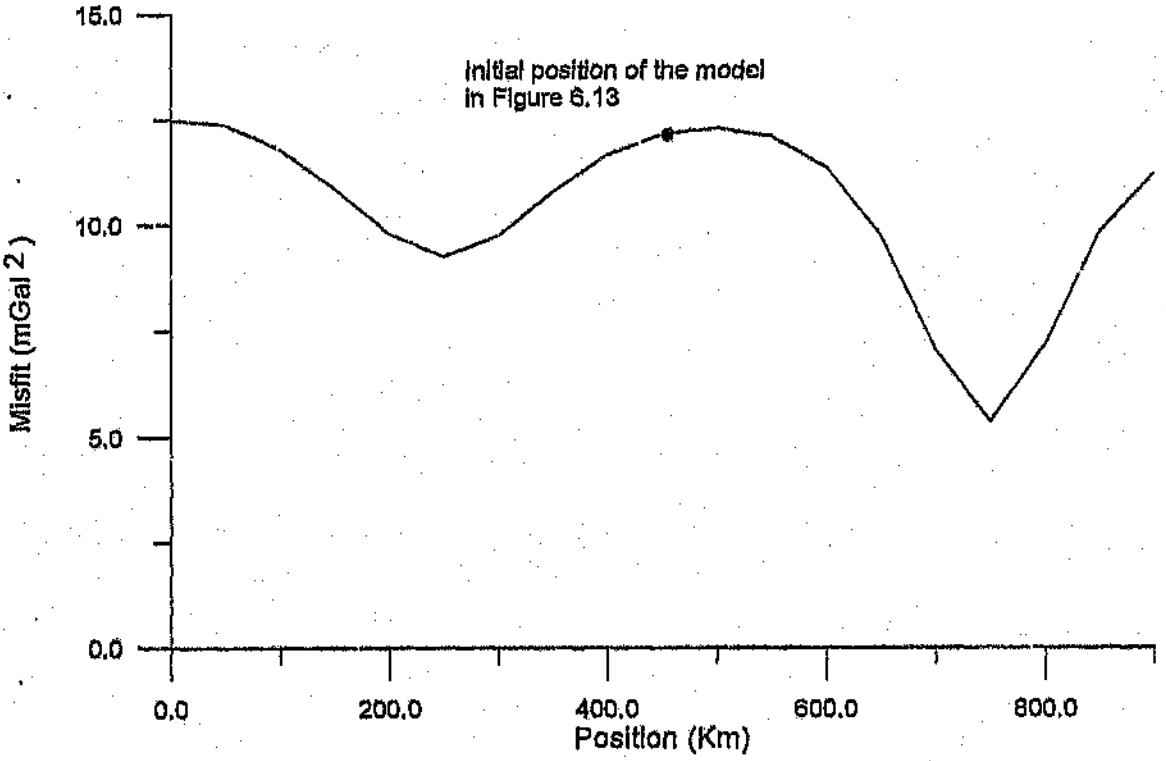

Figure 6.15 : Quartic fit to Misfit Surface

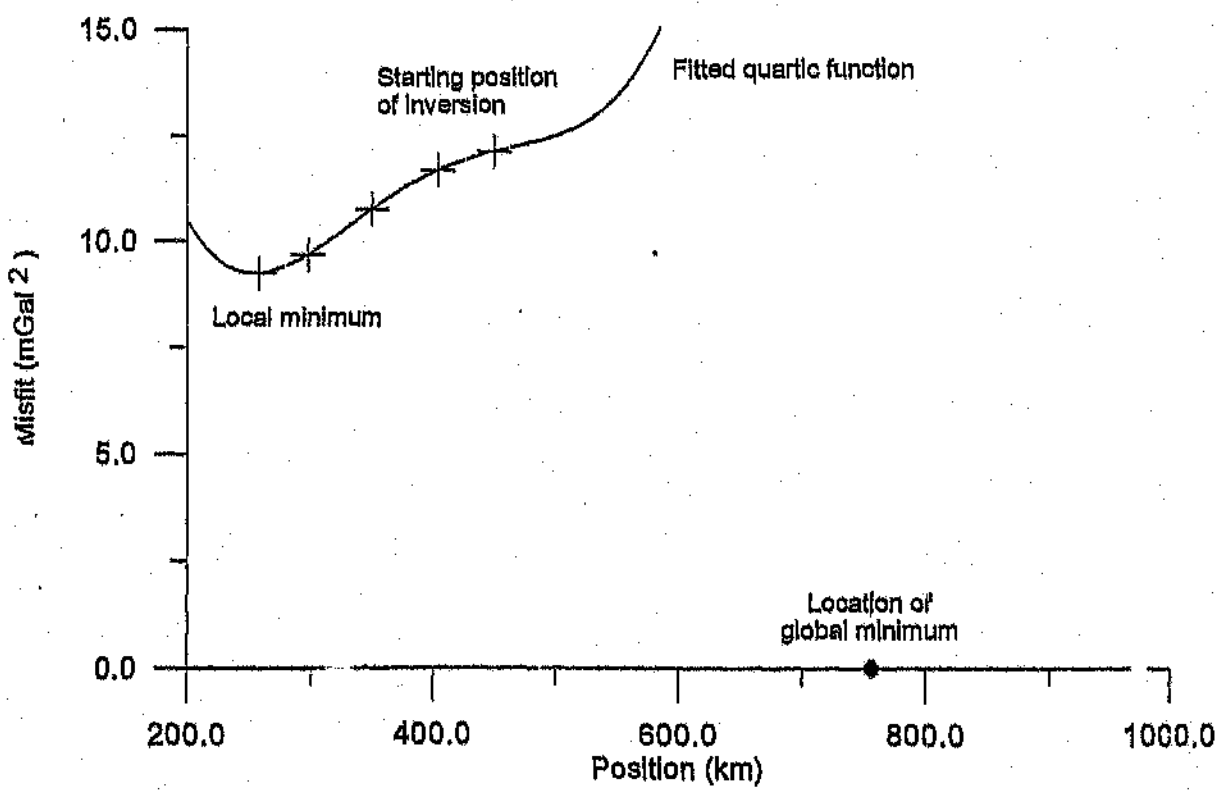

,and given 5 or more points then ;

$$y_1 = a + bx_1 + cx_1^2 + dx_1^3 + ex_1^4 \quad (6.7)$$

$$y_2 = a + bx_2 + cx_2^2 + dx_2^3 + ex_2^4$$

$$\vdots \qquad \vdots \quad \vdots \quad \vdots$$

$$y_5 = a + bx_5 + cx_5^2 + dx_5^3 + ex_5^4$$

,which can be placed in matrix form and solved to give the coefficients a,b,c,d,e .

$$\begin{vmatrix} 1 & x_1 & x_1^2 & x_1^3 & x_1^4 \\ 1 & x_2 & x_2^2 & x_2^3 & x_2^4 \\ 1 & x_3 & x_3^2 & x_3^3 & x_3^4 \\ 1 & x_4 & x_4^2 & x_4^3 & x_4^4 \\ 1 & x_5 & x_5^2 & x_5^3 & x_5^4 \end{vmatrix} \begin{vmatrix} a \\ b \\ c \\ d \\ e \end{vmatrix} = \begin{vmatrix} y_1 \\ y_2 \\ y_3 \\ y_4 \\ y_5 \end{vmatrix} \quad (6.8)$$

However this can prove unsatisfactory, as shown in Figure 6.15, where no second (and deeper) minimum is predicted. Use of the information of the gradient at each position can remedy this problem. Differentiating equation 6.6 with respect to x gives ;

$$dy/dx = b + 2cx + 3dx^2 + 4ex^3 \quad (6.9)$$

,and some of the rows in the matrices in equation 6.8 can be replaced (in this case the last two) with terms from equation 6.9 ;

$$\begin{vmatrix} 1 & x_1 & x_1^2 & x_1^3 & x_1^4 \\ 1 & x_2 & x_2^2 & x_2^3 & x_2^4 \\ 1 & x_3 & x_3^2 & x_3^3 & x_3^4 \\ 0 & 1 & 2x_4 & 3x_4^2 & 4x_4^3 \\ 0 & 1 & 2x_5 & 3x_5^2 & 4x_5^3 \end{vmatrix} \begin{vmatrix} a \\ b \\ c \\ d \\ e \end{vmatrix} = \begin{vmatrix} y_1 \\ y_2 \\ y_3 \\ dy/dx|_{x4} \\ dy/dx|_{x5} \end{vmatrix} \quad (6.10)$$

Figure 6.13 : Local Minimum Problem

a) Model used for Inversion

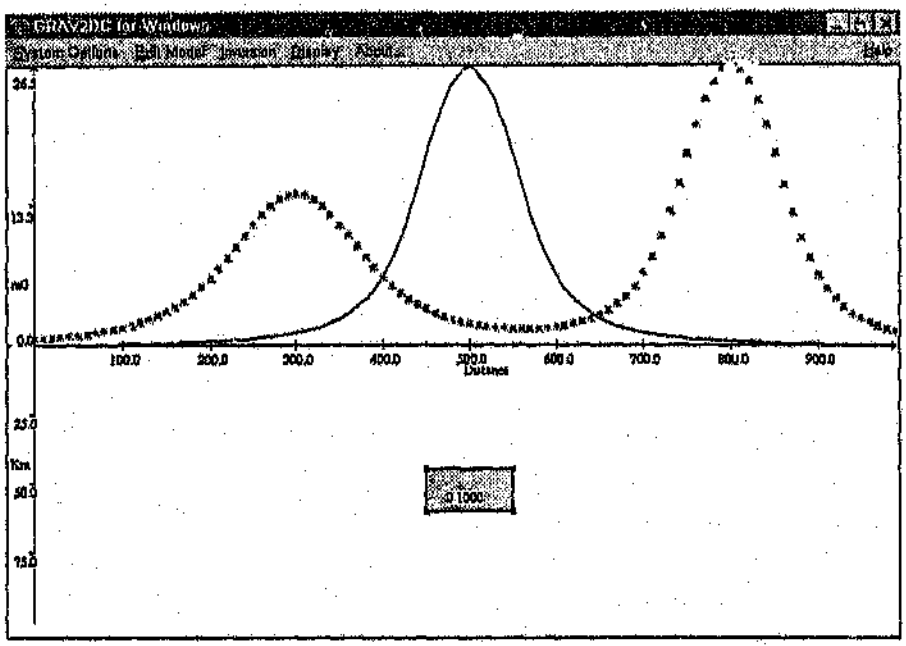

b) Model used to generate observed data in a)

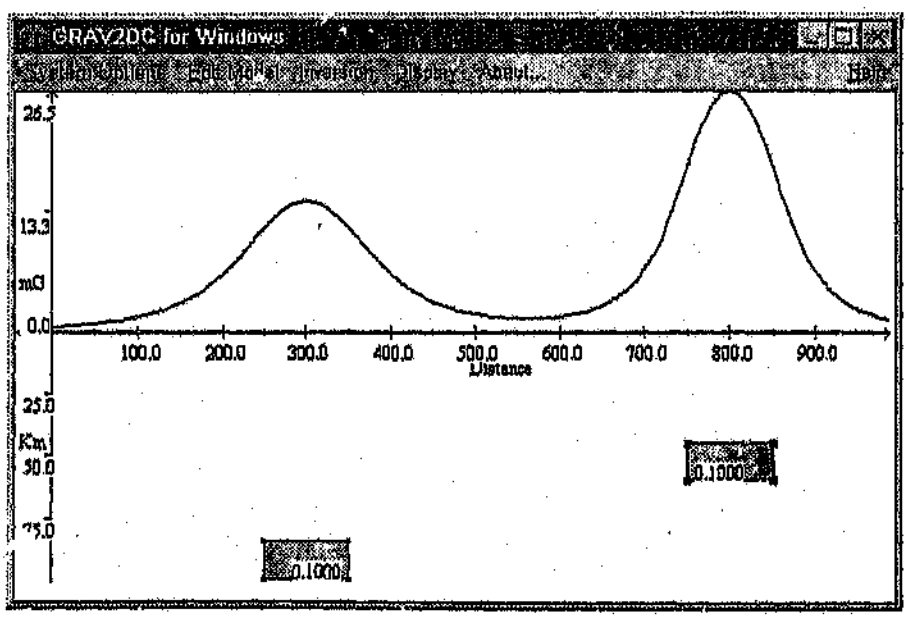

of the body being inverted together with its horizontal position. The comparison of ridge-regression inversion and parabolic interpolation for this case is shown in Figure 6.12. Again parabolic interpolation can be seen to out perform the ridge-regression inversion, particularly when the fact that each iteration of the former is computationally far less demanding than that of the latter, requiring only a forward model to be run and (for the latter iteration) a parabola to be fitted, is taken into account.

6.5 Avoidance of Local Minima

The optimisation scheme described in 6.3 is as likely to become trapped by local minima as any of the inversion techniques described in chapter 1 (apart from the Monte Carlo method). However, if the assumption of the quadratic form of the misfit surface around a minimum is correct, then the general form of any neighbouring minimum is also known. Figure 6.13a shows a situation where the body, when inverted in a horizontal plane from the starting position shown, will converge on the local minimum at a position of 250km rather than on the global minimum at 750km. The model used to generate the observed data used is shown in Figure 6.13b, and the misfit surface is shown in Figure 6.14 .

If both minima have a quadratic form, then their combination produces a quartic equation ;

$$y = a + bx + cx^2 + dx^3 + ex^4 \qquad (6.6)$$

Figure 6.12 : Comparison of the Ridge-Regression and Parabolic Inversion Techniques in the Inversion of Body Horizontal Position and Angle of Rotation for a Gravity Model

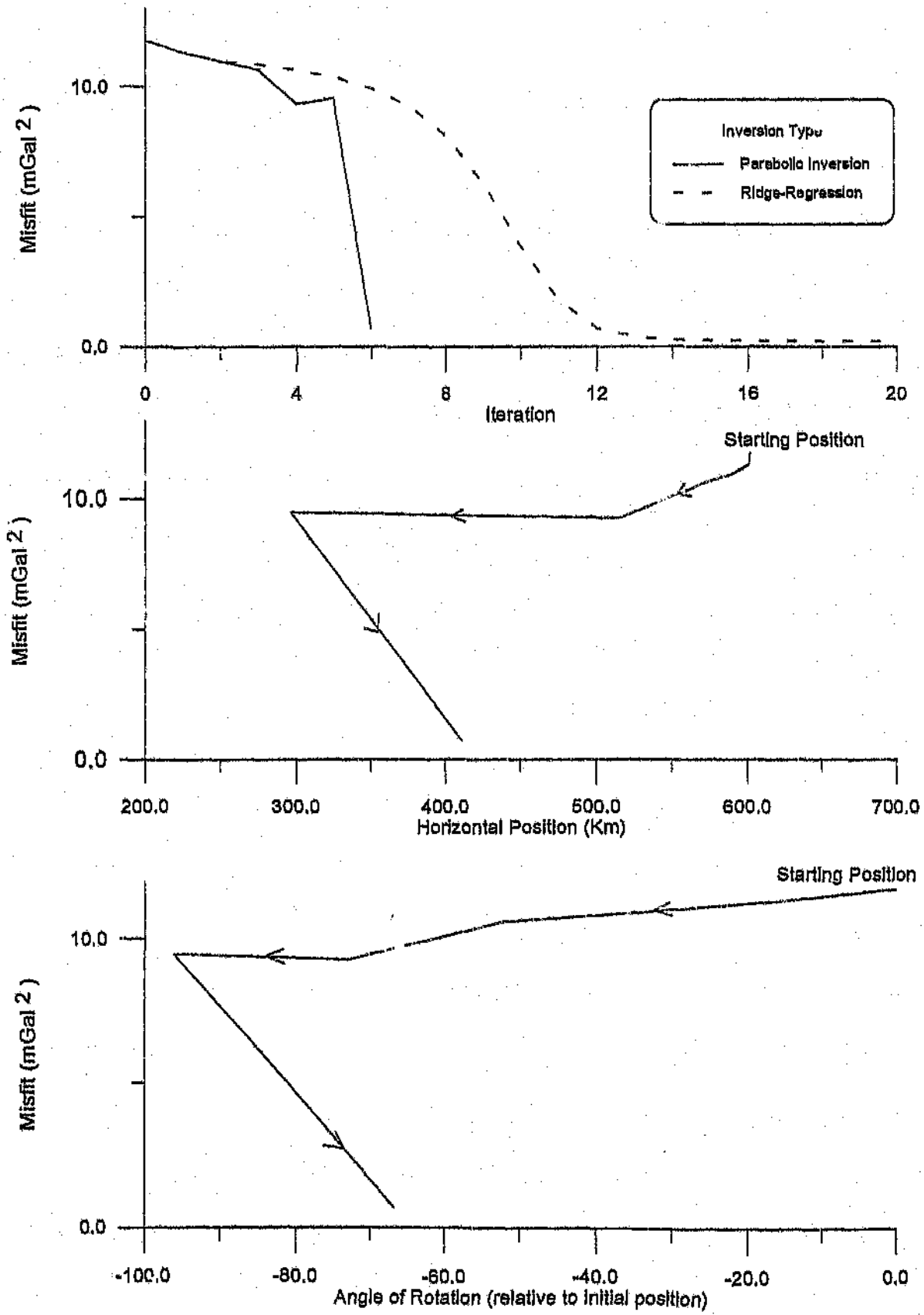

Figure 6.11 : Comparison of Parabolic Inversion and Ridge-Regression Inversion for the Inversion of Body Position and Depth in a Gravity Model

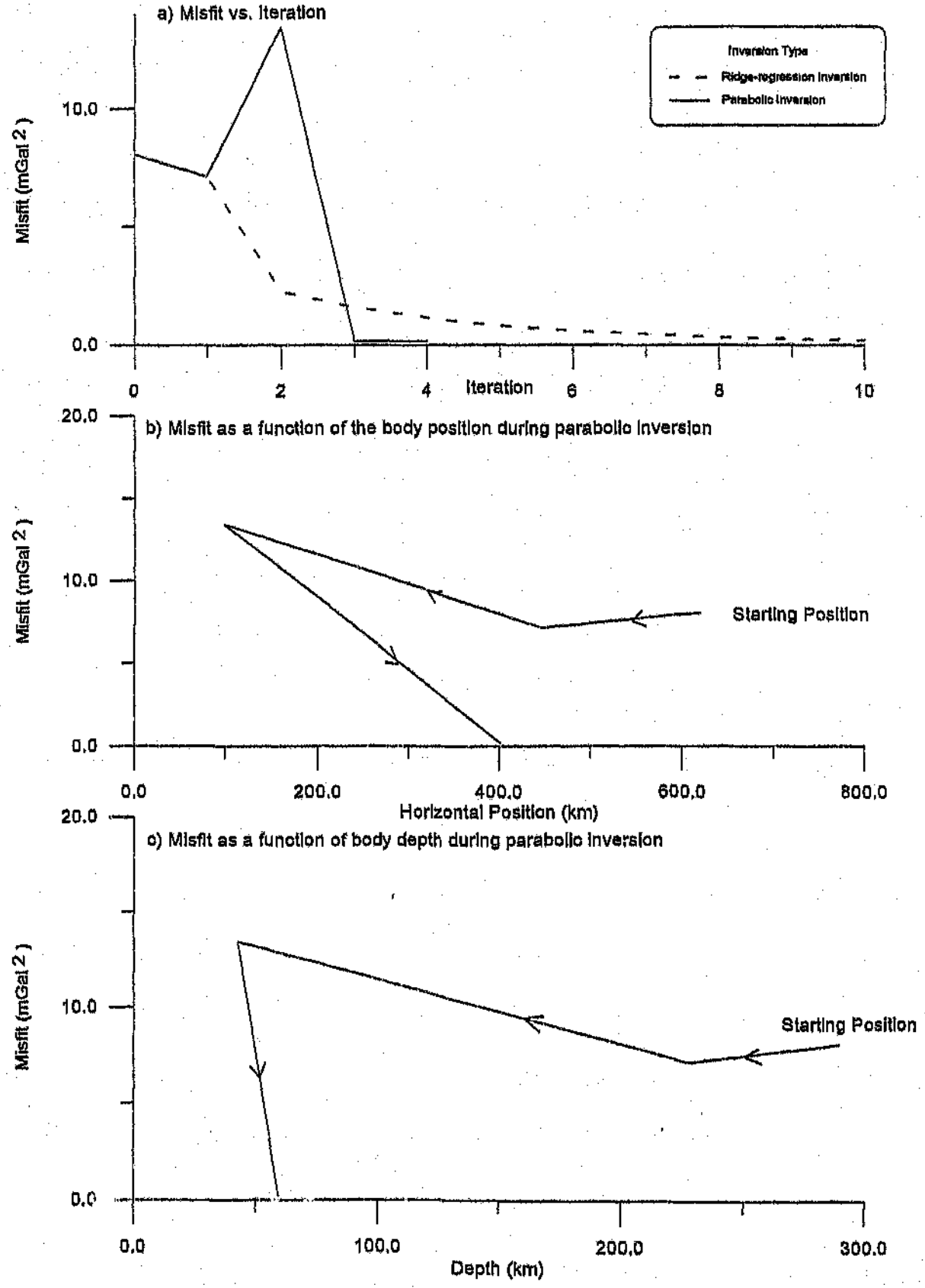

than attempts to fit n dimensional paraboloids to the misfit surface.

The strategy used in section 6.2 must be modified to cope with the multiparameter inversion situation. As in 6.2, the first change to the parameter values is accomplished via an iteration of ridge-regression inversion. Each parameter is then multipled by a constant value on successive iterations, until the misfit increases compared to the previous iteration. Figure 6.10 shows a schematic path across the misfit surface for the two parameter case. The n dimensional misfit trajectory is then projected onto n individual parabolas, one for each parameter. The improved values for each parameter are then established via parabolic inversion, as before.

This is demonstrated using the gravity model in Figure 6.2 . The position and depth of the body were simultaneously inverted, and the misfit was plotted as a function of iteration for ridge-regression inversion and the parabolic inversion method in Figure 6.11a. Figure 6.11b shows the trajectory of the misfit for the horizontal position and Figure 6.11c shows the misfit trajectory for the depth. The improvement in the rate of convergence of the parabolic inversion method can be seen, since it reached the minimum in under half of the number of iterations of the ridge-regression technique. Note however that its success depends on both the parameters under inversion moving toward the minima on the first iteration ; if either does not, then it will not be possible to construct a parabola around the minimum for that parameter.

The model in Figure 6.2 was used again, this time with the angle of rotation

Figure 6.10 : Misfit Surface for the Model in Figure 6.2 for the Parameters of Depth and Horizontal Position

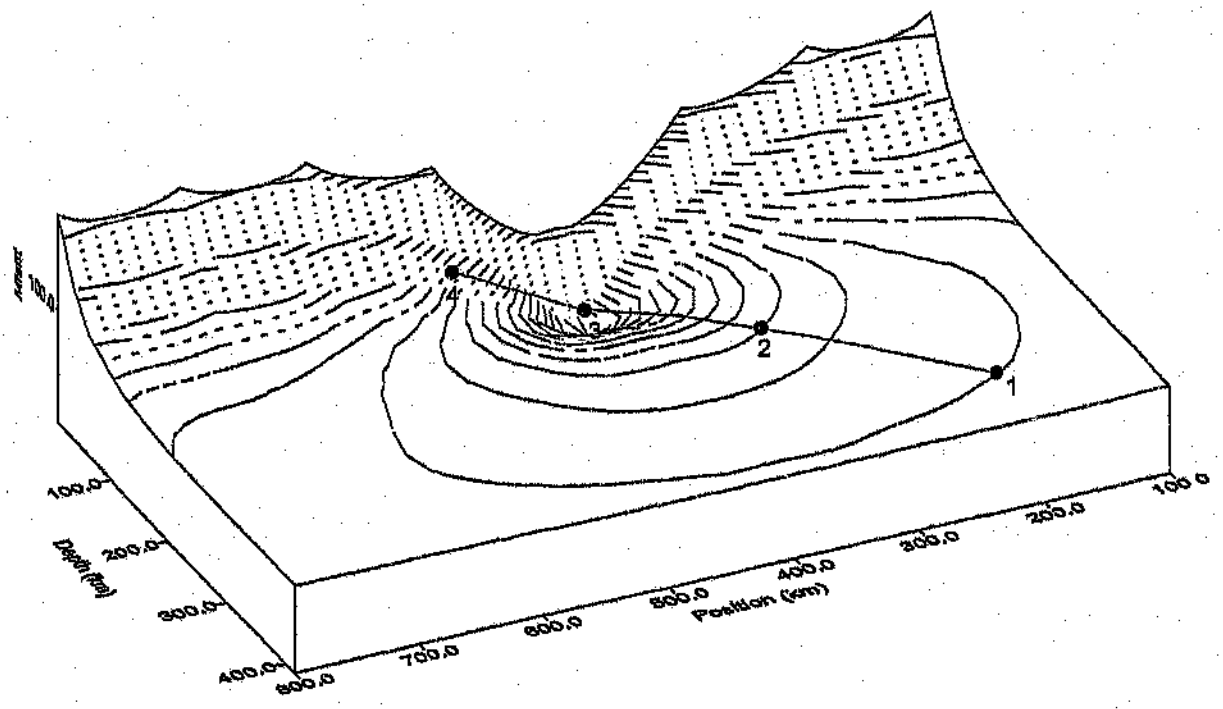

A schematic misfit trajectory is plotted on the misfit surface, starting at the point marked 1 and proceeding to the point marked 4. Parabolic interpolation is then used to take it to the minimum.

Figure 6.9 : Comparison of Parabolic Inversion and the Ridge-Regression Technique in the Inversion of Gravity Data - 50% Noise Added

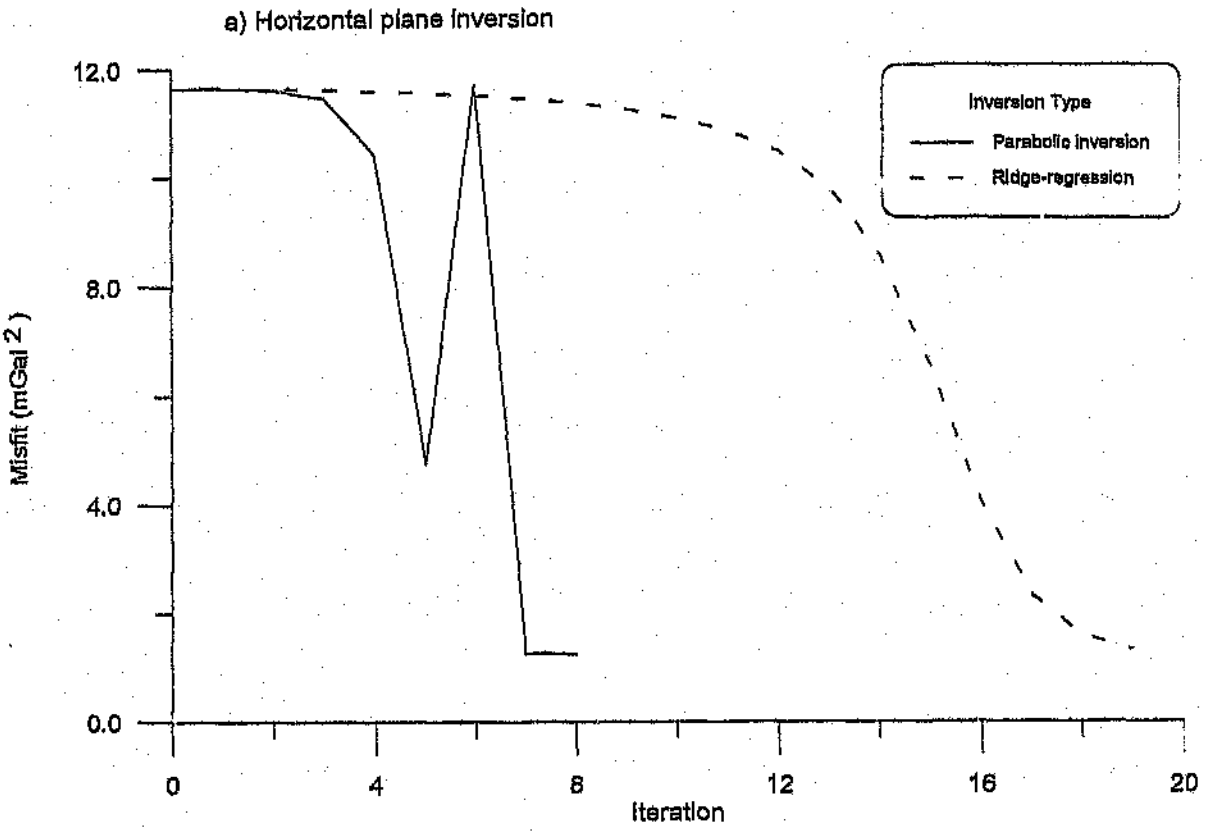

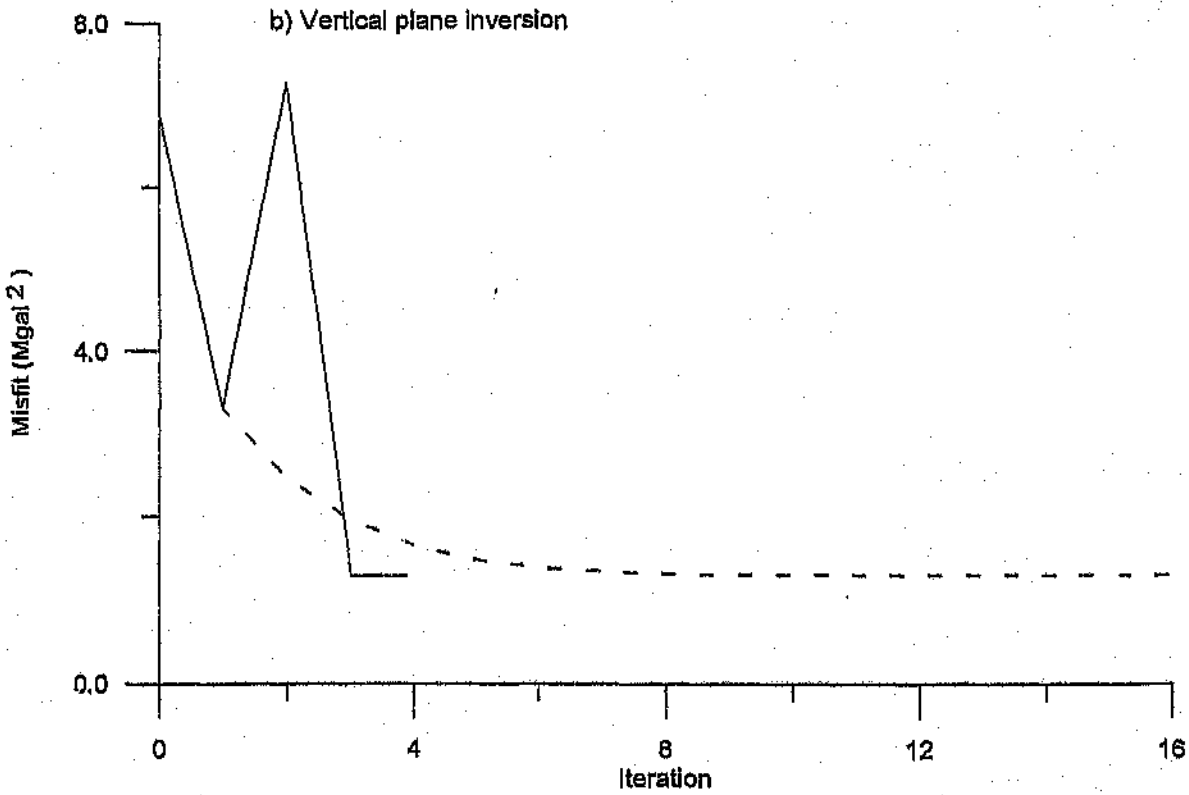

whole surface in the vicinity of the minimum) was however found to be more sensitive to the noise level. The noise results in the minimum achievable misfit being non-zero. In addition, the use of the gradient to determine the form of the quadratic surface is not recommended if the data are noisy, since the gradient is much more sensitive to noise than the misfit itself. Inverting the model in Figure 6.8 from the same starting positions as before produced an estimate of 645km for the horizontal position (compared to 400km) and a depth of 26.9km (compared to 35.5km).

6.4 Extension to Higher Dimensions

As the number of parameters being inverted increases, so does the number of dimensions of the misfit surface, and the problem becomes correspondingly more difficult to solve. For n parameters, the problem becomes that of fitting an n dimensional paraboloid on the n+1 dimensional misfit surface. The misfit surface for the model in Figure 6.2, when both the position and the body depth are inverted, is shown in Figure 6.10 . The equation for a general conicoid in three dimensions (corresponding to the case where two parameters are being inverted) (Blakey, J., 1952 p.88) ;

$$ax^2 + by^2 + cz^2 + 2fyz + 2gzx + 2hxy + 2ux + 2vy + 2wz + d = 0 \qquad (6.5)$$

The large number of coefficients (a,b,c,d,f,g,h,u,v,w) is a measure of the difficulty involved in the inverse process. As the number of parameters being inverted increases, the number of coefficients to be determined by the parabolic technique becomes unmanageable and the ridge-regression method will perform more efficiently

Figure 6.7 : Gravity Model Used for Body Vertical Position Inversion

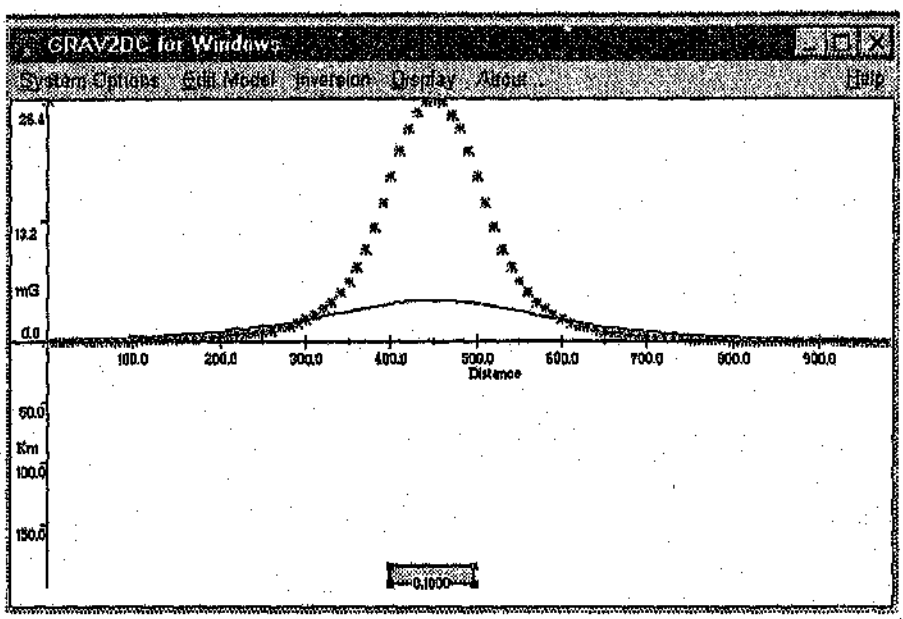

Figure 6.8 : The Gravity Model of Figure 6.5 with Noise Added

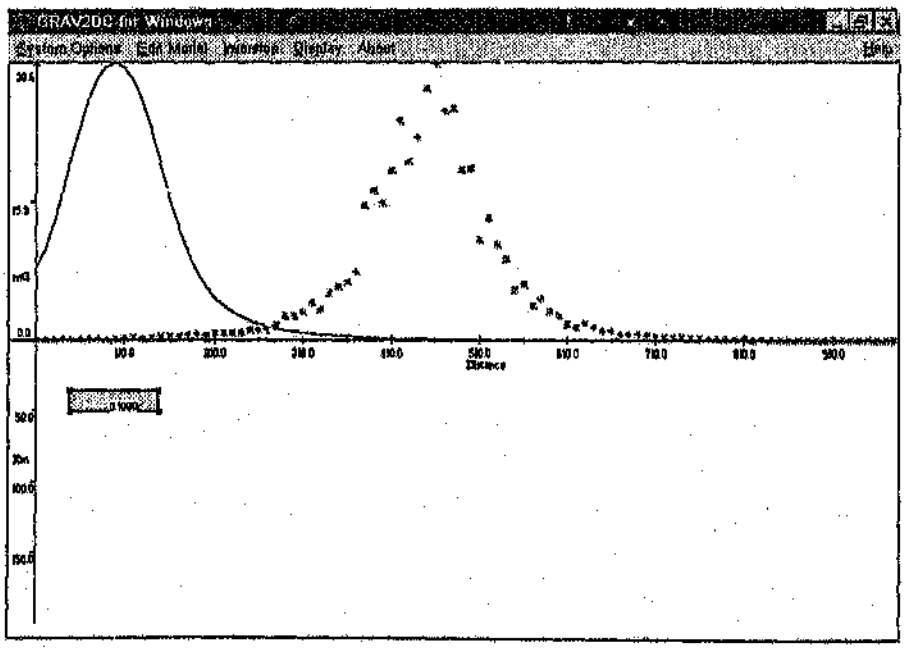

Constable, S.C., Parker, R.L., and Constable C.G., 1987. Occam's inversion : A practical algorithm for generating smooth models from electromagnetic sounding data. Geophysics v.52, p.289-300.

Cooke, D.A., and Schneider, W.A., 1983. Generalised linear inversion of reflection seismic data. Geophysics v.48 p.665-676.

Cooper, G.R.J., 1995. Non-Linear Dynamics and Gravity Inversion. Proceedings of the Centennial Geocongress. Johannesburg, p.957-960.

Cooper, G.R.J., and Jones, M.Q.W., 1998. Robust inversion of borehole temperature data. Geophysics (in press).

Craig, R.G., January 1989. Geophysical problems in nuclear waste disposal. Leading Edge, p.20-23.

Dimri, V., 1992. Deconvolution and inverse theory : Application to geophysical problems. Elsevier Science, 230p.

Gersztenkorn, A., Bednar, J.B., and Lines, L.R., 1986. Robust iterative inversion for the one dimensional acoustic wave equation. Geophysics v.51, p.357-368.

Gibowicz, S.J., and Kijko, A., 1994. An introduction to mining seismology. Academic Press, 300p.

Bergé, P., Pomeau, Y., and Vidal, C. 1984. Order within Chaos - Towards a Deterministic Approach to Turbulence. Wiley & Sons, New York. 329 p.

Blakey, J., 1952. Degree mathematics ; formulae and examples. Cleaver-Hulme London, 137p.

Blakely, R.J., 1995. Potential theory in gravity and magnetic applications. Cambridge University Press, New York, 435 p.

Blue Sky Software, 1991. RoboHelp Help Compiler. 7486 La Jolla Blvd, Suite 3, La Jolla, CA 92037, U.S.A.

Borland International, 1992. Turbo Pascal for Windows. 100 Borland Way, P.O. Box 660001, Scotts Valley, CA 95067-0001, U.S.A.

Bricker, R.I., 1990. Object oriented development, a logical approach to control system design. University of the Witwatersrand M.Sc. thesis.

Carlslaw, H.S., and Jaeger, J.C., 1959. Conduction of heat in solids. Oxford University Press, London 497p.

Cohen, J.K., and Bleistein, N., 1979. Velocity inversion procedure for acoustic waves. Geophysics v.44 p.1077-1087.

REFERENCES

Abarbanel, H.D.I., Brown, R., Sidorowich, J.J., and Tsmring, L.S., 1993. The analysis of observed chaotic data in physical systems. Reviews of Modern Physics v.65 no.4, p.1331-1392.

Abarbanel, H.D.I., 1995. Analysis of Observed Chaotic Data. Springer-Verlag, New York 272p.

Anderssen, R.S., Worthington, M.H., and Cleary, J.R., 1972. Density modelling by Monte Carlo Inversion - I Methodology. Geophys. J.R.astr. Soc v.29, p.433-444.

Baas, A., 1993. An object-oriented component based approach to building real-time software systems. University of the Witwatersrand M.Sc. thesis.

Barnsley, M.F., 1986. Making chaotic dynamical systems to order. chaotic dynamics and fractals p.53 .Academic Press, London. Barnsley, M.F. and Demko, S.G. (editors). 301p.

Beltrami, H., and Mareschal, J.-C., 1995. Resolution of ground temperature histories inverted from borehole temperature data. Global and Planetary Change v.11, p.57-70.

Beresford, M.R., 1996. Chaotic behaviour of share prices on the Johannesburg stock exchange. MBA thesis, University of the Witwatersrand business school, 59p.

to the inversion of one or two parameters.

In summary, the Gauss-Newton method of inversion is an excellent general purpose tool for geophysical data, but other methods can improve upon it under particular circumstances, depending on the nature of the problem under investigation.

7.2 Suggestions for Further Work

The next steps that can be taken with the chaotic inversion of chapter 5 are the *prediction* and *control* of the inverse process. Firstly, can the trajectory of the inverse process through parameter space be predicted a few iterations ahead of the current position ? If so, is doing this computationally less demanding than just performing the iterations anyway ? Secondly, can the trajectory be forced into a region of parameter space corresponding to a small misfit value ? This would be done by modifying a model parameter value at a particular position in parameter space, and hence altering the trajectory. The problem with both of these ideas is that current methods of control of chaotic trajectories require the trajectory to have visited the desired region of phase (parameter) space many times previously, to enable a picture of the dynamics there to be built up (Abarbanel, H.D.I., 1993). However for an inverse problem once a minimum (local or otherwise) has been established nothing further would be gained by forcing the trajectory back to that position in parameter space. So a new approach to these portions of the current theory of chaotic systems would be required, but it is felt that such a change is not infeasible.

inverse process reduced the fractal dimension of the set.

In Chapter 5 a modification to the Gauss-Newton inversion method was introduced which caused the inverse process to become chaotic, for parameters which had a non-linear geophysical response. The chaotic motion was studied in detail, and it was found that it was possible to move the system from a chaotic state to a periodic state or to a constant parameter value by increasing the damping of the inversion. The chaotic inverse process was used as an alternative to the Monte Carlo inverse method for a two parameter gravity model, where it was able to reconstruct the misfit surface successfully. It was also used to force the inverse process out of a local minimum to other regions of parameter space where other, deeper minima were encountered..

Chapter 6 examined the use of knowledge of the form of the misfit surface as an aid to the inverse process. The fitting of quadratic functions proved useful in that it was computationally unintensive and allowed more rapid convergence to the minimum than would have been achieved by the Gauss-Newton method. If minima are of quadratic form, then it proved possible to detect other minima that lie adjacent to the current one by fitting quartic functions to the misfit surface. The fitting of quadratic and quartic functions was insensitive to small amounts of noise in the data. The main drawback of the method was that the large number of terms required to define the misfit surface when many parameters were being inverted could only be determined after a large number of inversion iterations, and this could be greater than the number of iterations required by the Gauss-Newton method. Hence the method

CHAPTER SEVEN : CONCLUSIONS AND SUGGESTIONS FOR FURTHER RESEARCH

7.1 : Conclusions

In order to perform the investigations described above, a large quantity of computer software had to be written. The magnetic and gravity modelling software used in chapters 4-6 was written using the object-oriented approach, which made the code easier to debug and maintain.

In this project several different approaches to the geophysical inverse problem were considered. Chapter 3 looked at the application of L_1 rather than L_2 inversion to borehole temperature data, and found that varying the norm of the inversion during the inverse process could reduce by 50% the number of iterations required for the inversion to converge to a suitable model. The selection of which norm to use was based on the statistics of the residuals. Chapter 3 also considered various damping schemes, and found that the use of the misfit in controlling the damping could produce the smallest model that gave a good fit to the data, in the least number of iterations. Such models indicated an increase in ground surface temperature of 1-2°C over the last 125 years, which agreed with other known climatological data.

Chapter 4 investigated which initial model parameter configurations converged to which minima, for magnetic data, using the Gauss-Newton method. This set of initial models had a fractal nature, providing at least two model parameters which had a non-linear geophysical response were being inverted. Increasing the damping of the

Figure 6.22 : Quartic Fit to Misfit Surface for the Model in Figure 6.21

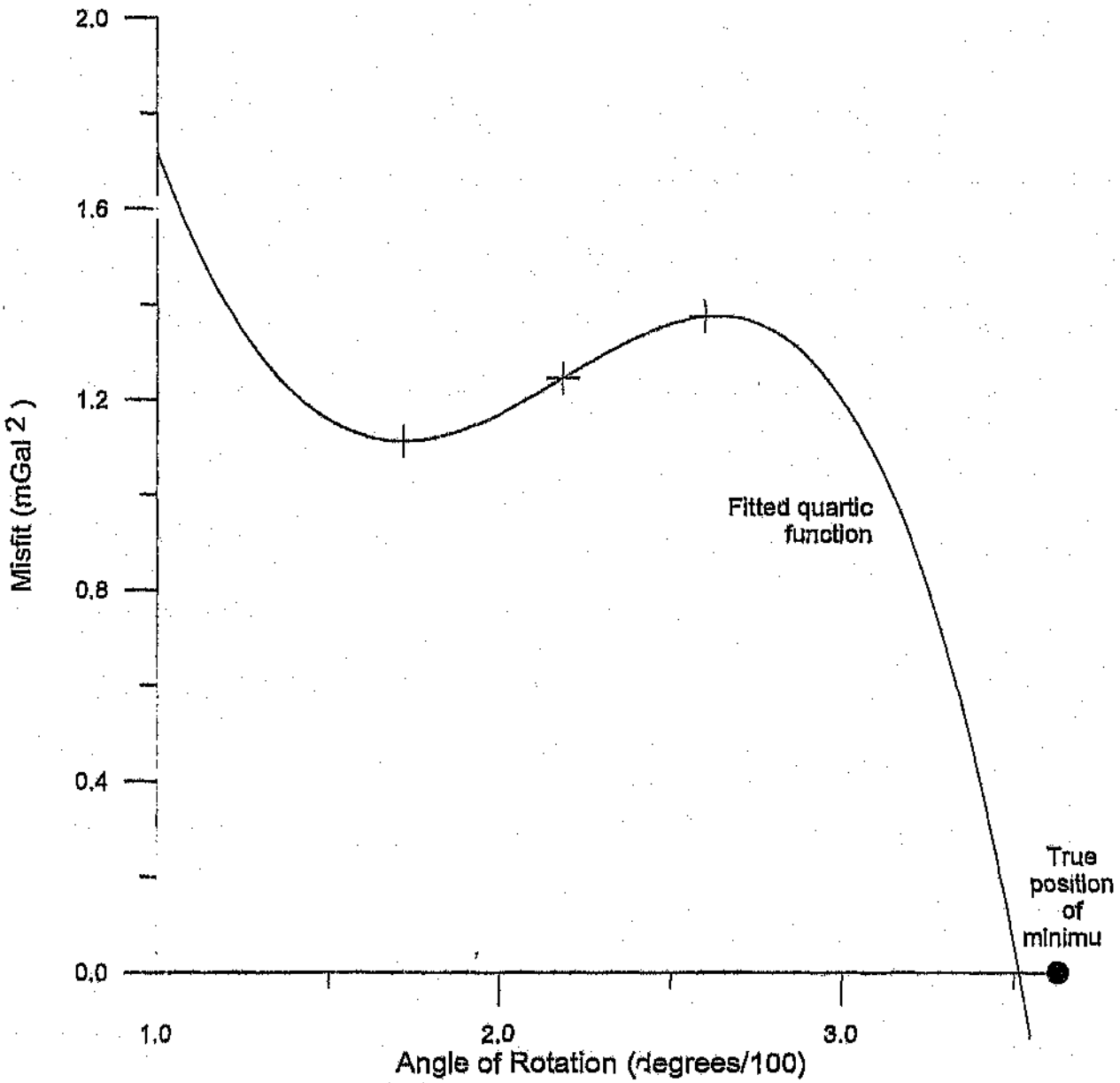

Figure 6.20 : Quartic fit to Misfit Surface using Data Points and Surface Gradient for the Model in Figure 6.19

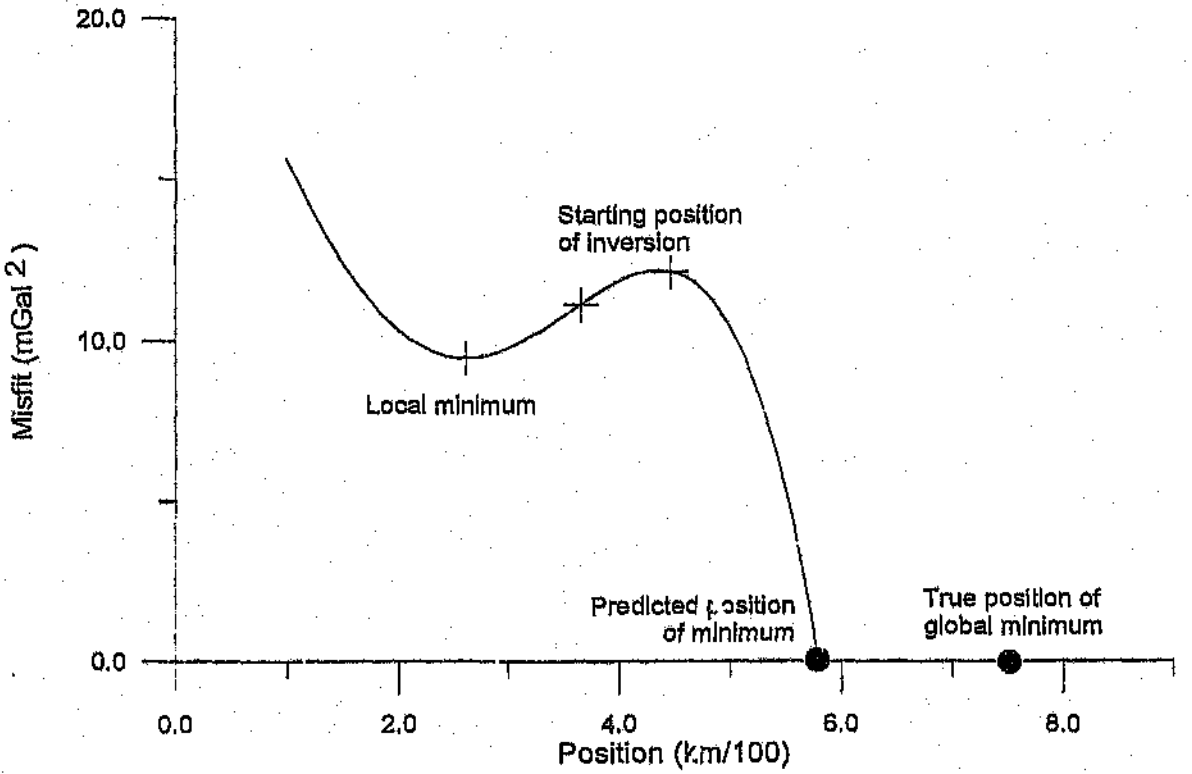

Figure 6.21 : The Model in Figure 6.17 with Noise Added

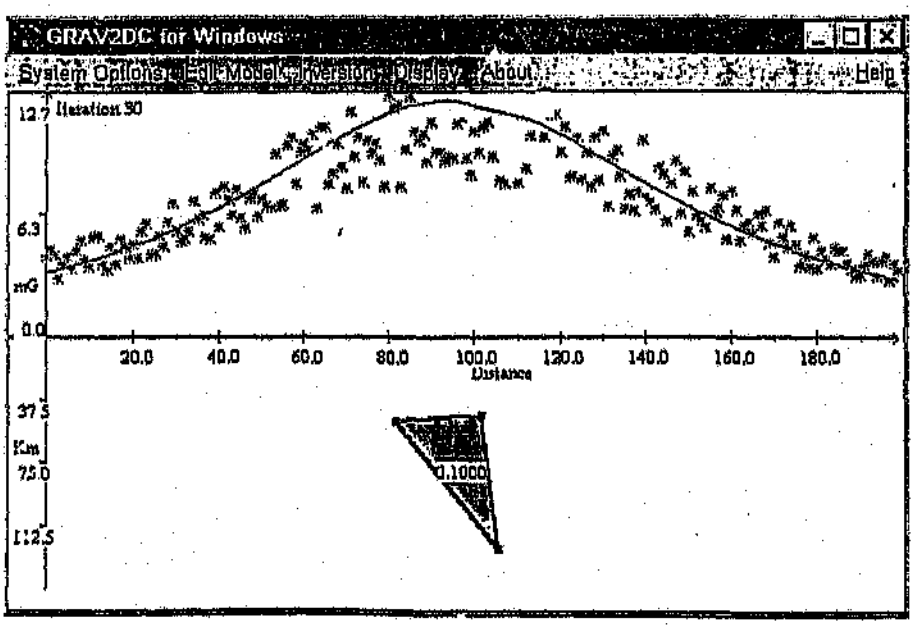

the fitting of the quadratic functions themselves. The parabolic interpolation method is best suited to inversion problems with small numbers of parameters, since the difficulty of fitting polynomials to the misfit surface increases rapidly as the number of parameters increases. The number of inversion iterations required to provide sufficient data to fit an n dimensional polynomial can become greater than the number of iterations required by the ridge regression inversion technique to fit the data when n is large.

Figure 6.18 : Misfit Surface for the Rotation of the Body in Figure 6.17

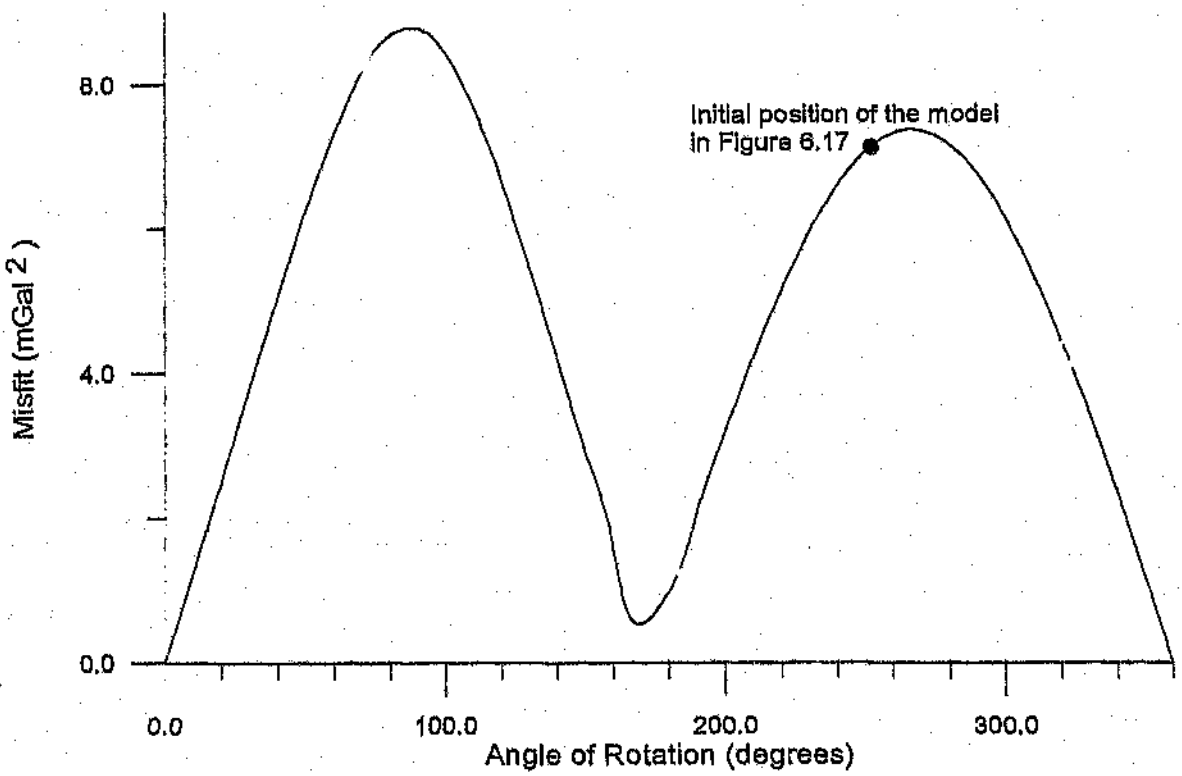

Figure 6.19 : The Model in Figure 6.13 with Noise Added



from this point reached the global minimum in three iterations.

6.5.1 Effect of Noise

The data in the model in Figure 6.13 had 50% uniformly distributed noise added to it to produce the model in Figure 6.19. This was inverted as described above and a quartic polynomial fit to three points and two gradients from the misfit surface. The results are shown in Figure 6.20, from which it can be seen that position of the predicted minimum moved from 600km (the noise-free solution) to 580km. Hence even the addition of 50% random noise only changed the result by 3% (in this case).

The gravity model in Figure 6.17 also had 50% normally distributed random noise added to it, to produce the model shown in Figure 6.21, and this was inverted as before. The predicted minimum position is at 352 degrees, which is actually closer to the correct position of 360 degrees than was obtained above for the noise free model. The fit is shown in Figure 6.22 .

6.6 Conclusions

Knowledge of the form of the misfit surface can be used to optimise the inversion process. The misfit surface was assumed to be quadratic in form in the regions surrounding a minimum, and this enabled the position of the minimum to be estimated. In addition, the position of other nearby minima can be estimated providing the gradient of the misfit surface is used and a quartic polynomial is fitted to the misfit surface. The technique proved insensitive to noise in the data, although calculations of the gradient of the misfit surface were more affected by noise than was

Figure 6.16 : Quartic fit to Misfit Surface using Data Points and Surface Gradient

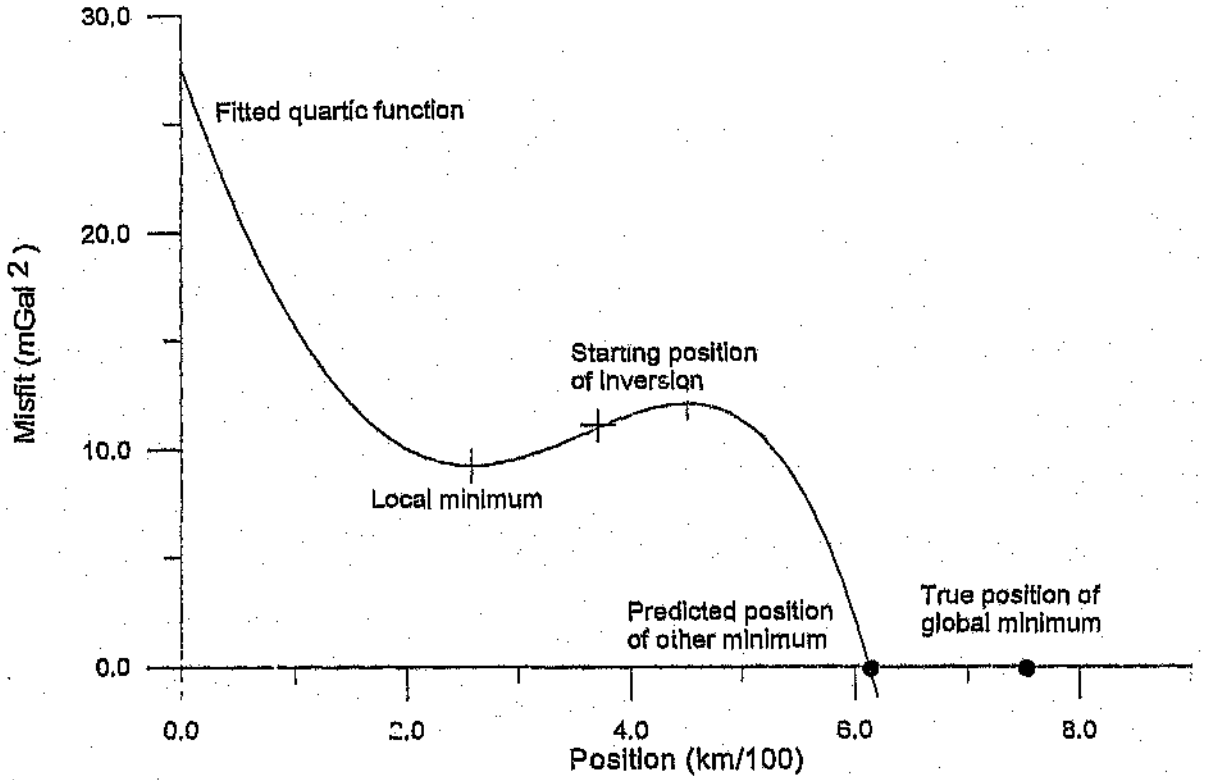

Figure 6.17 : Inversion of Angle of Rotation of Body

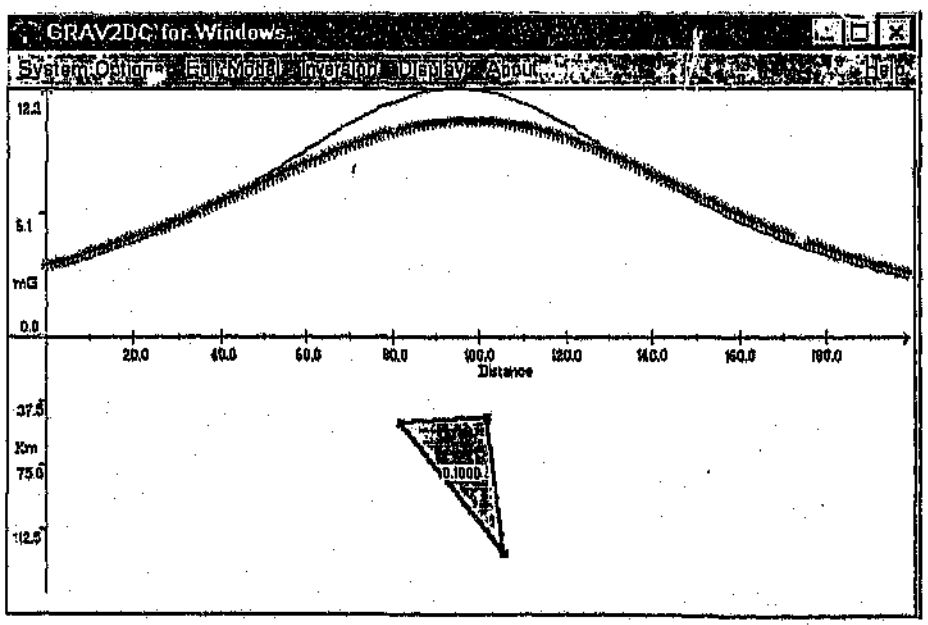

Telford, W.M., Geldart, L.P., Sheriff, R.E., and Keys, D.A. 1990. Applied geophysics (2nd ed.). Cambridge University Press. 770p.

Thompson, P.H., Judge, A.S., and Lewis, T.J., 1995. Thermal parameters in rock units of the Winter Lake-Lac de Gras area, Central Slave province, Northwest Territories - implications for diamond genesis. Current Research 1995-E ; Geological Survey of Canada p.125-135.

Tritton, D.J., 1986. Ordered and chaotic motion of a forced spherical pendulum. European Journal of physics v.7 p.162.

Turcotte, D.L., 1997. Fractals and chaos in geology and geophysics (2nd ed.). Cambridge University Press, New York 398p.

Tyson, P.D., Mason, S.J., Jones, M.Q.W., and Cooper, G.R.J., 1997. Global Warming in South Africa : Evidence from Geothermal Profiles. Submitted to Nature.

Vozoff, K., and Jupp, D.L.B., 1975. Joint inversion of geophysical data. Geophysical Journal of the Royal Astronomical Society v.42 p.977-991.

Welsz, D.A., and Oliveira, M., 1984. Fractal structures formed by kinetic aggregation of aqueous gold colloids. Phys. Rev. Lett., v.52 p.1433-1436.

Savit, R., 1992. Chaos on the trading floor. In the New Scientist guide to chaos p.174. Penguin Books. Hall, N. (Ed.)

Scott, S., 1992. Clocks and chaos in chemistry. In the New Scientist guide to chaos p.108. Penguin Books. Hall, N. (Ed.)

Sheer, J., Burton, R., and Bluhm, S., 1984. Recent developments in the cooling of deep mines. The South African Mechanical Engineer, v.34, p.2-8 .

Steward, D.V., 1979. Software engineering with systems analysis and design. Brook/Cole, California, 450p.

Stu i, D., and Stoyan, H., 1994. Fractals, random shapes and point fields : methods of geometrical statistics. Wiley & Sons, New York 389 p.

Swan, T., 1991. Turbo Pascal for Windows 3.0 programming. Bantam Books New York, 876 p.

Tan, C., Varghese, M., Varaiya, P., and Wu, F.F., November 1995. Bifurcation, Chaos, and Voltage Collapse in Power Systems. Proceedings of the IEEE vol.83 no. 11 p.1484-1497.

Takens, F., 1981. Dynamical systems and turbulence. Springer Verlag New York, 302p.

Rasmussen, R., and Pedersen, L.B., 1979. End corrections in potential field modelling. Geophysical Prospecting, v.27, p.749-760 .

Richards, J.A., 1993. Remote sensing digital analysis, an introduction (2nd ed.). Springer-Verlag, New York, 340 p.

Richardson, S.W., and Oxburgh, E.R., 1978. Heat flow, radiogenic heat production and crustal temperatures in England and Wales. Earth Planet. Sci. Lett., v.5 p.323-337.

Royden, L., Sclater, J.G., and Von Herzen, R.P., 1980. Continental margin subsidence and heat flow : important parameters in formation of petroleum hydrocarbons. A.A.P.G. bulletin v.64 no.2, p.173-187 .

Ruelle, D., 1992. Chaotic evolution and strange attractors. Cambridge University Press, New York 96p.

Ruelle, D., and Takens, F., 1971. On the nature of turbulence. Commun. Math. Phys. v.20, p.167-92

Sambridge, M., and Drijkoningen, G., 1992. Genetic algorithms in seismic waveform inversion. Geophysical Journal International v.109, p.323-342.

Savit, R., 1988. When Random is not Random: An Introduction to Chaos in Market prices. J. Future Markets, v.8, p.271

University of the Witwatersrand Ph.d. thesis.

Oldenburg, D.W., 1974. The inversion and interpretation of gravity anomalies. Geophysics v.39, p.526-536.

Oristaglio, M.L., and Worthington, M.H., 1978. Inversion of surface and borehole electromagnetic data for two-dimensional electrical conductivity models. Geophysical Prospecting v.28, p.633-657.

Pippard, A.B., 1985. Response and stability : an introduction to physical theory. Cambridge University Press, New York 228 p.

Pollack, H.N., 1993. Climate change inferred from borehole temperatures. Global Planet Change v.7, p. 173-179.

Pollack, H.N., and Cercone, K.R., 1994. Anomalous thermal maturities caused by carbonaceous sediments. Basin Research, v.7, p.47-51 .

Press, F., 1969. Earth Models obtained by Monte Carlo Inversion. Journal of Geophysical Results v. 73

Press, W.H., Teukolsky, S.A. Vettering, W.T., and Flannery, B.P., 1992. Numerical recipes, the art of scientific computing (2nd ed.). Cambridge University Press, New York, 963p.

systems. Cambridge University Press, New York 367p.

Matlab, 1997. The MathWorks Inc., 24 Prime Park Way, Natick, MA 01760, USA.

May, R.M., 1974. Biological populations with non overlapping generations: stable points, stable cycles, and chaos. Science v. 186 p.645-647.

May, R.M., and Oster, G.F., 1976. Bifurcations and dynamic complexity in simple ecological models. Amer. Nature v.110 p.573-599.

Menichetti, V., and Guillen, A., 1983. Simultaneous interactive magnetic and gravity inversion. Geophysical Prospecting v.31 p.929-944.

Menke, W., 1989. Geophysical data analysis : Discrete inverse theory 2nd edition. Academic Press, 289p.

Meyer, B., 1988. Object oriented software construction. Journal of object oriented programming v.2, no. 3.

Nicolson, J.M., 1993. Object oriented design of cable selection softwar. for low voltage networks. University of the Witwatersrand M.Sc. thesis.

Nitch, D., 1992. A serial and parallel design of NEC2 to demonstrate the advantages of the object-oriented paradigm in comparison with the procedural paradigm.

analysis and generalised linear inversion for deriving statics and shallow bedrock velocities. M.Sc. thesis, Memorial University of Newfoundland.

Levenburg, K., 1944. A method for the solution of certain non-linear problems in least squares. Quarterly of Applied Mathematics v.2, p.164-168.

Lewis, T., and Wang, K., 1992. Geothermal research related to past climate. EOS Trans. Am. Geophys. Union v.73, p.265-269.

Lines, L.R., and Treitel, S. 1984. Tutorial : A review of least-squares inversion and its application to geophysical problems. Geophysical Prospecting v.32 p.159-186.

Madan, R.N., and Wu, C.W., 1993. Introduction to experimental chaos using Chua's circuit. In, Chua's circuit : A paradigm for chaos. Madan R.N. (Ed.)1045p. World Scientific Publishing, Singapore .

Mandelbrot, B., 1982. The fractal geometry of nature. W.H.Freeman, San Francisco, 468p.

Marquardt, D.W., 1963. An algorithm for least-squares estimation of non-linear parameters. Journal of the Society of Industrial and Applied Mathematics v.11 p.431-441.

Marek, M., and Schreiber, I., 1991. Chaotic behaviour of deterministic dissipative

J.Geophys. Res. v.93 no.B4, p.3243-3260 .

Jeffrey, A., 1979. Mathematics for scientists and engineers (2nd ed.). Nelson and Sons, Surrey UK 734p.

Jones, M.Q.W., Tyson, P.D., and Cooper, G.R.J., 1997. Modelling climatic change in South Africa from perturbed borehole temperature profiles. Quaternary Science (in press).

Kaye, B.H., 1989. A random walk through fractal dimensions. V.C.H., Germany 421p.

Kaye, B.H., and Clarke, G.G., 1985. The fractal description of extra terrestrial fine particles. Part. Charact., v.2 p.143-148.

Kijko, A., 1994. Seismological outliers : L_1 or adaptive L_p norm application. Bulletin of the seismological society of America, v.84 no.2 p.473-477

La Salle, J., and Lefschetz, S., 1961. Stability by Lyapunov's Direct Method, with Applications. Academic Press, New York, 134 p .

Lauwerier, H.A., 1986. One dimensional iterated maps. In Chaos, Princeton University Press New Jersey, A.V.Holen (ed.)324p.

Leslie, I., 1995. A comparison of the methods of engineering seismic refraction

Gleick, J., 1987. Chaos. Abacus Press, London 352 p.

Gowan, H.K.M., 1991. An investigation into the viability and advantages of object-oriented programming in the implementation of a long range predictive controller. University of the Witwatersrand M.Sc. thesis.

Hampson, D., and Russel, B., 1984. First-break interpretation using generalised linear inversion. Canadian Society of Exploration Geophysicists v.20 p.40-54.

Hilborn, R.C., 1994. Chaos and nonlinear dynamics. Oxford University Press, New York 654 p.

Horne, S., and MacBeth, C., 1994. Inversion for seismic anisotropy using genetic algorithms. Geophysical Prospecting v.42 p.953-974.

Harter, H.L., 1972. The method of least squares and some alternatives. A.R.L. technical report 72-0129, Aerospace research laboratories, Wright-Patterson Air Force Base, Ohio AD 752211

Inman, J.R., 1975. Resistivity inversion with ridge regression. Geophysics v.50 p.2112-2131.

Jones, M.Q.W., 1988. Heat flow in the Witwatersrand basin and environs and its significance for the South African shield geotherm and lithosphere thickness.

Author: Cooper, Gordon Robert John.
Name of thesis: Aspects of the theory of inversion as applied to geophysical problems.

PUBLISHER:
University of the Witwatersrand, Johannesburg
©2015

LEGALNOTICES:

Copyright Notice: All materials on the University of the Witwatersrand, Johannesburg Library website are protected by South African copyright law and may not be distributed, transmitted, displayed or otherwise published in any format, without the prior written permission of the copyright owner.

Disclaimer and Terms of Use: Provided that you maintain all copyright and other notices contained therein, you may download material (one machine readable copy and one print copy per page)for your personal and/or educational non-commercial use only.

The University of the Witwatersrand, Johannesburg, is not responsible for any errors or omissions and excludes any and all liability for any errors in or omissions from the information on the Library website.